For Reviewer comments 1 RC1

We thank this Reviewer for thoughtful and constructive comments on our manuscript. We appreciate the time s/he invested in the review. We believe that our revised manuscript addresses all the comments. In this regard, we have revised and rewritten a few sections such as Abstract, method, results, discussion and conclusion in the revised manuscript. Quality control and revision of dissipation estimates, as well as current calculations were also done to ensure the validity of our results. We thought it useful to point out its detailed revisions (lines and sections) in the reply to your comments. Below (highlighted in blue and magenta) is an itemized response to the different issues raised in the review.

Review

Turbulent dissipation from AMAZOMIX off the Amazon shelf along internal tides paths

Kouogang et al.

Summary

This manuscript describes measurements of currents, hydrography, and turbulence at numerous sites near the Amazon outflow, where internal tides are also generated at the slope. The dataset appears suited to study the questions posed by the authors. Do internal tides affect the mixing? Does the mixing affect nutrient fluxes?

However, I have some concerns about the analysis listed below. Since many of the details of the analysis are not presented, it is difficult for me to evaluate what has been done. Some of the more prominent ones include:

tidal decomposition of the currents,

use/decomposition of shear,

description/applicability of the finescale parameterizations used,

and shaded color plots of SADCP velocity that include transits and times on station.

There are also presentation/stylistic problems that make the manuscript very difficult to read. Many of them are major, but also getting down to such points as the labelling of figures and sections. Some examples are listed below. It is well beyond the scope of a review to point all of these out. Furthermore, the cumulative difficulty of numerous minor things (let alone the more major ones) turns into a major distraction to the detriment of the hard work done and the science. The senior authors must make considerably more effort in this regard.

Major comments

1. SI units should be written W kg-1 not W.kg-1 and 90 km not 90km and so on.

R: Thanks for your remarks.

We have revised the SI units throughout the revised manuscript.

an example, in lines 22-24 of the revised manuscript, is shown below:

“

> Near generation sites, mixing rates were elevated, between [10^{-6}, 10^{-5}] W kg^{-1}, with IT shear contributing ~65 %, compared to mean baroclinic current (BC) shear. Along IT pathways and in far-field IT regions, mixing decreased to [10^{-8}, 10^{-7}] W kg^{-1} but remained substantial, driven by nearly equal contributions from IT and BC shear.

“

2. 50.4% on line 29. Please state the error and adjust the significant figures accordingly.

R: Thanks for your remarks.

We have revised as suggested

The error, associated with the contribution of tidal and mean shear, was estimated with the standard deviation. It is relatively small. you will find the error we have declared in table A1 of the revised manuscript.

3. line 34 - A “guide for the mixing parameterization in future numerical simulation” is mentioned. What is the guidance?

R: Thanks for your remark.

Indeed, we have revised all the Abstract and sentence in line 29-30 of the revised manuscript:

“

These findings provide valuable insights for developing parameterizations of tidal and mean shear mixing for ocean or coupled models, with significant implications for regional biogeochemistry and the climate system.

”

4. Section 2.2- some of the microstructure processing steps should be shown in either the main text, appendix, or supplementary material. In particular, I would like to see some examples of the spectral fits.

R: Thanks for your suggestions.

We have incorporated additional microstructure processing steps and spectral fits into both the main text and the appendix. Revisions and checks of the VMP profile processing, and dissipation estimates have been carried out, along with quality assurance tests, in alignment with all reviewers' comments and ATOMIX's recommendations (Lueck et al., 2024).

a) First, the revisions were focused on the VMP profile processing, particularly on:

- Parameters controlling shear spectra estimation, such as record lengths (L), which are cosine-windowed and overlapped (O) by 50%.
- Parameter for extracting the section or profile (continuous part of the time series), including the minimum depth of extraction (Pmin).

For shallow stations, we used L = 5 s and O = 2.5 s, instead of the previous L = 4 s and O = 2 s. Parameters for deep stations remain unchanged (L = 8 s and O = 4 s).

Additionally, we adjusted the minimum depth of extraction to Pmin = 10 m for deep stations and Pmin = 3 m for shallow stations, compared to the previously used value of Pmin = 1 m for both station types.

b) Second, the revisions and checks focused on the quality assurance measures for dissipation estimates, with quality control checks and adjustments applied across all stations (e.g., S2, S7, S12, S14).

For instance, at station S14, previous dissipation estimates showed some peaks at various depths, particularly between 100–200 m, 300–400 m, and 500–700 m. While the fraction of shear data affected by despiking during processing was <0.05, the figure of merit (FM)—used to filter out poor-quality data—for shear probe 1 was >>1.4 at certain depths (e.g., around 327 m compared to 122 m, as shown in figure RC1.1 below). In contrast, the FM for shear probe 2 remained <1.4.

After checks, quality control of dissipation estimates have been revised for all stations (e.g., S6, S10, S14). We have retained only dissipation estimates from either one or both probes that met the quality assurance criteria (FM < 1.4 and fraction of despiked shear data <0.05, as recommended by ATOMIX), as shown at S6 and S10 for example (figure RC1.2 below).

The final dissipation estimate was computed as the average of the estimates from both shear probes, followed by the mean of the dissipation profiles for the station, as illustrated in figure RC1.3 below.

The revision of section “methods/TKE dissipation rates” can be found in lines 121-151 of the revised manuscript, as shown below:

“

2.2 Methods

TKE dissipation rates

The VMP data are processed using ODAS Matlab library (developed by Rockland Scientific International, Inc) to infer the TKE dissipation rate (ε). The processing methods for the VMP data are briefly described here and adhere to the recommendations of ATOMIX (Analyzing ocean turbulence observations to quantify mixing), as reported by Lueck et al. (2024), and have been validated against the benchmark estimates (presented in Fer et al., 2024).

First, the VMP data are converted into physical shear units, and the time series are prepared. Continuous sections of the time series are selected for dissipation estimation. Before spectral estimation, the aberrant shear signals caused by vessel wake contamination are removed. Collisions of the shear probe with plankton and other particles are removed using the de-spiking routine. The records from each section are then high-pass filtered (e.g., at station S6 and S10; Fig. 2a, and Fig. A1, Appendix).

Shear spectra are estimated using record lengths (L) and Fast Fourier Transform segments of 2 s, which are cosine windowed and overlapped by 50% (e.g., at station S6 and S10; Fig. 2b, and Fig. A1, Appendix). Additionally, vibration-coherent noise is removed. Different L and overlap (O) settings were selected and tested based on the environment (e.g., deep vs. shallow water), following Fer et al. (2024). For shallow stations, L (O) was shortened to 5 s (2.5 s), in contrast to the 8 s (4 s) used for deeper stations, due to evidence of overturns observed in AMAZOMIX acoustic measurements at deeper stations (Koch-Larrouy et al., 2024; in preparation). This adjustment helped to optimize the spatial resolution of dissipation estimates in shallow water stations.

Finally, ε is determined using the spectral integration method and by comparison with the Nasmyth empirical spectrum (Nasmyth, 1970). Quality assurance tests are carried out in accordance with ATOMIX's recommendations (Lueck et al., 2024). A figure of merit < 1.4 is used to exclude bad data (e.g., at station S6 and S10; Fig. 2b, and Fig. A1, Appendix), and the fraction of data affected by de-spiking is < 0.05.

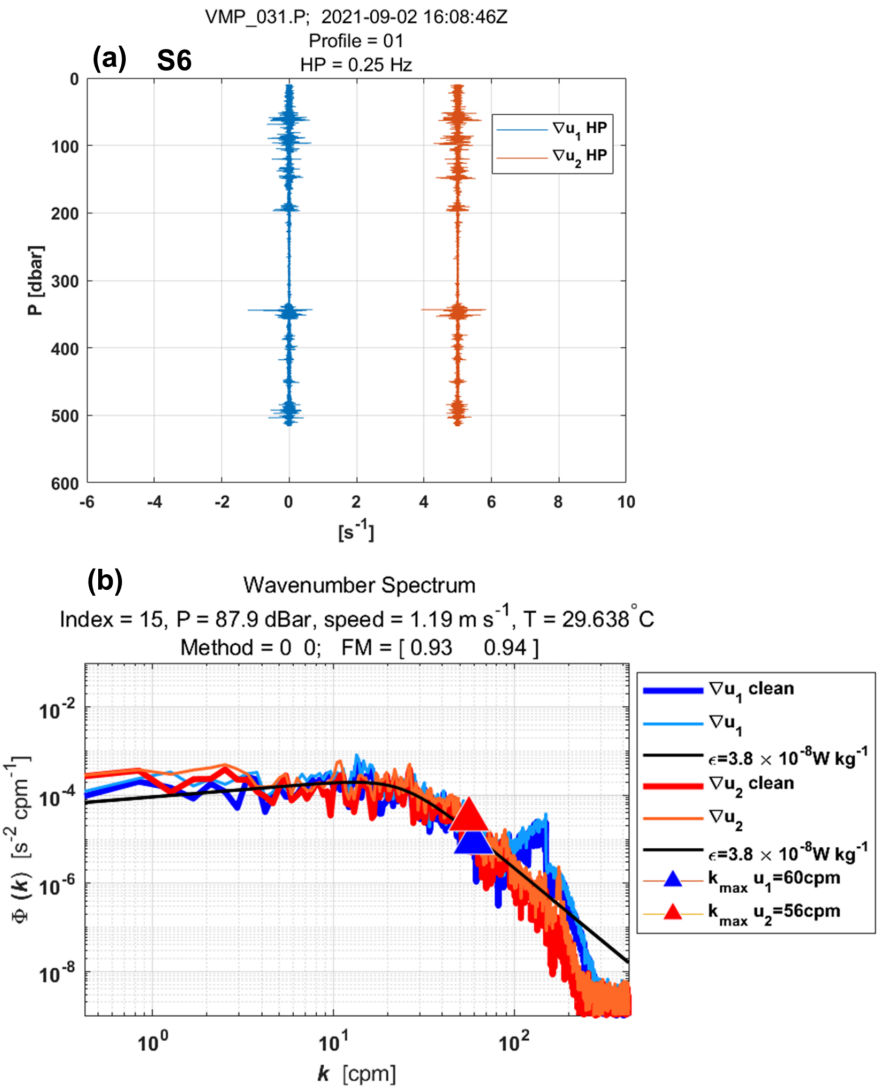

Figure 2: Example of wavenumber spectra from a dissipation structure segment used to determine the dissipation rate at station S6 at a pressure of 87.9 dBar. (a) Cleaned and high-pass filtered signals from shear probe 1 (blue) and shear probe 2 (red, offset by 5 s^{-1}). (b) Wavenumber spectra for shear probes 1 and 2. Thick lines (blue for probe 1, red for probe 2) show shear spectra with coherent noise correction, while thin lines (sky blue for probe 1, orange for probe 2) show spectra without correction. Triangles mark the maximum wavenumber used for dissipation rate estimation. Black lines represent Nasmyth reference spectra for estimated dissipation rate of 3.8 x 10^{-8} W kg^{-1} for both shear probes. Dissipation rate estimates for shear probe 1 and shear probe 2 at a pressure of 87.9 dBar yielded a figure of merit of 0.93 and 0.94, respectively.

”

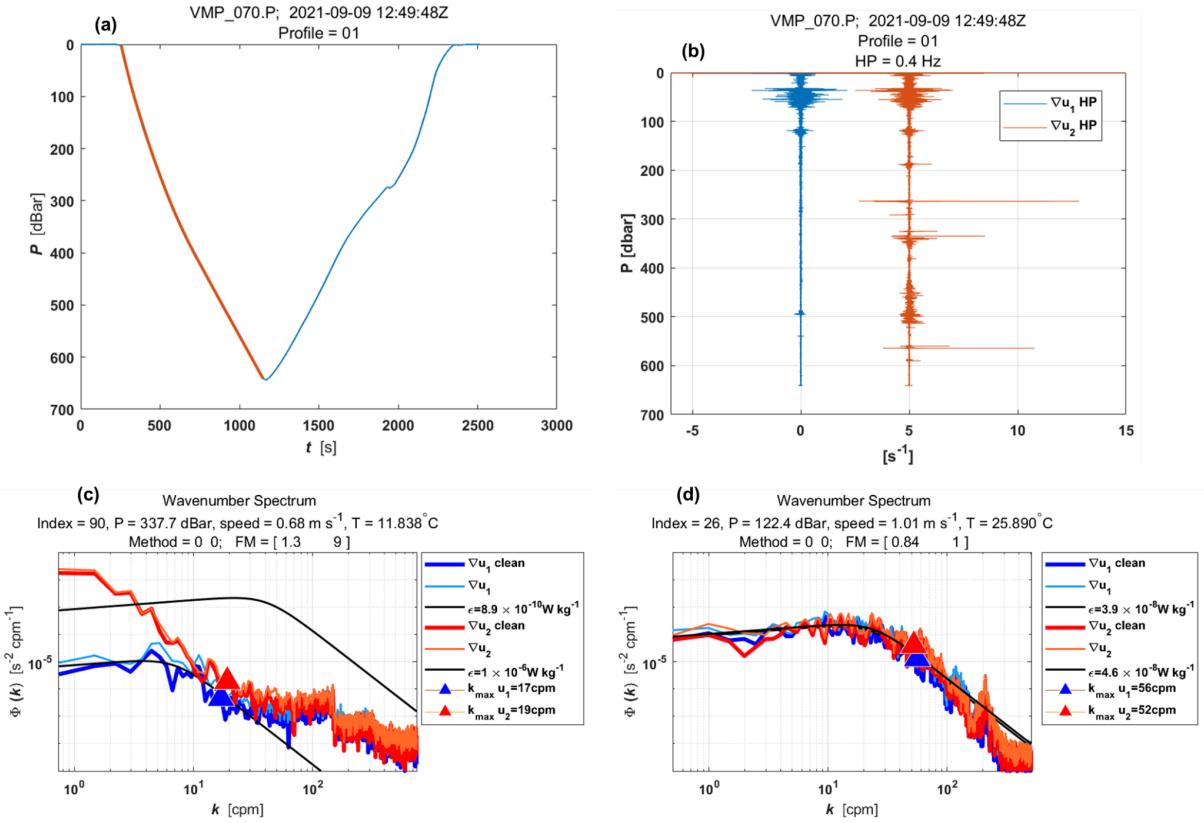

Figure RC1.1: Example of wavenumber spectra from a dissipation structure segment used to determine the dissipation rate at station S14 at a pressure of 337.7 dBar. (a) Pressure record for the entire data file (blue) and the specific segment being analyzed (red). (b) Cleaned and high-pass filtered signals from shear probe 1 (blue) and shear probe 2 (red, offset by 5 s^{-1}). (c) Wavenumber spectra for shear probes 1 and 2. Thick lines (blue for probe 1, red for probe 2) show shear spectra with coherent noise correction, while thin lines (sky blue for probe 1, orange for probe 2) show spectra without correction. Triangles mark the maximum wavenumber used for dissipation rate estimation. Black lines represent Nasmyth reference spectra for estimated dissipation rate of 8.9 x 10^{-10} W kg^{-1} and 1 x 10^{-6} W kg^{-1} for shear probes 1 and 2, respectively. Dissipation rate estimates for shear probes 1 and shear probe 2 at a pressure of 337.7 dBar yielded a figure of merit of 1.3 and 9, respectively. Panel (d) is similar to panel (c) but:- with Nasmyth reference spectra for estimated dissipation rate of 3.9 x 10^{-8} W kg^{-1} and 4.6 x 10^{-8} W kg^{-1} for shear probes 1 and 2. -wth dissipation rate estimates for shear probes 1 and 2 at a pressure of 122.4 dBar yielding a figure of merit of 0.84 and 1, respectively.

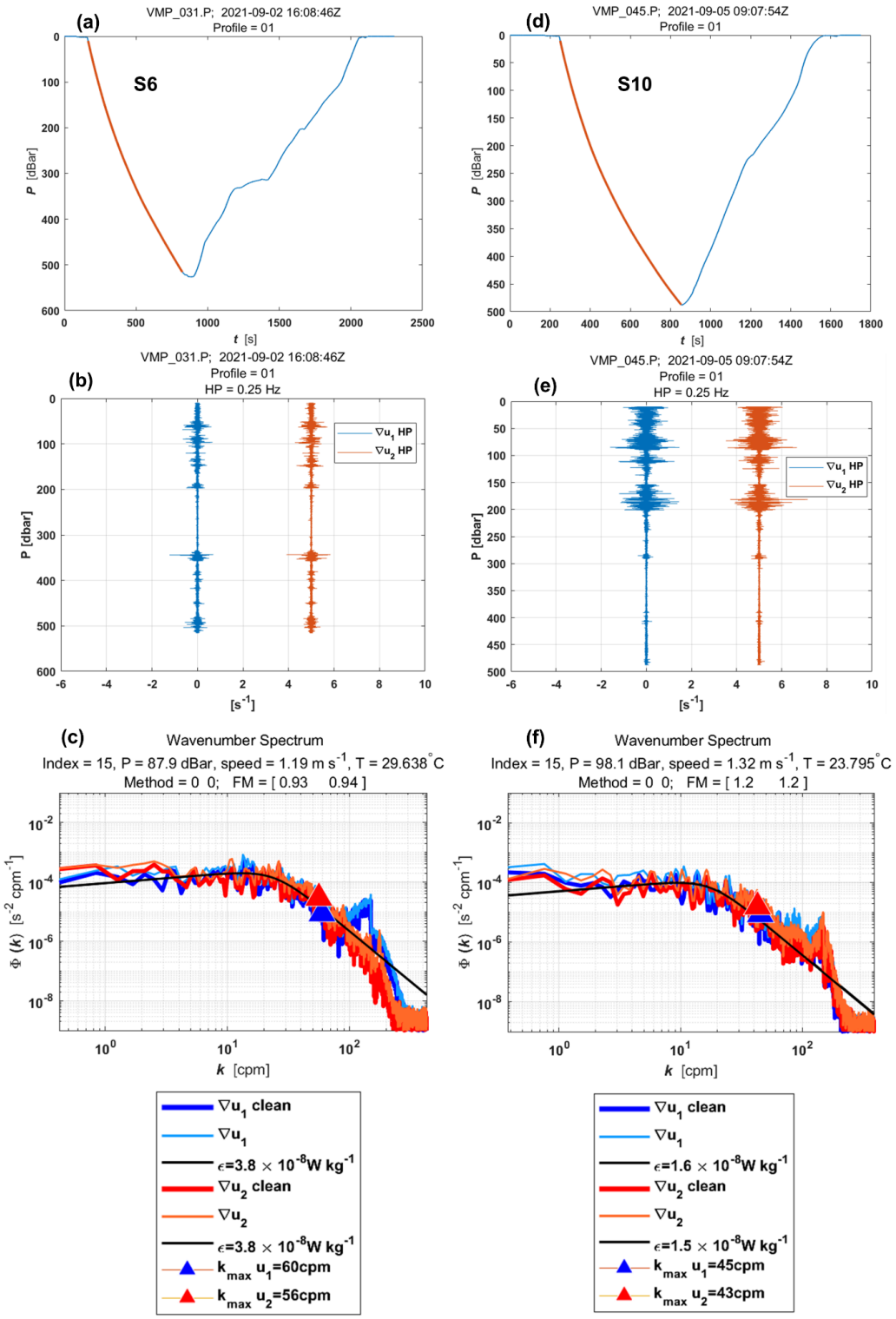

Figure RC1.2: Similar to Fig. RC1.1. but for stations (a)-(b)-(c) S6 and (d)-(e)-(f) S10. For S6 (panels c), Black lines represent Nasmyth reference spectra for estimated dissipation rate of 3.8 x 10-8 W kg-1 for both shear probes, and dissipation rate estimates for shear probes 1 and shear probe 2 at a pressure of 337.7 dBar yielded a figure of merit of 0.93 and 0.94, respectively. For S10 (panel f), Black lines represent Nasmyth reference spectra for estimated dissipation rate of 1.6×10^{-8} W kg^{-1} and 1.5×10^{-8} W kg^{-1} for shear probes 1 and 2, respectively, and dissipation rate estimates for both shear probes at a pressure of 337.7 dBar yielded a figure of merit of 1.2.

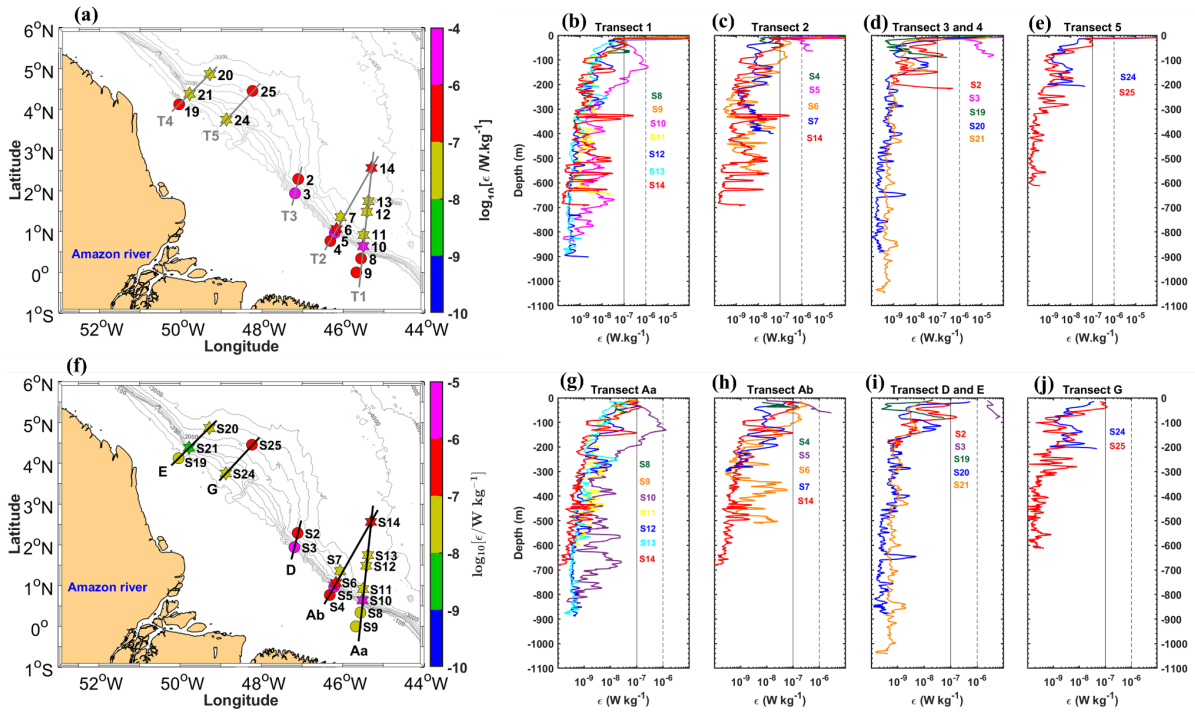

figure RC1.3: (a) Horizontal maximum and (b)-(c)-(d)-(e) vertical dissipation rates (ε, in W kg-1, on a logarithmic scale) before revisions and checks processes for all stations along transects T1 to T2. (f) Horizontal maximum and (g)-(h)-(i)-(j) vertical dissipation rates (ε, in W kg-1, on a logarithmic scale) after revisions and checks processes for all stations along transects Aa, Ab, D, E, and G. Distinct colors are used to represent each station within each transect. Dashed and solid black lines in panels (b) to (e) are included for comparison purposes.

5. Semidiurnal currents are obtained by removing the mean current over a tidal period from the baroclinic velocities. This will include other frequencies. In fact Figure 4 has everything: 6 hrs, 12 hrs, … It would be better to make a least squares fit of sines and cosines to the various tidal periods. With a short time series of 1 day, the frequency resolution is 1 cycle/day. So you could try fitting diurnal and semidiurnal, but recognizing that they are not formally distinct. Also the inertial period here is at least 5 days and so cannot be determined in your dataset. This is a key limitation that should be pointed out. At the equator every frequency just about is in the internal wave band.

How or even whether the currents should be separated in frequency seems to be a major question given the limitations of the data and the desire to examine dissipation.

R: Thanks for your comments and suggestions. Based on your suggestion we completely re-worked our methodology, it has gained in robustness.

Indeed, semidiurnal currents are obtained by removing the mean current over a tidal period from the baroclinic velocities. This could include other frequencies. We have tried to make a least squares fit of sines and cosines to the various tidal periods (diurnal and semidiurnal), as you recommended. This fitting only resolved for the S14 station, which is 42 hours long, compared to the other shorter stations of 17 hours. This may be due to the length of the time series.

Below we present the result at S14. Figure RC1.4 shows the time series of the data collected and Figure RC1.5 and RC1.6 shows the diurnal and semidiurnal fitting at S14.

Indeed, with a short time series of 1 day, the frequency resolution is 1 cycle/day. We recognize that diurnal and semidiurnal fitting are not formally distinct, and that the inertial period here is at least 5 days and so cannot be determined in our dataset. We have pointed out this key limitation, as you recommended, in the manuscript in the lines 187-193 of the revised manuscript.

We know that our time series data are shorter than 17 h hours at all long stations, except for S14 (long of 42 hours). Indeed, the diurnal and semidiurnal periods fitting are not formally distinct and the inertial period (at least 5 days) cannot be determined in our dataset, limiting the currents separation in frequency and our desire to examine dissipation associated.

We have added the Figure RC1.4 and Figure RC1.5 in the Appendix of the revised manuscript (Figs. A4 and A5).

Indeed, even if currents need to be separated in frequency, this seems to be a major issue given the limitations of the data and the desire to examine dissipation. We have also pointed out this limitation in the manuscript in the lines 187-193 of the revised manuscript, as shown below:

“

> Note that continuously collected SADCP for some stations (e.g., S11) are not sufficiently resolved due to gaps filled by interpolating between time points. The similar processing are applied to the CTD-O_2 data collected alternately. SADCP time series data are less than 17 hours at all long stations, except for S14, which spans 42 hours. As a result, the diurnal and semidiurnal period fittings are not formally distinct (except at S14; Figs. A4 and A5, Appendix), and the inertial period (at least 5 days) cannot be resolved in our dataset. This limits our ability to separate currents by frequency and examine the associated dissipation.
>
> The velocity profiles from LADCP are glued into our SADCP time series data below ~ 500 m depth at long stations..

“

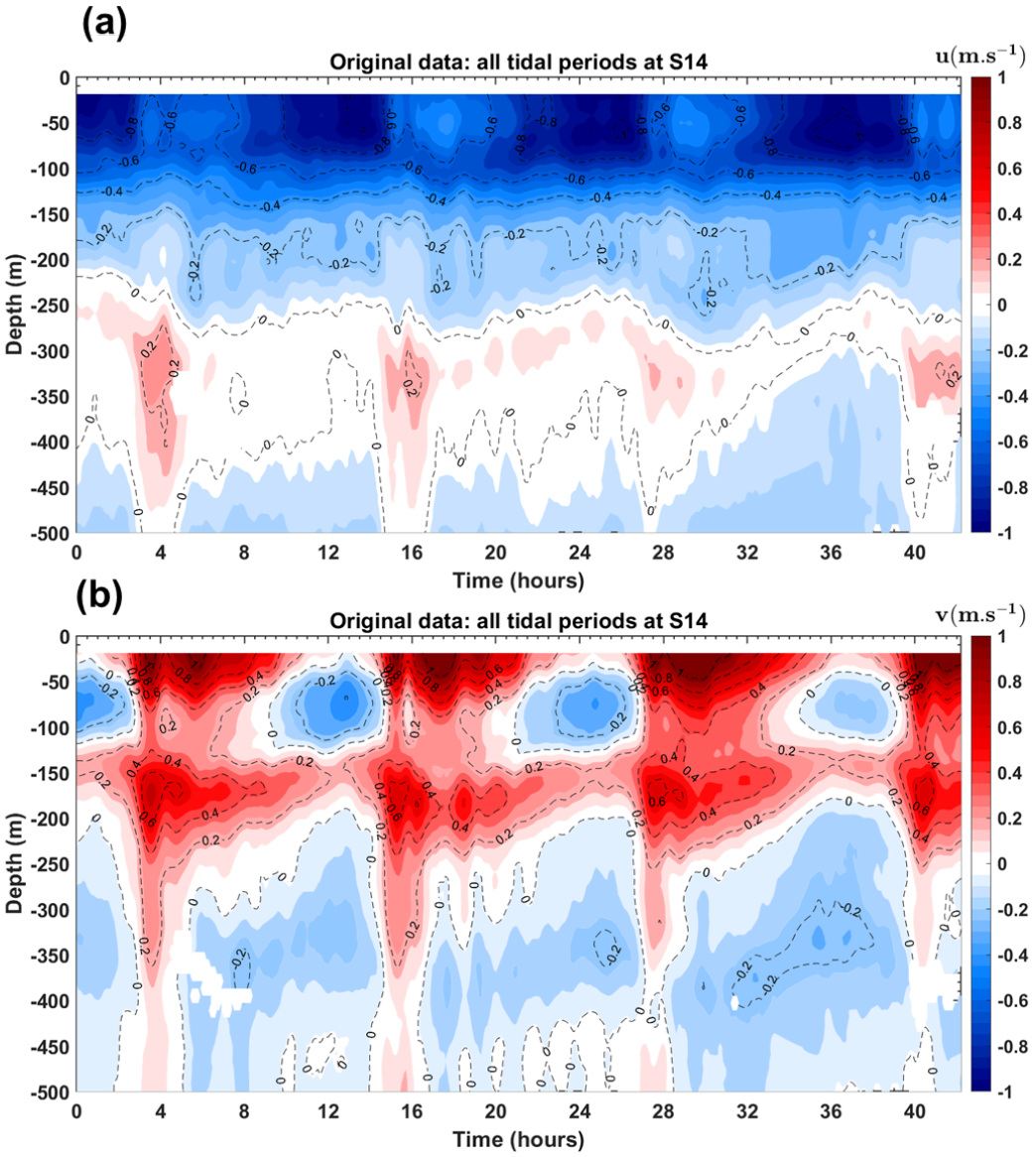

Figure RC1.4: Time series of (a) zonal and (b) meridional current of the original SADCP data at a fixed position for station S14. Time is scaled to start at t=0.

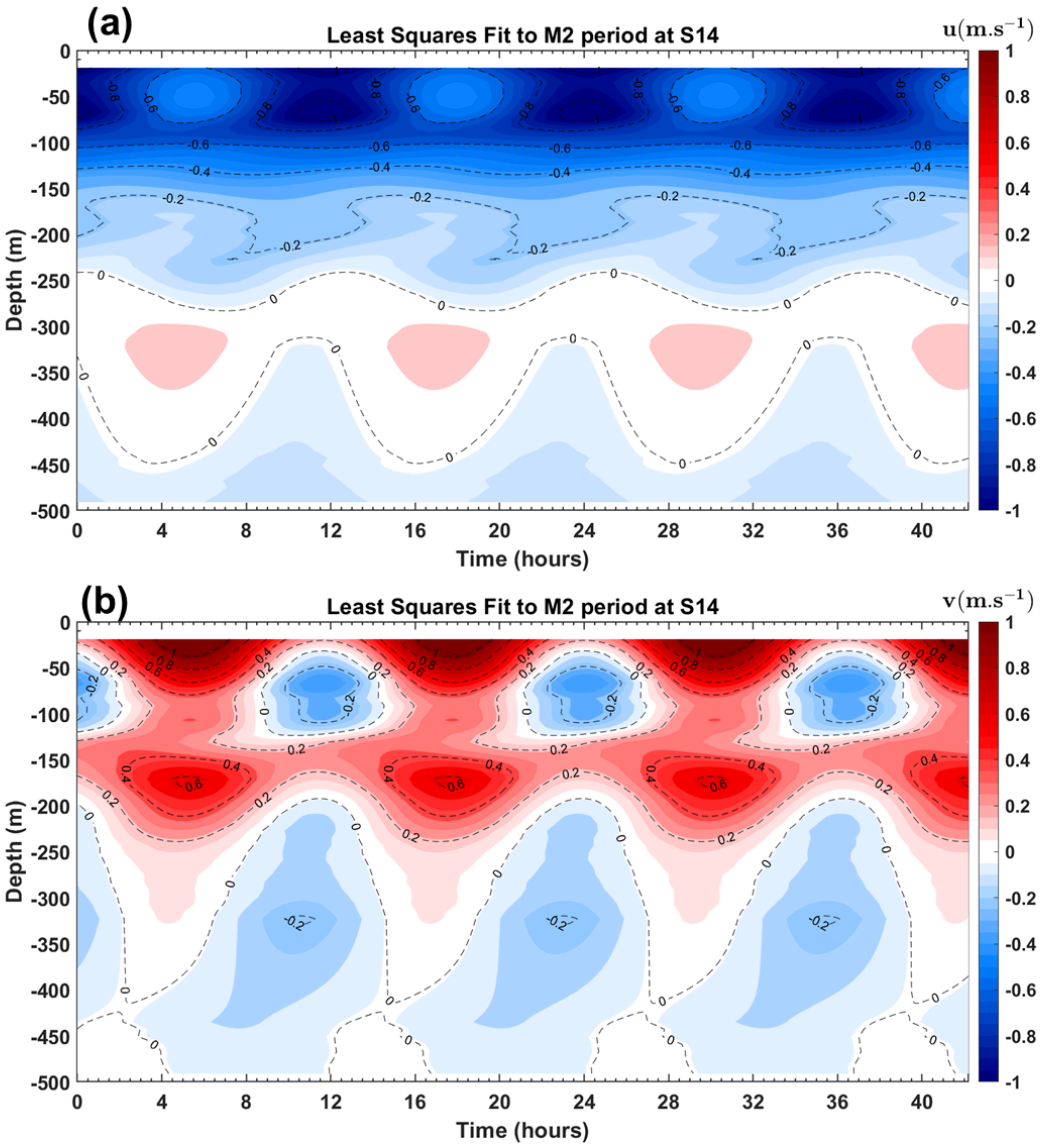

Figure RC1.5: Least squares fit of sines and cosines to M2 period for (a) zonal and (b) meridional current at station S14. Time is scaled to start at t=0.

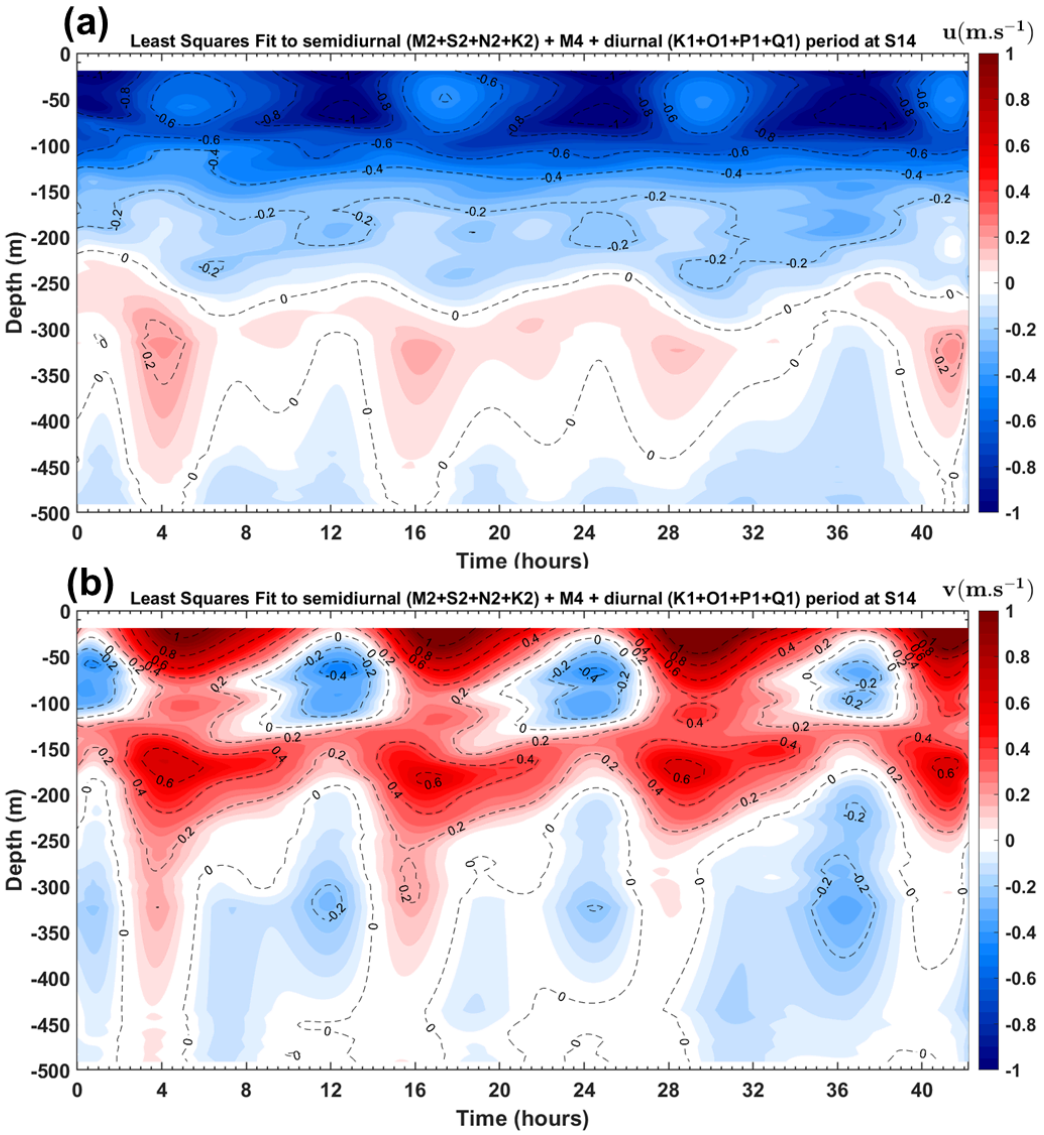

Figure RC1.6: Least squares fit of sines and cosines to semidiurnal (M2+S2+N2+K2) + M4 + diurnal (K1+O1+P1+Q1) periods for (a) zonal and (b) meridional current at station S14. Time is scaled to start at t=0.

The revision of section “methods/Baroclinic currents” can be found below in lines 175-208 of the revised manuscript:

“

Baroclinic currents

To analyze the processes explaining dissipation and mixing, particularly along internal tidal (IT) paths, we estimate shear instabilities associated with the semi-diurnal (M2) ITs and mean circulation, as well as their contributions to mixing.

The M2 tidal component of the tidal current is derived by calculating the baroclinic (semi-diurnal) tidal velocity $[u'', v'']$ (Fig. A3, Appendix), following these equations:

$$[u', v'] = [u, v] - [u_{bt}, v_{bt}], \quad (1)$$

$$[u_{bt},\ v_{bt}] = \frac{1}{H}\int_{-H}^{0}[u,\ v]dz, \quad (2)$$

$$[u'',\ v''] = [u',\ v'] - [\overline{u'},\ \overline{v'}]. \quad (3)$$

Here, $[u,\ v]$ represent total horizontal velocities (Fig. A3, Appendix) obtained from SADCP data. The components $[u',\ v']$ and $[u_{bt},\ v_{bt}]$ represent baroclinic and barotropic components of horizontal velocities, respectively (Fig. A3, Appendix). H is water depth. The baroclinic mean velocities $[\overline{u'},\ \overline{v'}]$ (Fig. A3, Appendix), calculated to estimate mean circulation along IT paths, are decomposed into along-shore $\overline{u'}_l$ and cross-shore $\overline{u'}_c$ velocities. The overbar denotes the average over a M2 tidal period.

Note that continuously collected SADCP for some stations (e.g., S11) are not sufficiently resolved due to gaps filled by interpolating between time points. The similar processing are applied to the CTD-O_2 data collected alternately. SADCP time series data are less than 17 hours at all long stations, except for S14, which spans 42 hours. As a result, the diurnal and semidiurnal period fittings are not formally distinct (except at S14; Figs. A4 and A5, Appendix), and the inertial period (at least 5 days) cannot be resolved in our dataset. This limits our ability to separate currents by frequency and examine the associated dissipation.

The velocity profiles from LADCP are glued into our SADCP time series data below ~ 500 m depth at long stations.

To evaluate shear instabilities associated with ITs and the mean background circulation, we compute the baroclinic tidal vertical shear squared ($S^{2''}$) and mean shear squared ($\overline{S^{2'}}$) (Fig. A3, Appendix), as follows:

$$S^{2''} = (\partial u''/\partial z)^2 + (\partial v''/\partial z)^2, \quad (4)$$

$$\overline{S^{2'}} = (\partial \overline{u'}/\partial z)^2 + (\partial \overline{v'}/\partial z)^2. \quad (5)$$

To evaluate the impact of bottom friction on mixing, we calculate kinetic energy $\varepsilon_f = \frac{1}{2}\rho_s(u_f^2)$ near the bottom boundary layer at shallow stations using friction velocity $u_f = u_b\sqrt{C_d}$, where C_d=2.5 x 10^{-3} is a drag coefficient obtained from the NEMO model. Huang et al. (2019) showed that the bottom boundary layer thickness spatially varies between 15-123 m in the Atlantic Ocean, with a median of ~ 30-40 m in the North Atlantic. We define bottom layer thicknesses in our study area based on measured bathymetry from CTD-O_2 and near-bottom currents from ADCP. Here, u_b is the total velocity averaged over a thickness of 20 m above the seabed for shallow stations and 40 m for deep stations.

The individual contributions of semi-diurnal ITs and mean circulation are then expressed as follows: $E''/(\overline{E'} + E'')$ for tidal contribution and $\overline{E'}/(\overline{E'} + E'')$ for mean circulation contribution. Here, $E = N^2S^2$. N is the buoyancy frequency and S is vertical shear. S can be substituted by $S^{2''}$ and $\overline{S^{2'}}$.

“

6. Shear. Based on the calculations for barotropic u, baroclinic u, and tidal u. I do not see why shear is different for baroclinic and tidal u.

Tidal u = baroclinic u - lowpassed u.

It seems like it should be almost the same as the shear in baroclinic u. I'm confused. It would be helpful to see more of the processing steps and their justifications for these steps.

R: Thanks for your comments.

We have explained with more care the methodology step by step. Please see the previous response to your comment n°5.

Perhaps there is a problem with the short time series or large tidal isopycnal displacements. I suggest plotting some profiles of u and shear for barotropic, baroclinic, and tidal u to make sure these calculations are correct.

R: Thanks for your comments.

Indeed, our time series from SADCP are shorter than 17 hours at all long stations, except for S14 (long of 42 hours). Our calculations, as shown below, seem correct to be used. Please see below the example for S14 over a (M2) tidal cycle, the plots of u and shear for total, barotropic, total baroclinic, and baroclinic tidal, and mean baroclinic in figures RC1.7. We have added this example in the Appendix of the revised manuscript (Fig. A3)

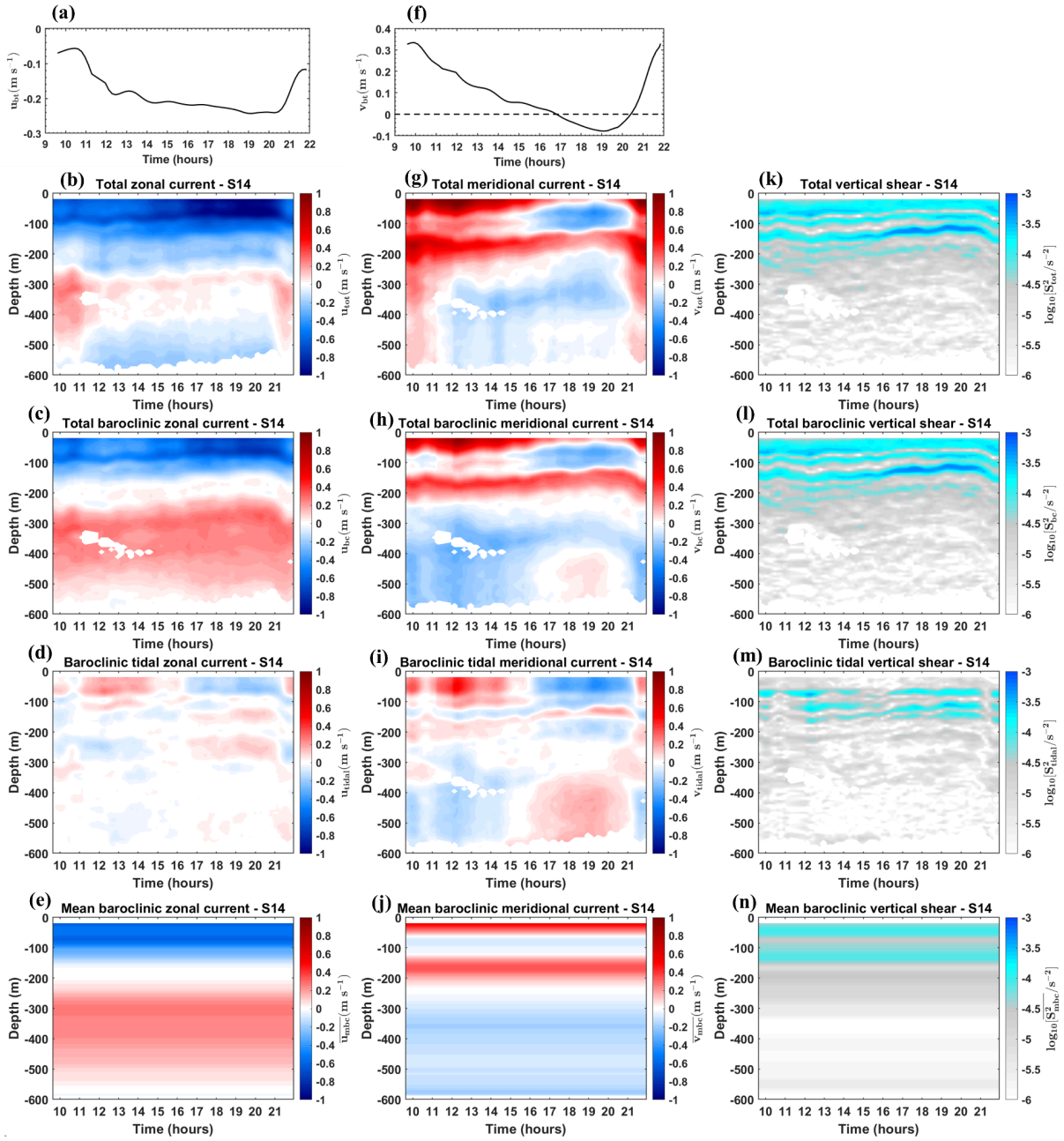

Figure RC1.7: For Station S14. zonal currents for (b) total, (a) barotropic, (c) total baroclinic, (d) semi-diurnal baroclinic tidal, and (e) mean baroclinic. Meridional currents for (g) total, (f) barotropic, (h) total baroclinic, (i) semi-diurnal baroclinic tidal, and (j) mean baroclinic. Vertical shear for (k) total, (l) total baroclinic, (m) semi-diurnal baroclinic tidal, and (n) mean baroclinic.

Also you could try doing these calculations on an isopycnal since it looks like the velocity structure is being heaved up and down by the internal waves. That could lead to artifacts in the calculations on depth surfaces. For example in Figure 4a1, on sigma = 26, current is negative.

R: Thanks for your comments.

We performed the calculations on the 26 kg/m³ isopycnal as suggested and presented the results in the figure RC1.8 below. But we think that these results are not so robust since CTD data were collected alternately and needs to be interpolated between time points (e.g., between 17:00 and 20:00 at station S10). Consequently, the density data are not sufficiently resolved to allow the currents to be projected on over the tidal period. Doing this would introduce potential artifacts in the calculations on an isopycnal. So we decided to stick with our first calculation, pointing out in lines 187-193 of the revised manuscript:

"

Note that continuously collected SADCP for some stations (e.g., S11) are not sufficiently resolved due to gaps filled by interpolating between time points. The similar processing are applied to the CTD-O_2 data collected alternately. SADCP time series data are less than 17 hours at all long stations, except for S14, which spans 42 hours. As a result, the diurnal and semidiurnal period fittings are not formally distinct (except at S14; Figs. A4 and A5, Appendix), and the inertial period (at least 5 days) cannot be resolved in our dataset. This limits our ability to separate currents by frequency and examine the associated dissipation.

The velocity profiles from LADCP are glued into our SADCP time series data below ~ 500 m depth at long stations.

"

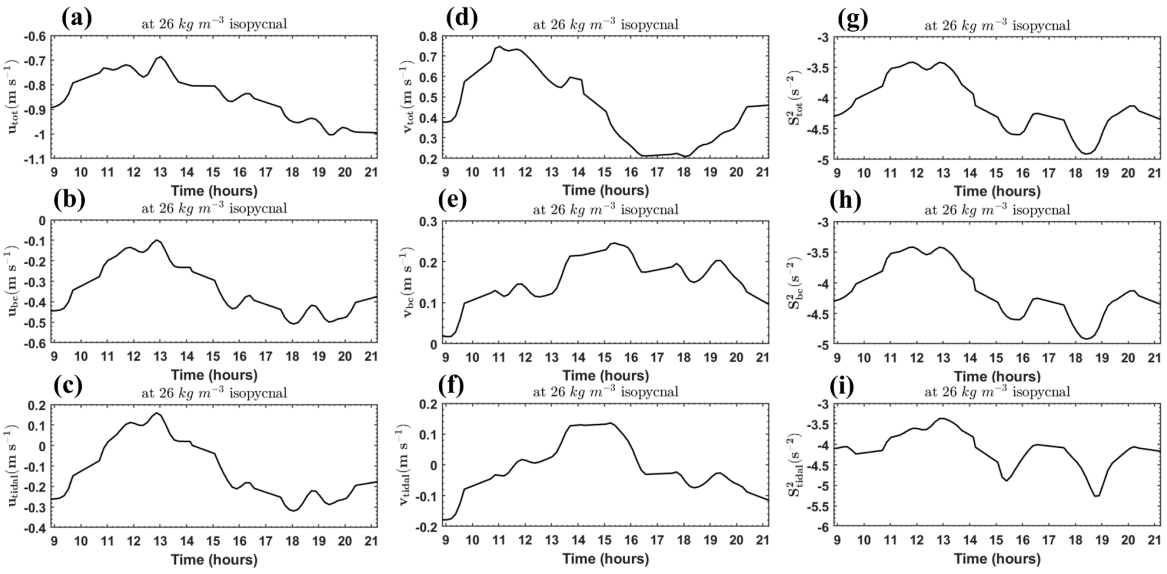

Figure RC1.8: For Station S10, calculations on the 26 kg/m³ isopycnal. zonal currents for (a) total, (b) total baroclinic, and (c) semi-diurnal baroclinic tidal. Meridional currents for (d) total, (e) total baroclinic, and (f) semi-diurnal baroclinic tidal. Vertical shear for (g) total, (h) total baroclinic, and (i) semi-diurnal baroclinic tidal.

At 120 m, current switches sign multiple times. As far as I can tell, there are no plots of shear.

Also I do not understand why only one component of the current is shown. Using both components is needed to understand propagation of internal tides either vertically or horizontally (alongshelf vs cross-shelf).

Section 3.2.2 uses a lot of words that could be instead expressed concisely in a map with current vectors. Different colours could indicate different depths.

R: Thanks for your comments.

We have added in the revised manuscript plots of the shear of shear for tidal U and mean U at selected stations (e.g., S10, S11, and S14; in Fig. 6, and Figs. A15 to A18, Appendix) and also reported here in figure RC1.9 below

Indeed, at 120 m, the current switches direction multiple times. We have added in the revised manuscript a 2D map of mean current (vectors) and also reported here in figure RC1.12 below.

Indeed, both zonal (u) and meridional (v) components are essential for understanding the propagation of internal tides, whether vertically or horizontally (along-shelf vs. cross-shelf). As we more focused on zonal (u) and meridional (v) components of ITs, we have added these components in the revised manuscript at selected stations (e.g., S10, S11, and S14; in Fig. 5, and Figs. A9 to A15, Appendix) and also reported here in figure RC1.10 and RC1.11 below.

Additionally, we have visualized the mean baroclinic current using a map with current vectors (as reported here in RC1.12).

In response to all reviewer comments, we have revised several sections of the manuscript, including “Methods,” “Results,” and “Discussion and Conclusion,” spanning lines 121–567 of in the revised manuscript.

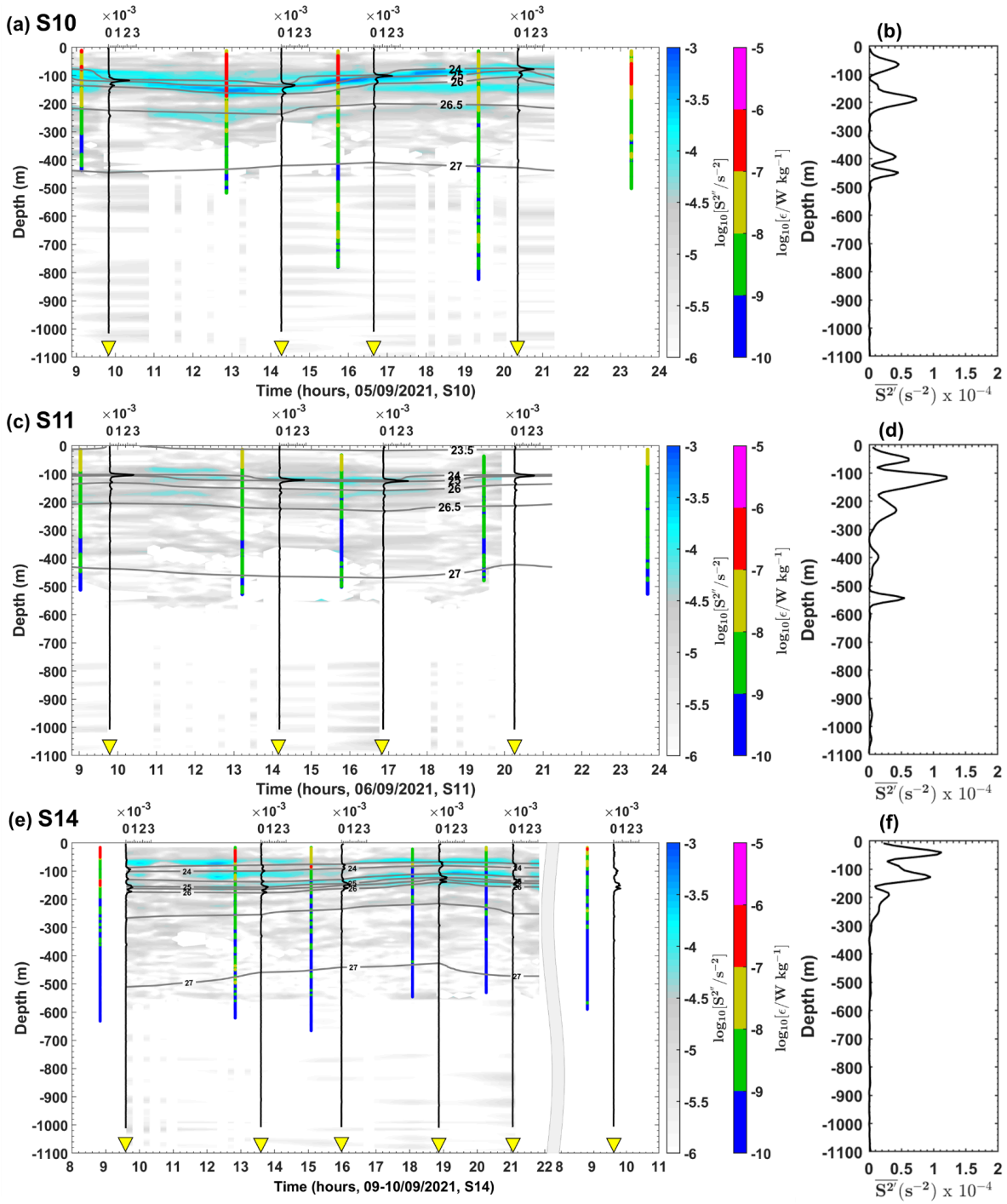

Figure RC1.9: *Semi-diurnal baroclinic vertical shear squared ($S^{2'}$, in m s^{-1}, on a logarithmic scale) for stations (a) S10, (c) S11, and (e) S14. Panels (a), (c), and (e) also display the buoyancy frequency squared (N^2, in s^{-2}) represented by vertical black lines, potential density represented by grey contours, and dissipation rate profiles (ε, in W kg^{-1}, on a logarithmic scale) represented by vertical colored bars. Mean baroclinic vertical shear squared ($\overline{S^{2'}}$, in m s^{-1}) for stations (b) S10, (d) S11, and (f) S14.*

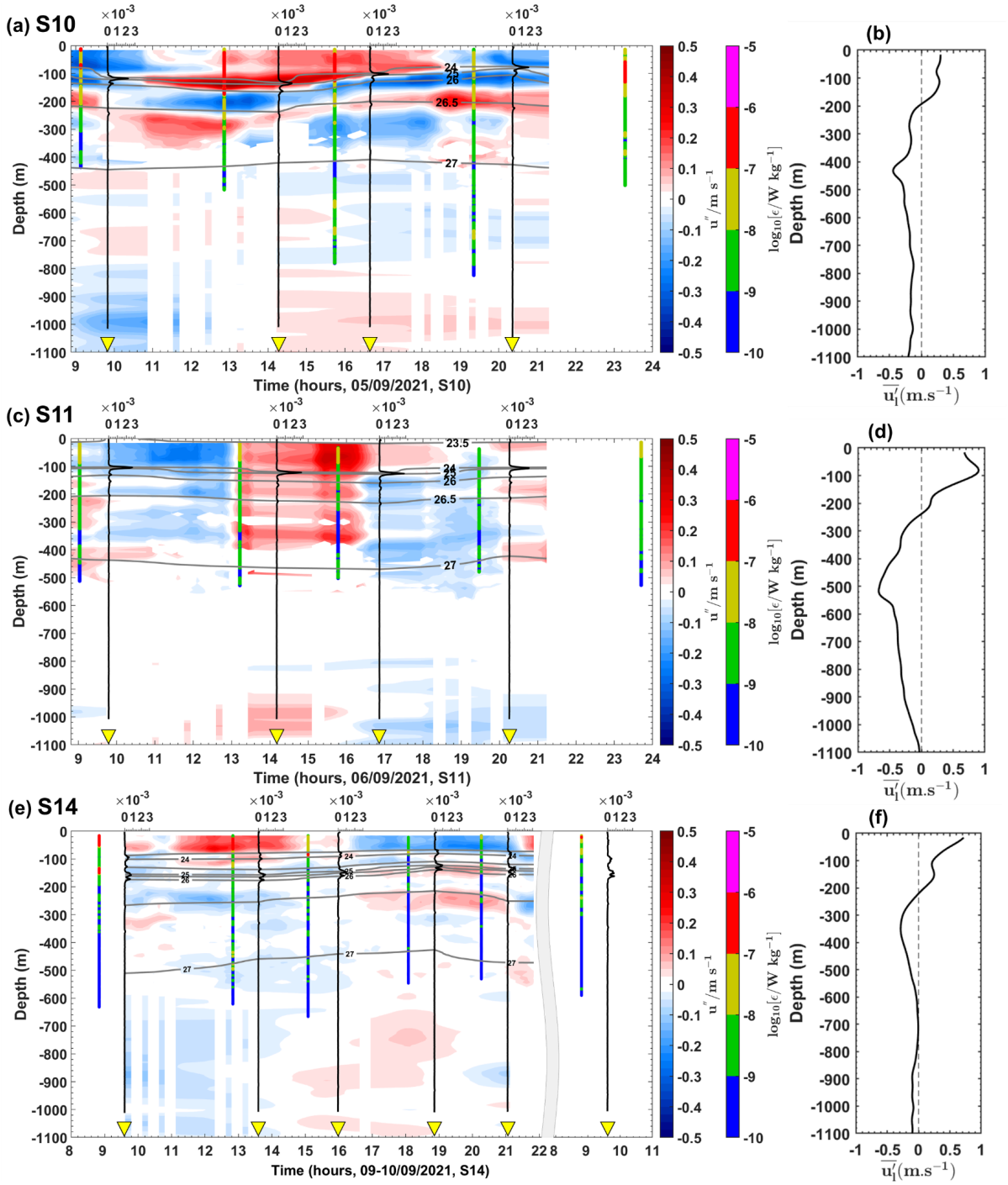

Figure RC1.10: *Semi-diurnal baroclinic zonal currents (u", in m s^{-1}) from the ADCP for stations (a) S10, (c) S11, and (e) S14. Panels (a), (c), and (e) also display the buoyancy frequency squared (N^2, in s^{-2}) represented by vertical black lines, potential density represented by grey contours, and dissipation rate profiles (ε, in W kg^{-1}, on a logarithmic scale) represented by vertical colored bars. Along-shore mean baroclinic currents ($\overline{u'}_l$, in m s^{-1}) from the ADCP for stations (b) S10, (d) S11, and (f) S14.*

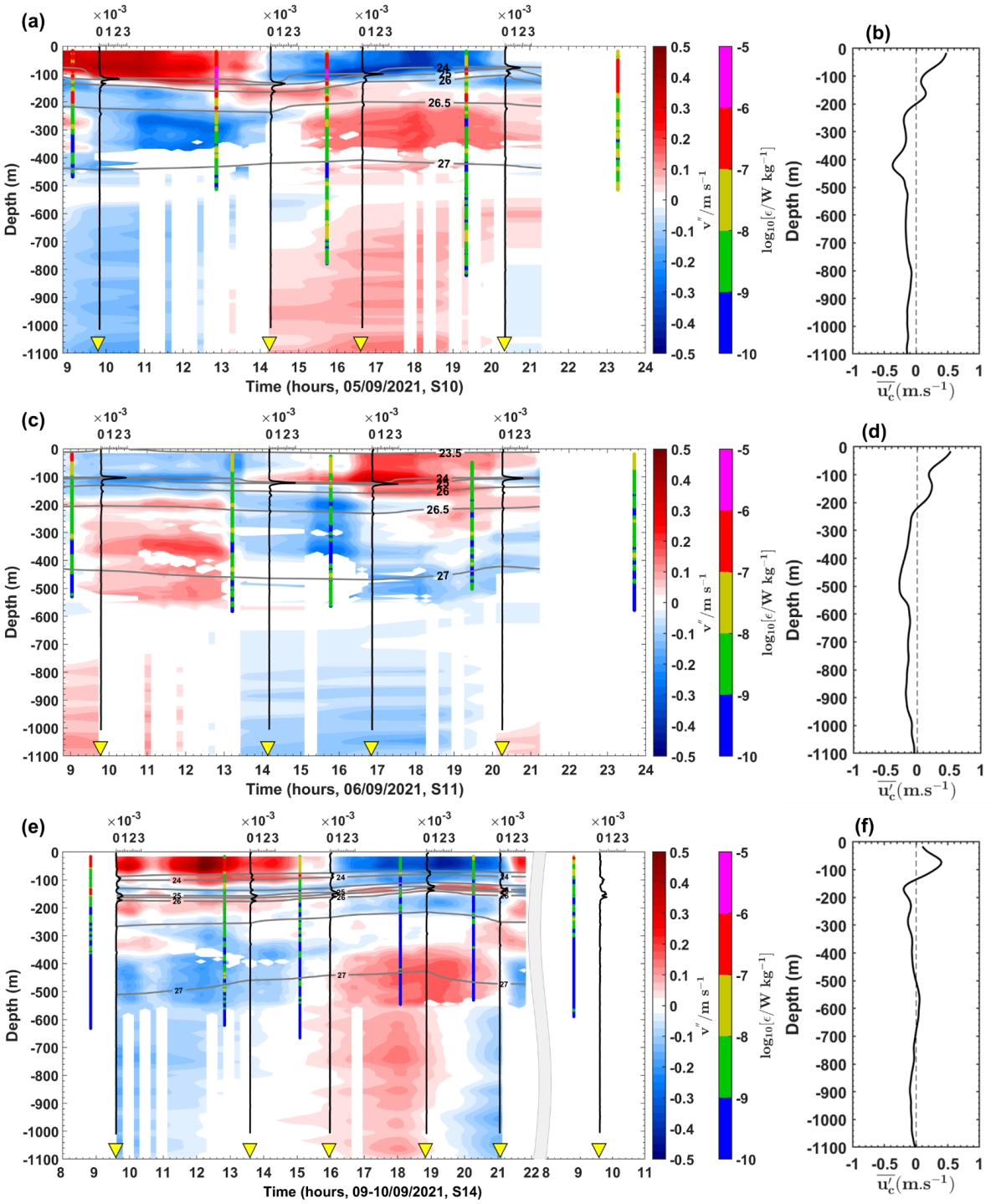

figure RC1.11: *Semi-diurnal baroclinic meridional currents (u", in m s^{-1}) from the ADCP for stations (a) S10, (c) S11, and (e) S14. Panels (a), (c), and (e) also display the buoyancy frequency squared (N^2, in s^{-2}) represented by vertical black lines, potential density represented by grey contours, and dissipation rate profiles (ε, in W kg^{-1}, on a logarithmic scale) represented by vertical colored bars. Cross-shore mean baroclinic currents ($\overline{u'}_l$, in m s^{-1}) from the ADCP for stations (b) S10, (d) S11, and (f) S14.*

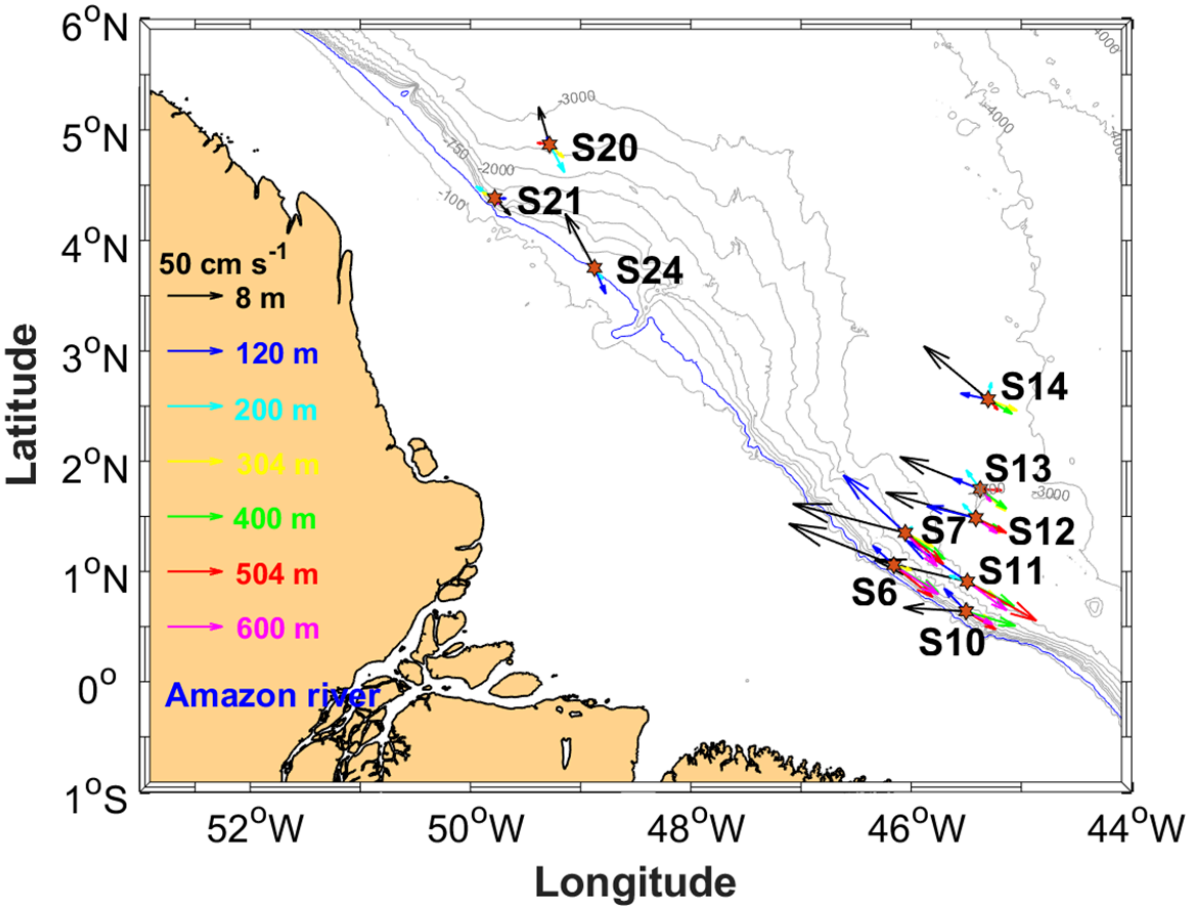

Figure RC1.12: Map of mean baroclinic currents (vectors) at stations. Colored arrows are used to distinguish the currents at different depths: Black, blue, cyan, yellow, green, red and magenta arrows at depth equal to 8 m, 120 m, 200 m, 304 m, 400 m, 504 m and 600 m, respectively. The blue line indicates the 200 m isobath.

7. Dissipation is estimated using parameterizations based on shear in the tidal current. Actual dissipation depends on the total shear or strain.

R: Thanks for your remarks.

Indeed, dissipation was estimated using parameterizations based on shear in the tidal current. MacKinnon-Gregg parameterization was applied as a proxy to evaluate the contributions of tidal and low-frequency shear, primarily for comparison purposes. However, no scientific results were derived from it.

Ultimately, thanks to all the reviewers comments, we decided to remove the section using this parameterization. Eventually, we will work on a separate paper to test the robustness of this parameterization against these observations.

In the present paper, we focused on vertical shear to separate the contributions of tidal and mean shear. Revisions can be found in the "Methods" section in the revised manuscript.

8. Some more explanation of the applicability of MacKinnon-Gregg parameterization vs those based on Gregg (1989) is needed. The former is related to the limited bandwidth of internal

waves (in shallow water for example), while the latter is for a typical open ocean environment away from generation sites. How does this apply to your study sites?

R: Thanks for your comments.

Please see the previous response to your comment n°7.

9. Naming of the sites and transects. Maybe these are what are used on the cruise but they should be rearranged in a logical order to *help the reader*. It is completely confusing as it is. Consider another system, such as A B C D … for generation sites. If there's a transect near site A, it's transect A.

If there are 3 stations on transect A, they are sites A1 A2 A3 and counting higher offshore. Or labelled by isobath, A500, A1000, A2000… There may not be a generation site for each transect.

For example lines 265-267 read: "The highest baroclinic tidal current velocities were observed (between 25-48 cm.s-1) at sites Aa and Ab along T1-T2. Whereas lower tidal velocities (< 25 cm.s-1) are found in site F along T4 (e.g., at S20 and S21) compared to OUT-ITs stations (e.g., at S24)." So I have to use the map. This could read instead as: "The highest baroclinic tidal current velocities were observed (between 25-48 cm.s-1) at sites D and E along transects D and E. Whereas lower tidal velocities (< 25 cm.s-1) are found in site A along transect A (e.g., at A2 and A3) compared to OUT-ITs stations (e.g., at site B1)."

R: Thanks for your comments and suggestions.

We acknowledge that the nomenclature might be somewhat confusing, and your suggestions would indeed simplify understanding. However, we have chosen to retain the naming convention used in previous studies of this region. Specifically, the names A to F for the generation sites were already defined in earlier works (e.g., Magalhães et al., 2016; Tchilibou et al., 2022; Assene et al., 2024; de Macedo et al., 2023).

To maintain consistency with these studies, we have decided to adhere to the established naming convention. As a compromise between simplifying the nomenclature and preserving coherence with previous works, we have designated the transects with the same letters as their corresponding generation sites: Aa, Ab, D, E, G, as shown in figure 1 of the revised manuscript and reported here in figure RC1.13.

Revisions reflecting this choice can be found in the subsection "Baroclinic tidal current" (lines 301–306) of the revised manuscript.

As an example, the previous phrase "is now transform in :

"

> The baroclinic tidal velocities reveal a superposition of 3-5 tidal modes at IN-ITs stations (Figs. 5a, 5c, and 5e, and Figs. A9 to A15, Appendix). A greater number of modes is observed near the shelf-break (e.g., 4 modes at S6 and 5 modes at S10), while fewer modes are detected far from (e.g., 3 modes at S7, S12 and S14). Higher tidal velocities ranging from 25-50 cm s^{-1} are found between 80-350 m along transects Aa and Ab (e.g., at S6,

and S10). In contrast, lower tidal velocities, typically below 25 cm s^{-1}, are more pronounced along transect E (e.g., at S20, and S21) to OUT-ITs stations along transect G (e.g., at S24).

“

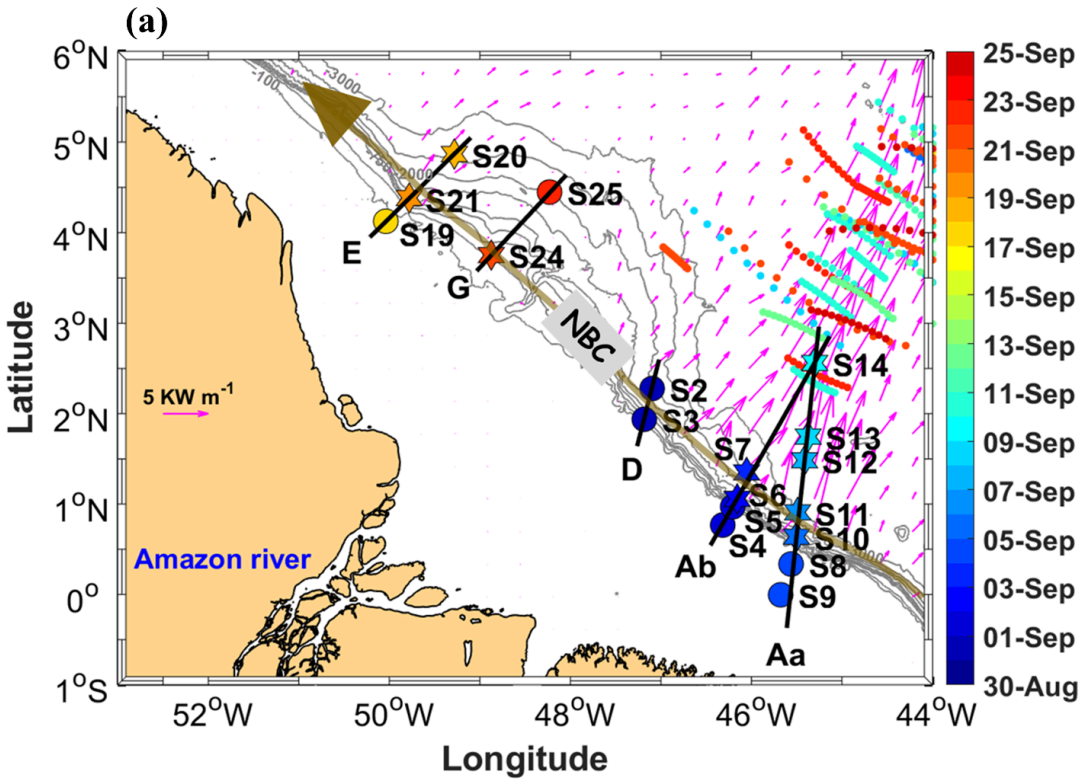

Figure RC1.13:*a) Map of a part of the AMAZOMIX 2021 cruise off the Amazon shelf, showing bathymetric contours (100 m, 750 m, 2000 m, and 3000 m isobaths) in gray. Colored circles and stars indicate short and long CTD-O2/L-S-ADCP stations, respectively, with the corresponding sampling dates represented by the color bar. Solid black lines depict SADCP transects (for Aa, Ab, D, G, and E). Magenta arrows show the 25-hour mean depth-integrated baroclinic IT energy flux (September 2015, from the NEMO model) originating from IT generation sites (Aa, Ab, D, and E) along the shelf break. The solid brown line represents the NBC pathways illustrating background circulation. Shattered colored lines highlight ISW signatures.*

10. Mixing is invoked as the explanation for increased nutrients. How about coastal upwelling? Where is the euphotic zone?

Thank you for this question, which gives us the opportunity to emphasize in the discussion that mixing is not the only significant process influencing the nutrient structure in the region.

Indeed, the nutrient inputs are controlled by several physical processes such as : Riverine Input, Coastal Upwelling, Internal Tides (ITs), Stratification Changes, and Eddies and Currents Off the Amazon shelf (Williams and Follows, 2003; Santos et al., 2008).

There is a very high variability of the euphotic layer in the region. It is very sensitive and heterogeneous from shelf to open ocean. The average estimated by in-situ observations is 13 m (Santos et al., 2008).

In our study, we tried to quantify the impact of internal tide on nutrient structuration. IT is indeed probably of a secondary order of importance in instantaneous but by its repetitiveness (12h, 14 Days), the cumulative effect of the tide over a year could impact the nutrient content. In addition, in a context of climate change this effect may be increased. (Yang et al., 2024)

In our study, we focused on quantifying what was measurable: specifically, vertical mixing, out of which approximately 50% was attributed to tidal processes. And, we also suggested that tidal mixing could contribute to nutrient inputs through vertical diffusivity since it has a strong contribution at the base of the mixed layer.

In the discussion, we contextualized these findings by emphasizing that mixing is not the only process influencing nutrient dynamics, and that upwelling also plays a significant role in nutrient supply.

Ultimately, we decided to remove and reserve all sections on “Nutrients fluxes” for a separate paper in progress.

11. Were adjustments to the shear parameterization based on the Gregg (2003), where it was shown that internal wave interactions may lead to little mixing at the equator?

R: Thanks for your comments and suggestions.

Please see the previous response to your comment n°7.

Minor comments

1. Line 107- While the bin size of the LADCP may be 8 m, its resolution will be about 50 m. Examine where the vertical wavenumber spectra fall off

R: Thanks for your comments.

We have examined the vertical wavenumber spectra. We fitted a slope to the spectrum in the steep region to estimate the roll-off wavenumber. For example, the spectrum falls off as $k^{-2.31}$ and $k^{-2.11}$ for the (a) zonal and (b) meridional at S14, as reported below in figure RC1.14.

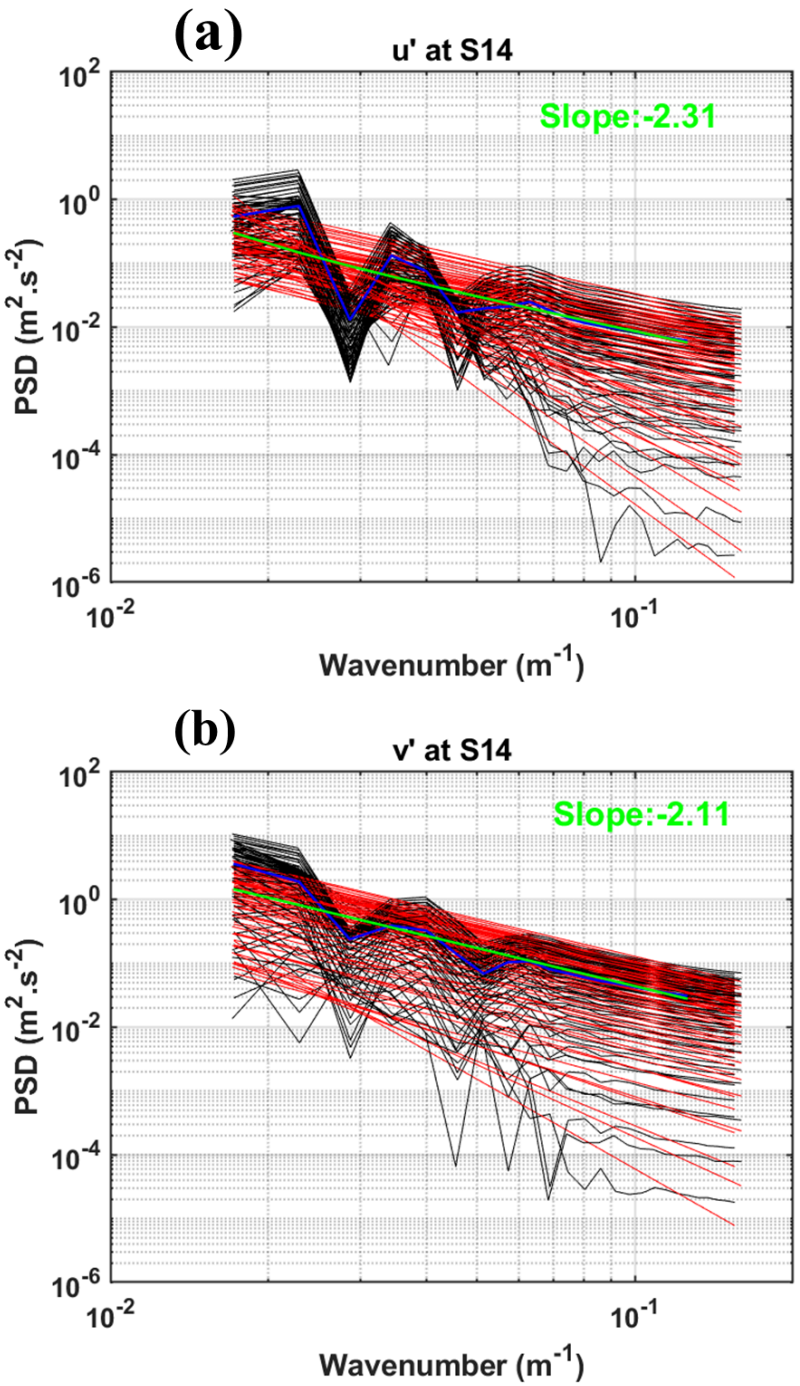

Figure RC1.14: Panels (a) and (b) show the vertical wavenumber spectra for perturbations in the total zonal and meridional currents, respectively, derived from LADCP data at station S14. Black curves represent the vertical wavenumber spectra for individual current profiles over time, while the blue curves indicate the spectra averaged across all time profiles. The red and green lines illustrate the linear fits to the spectra slopes for individual profiles and the mean spectrum, respectively. The fitted slopes of the mean perturbation spectra are indicated in green: (a) -2.31 for the zonal current and (b) -2.11 for the meridional current.

2. I would recommend a native english speaker help with some of the grammar, if possible. It's ok as is but could be much better. It will be less distracting for the reader. Then the reader will pay more attention to the science.

R: Thanks for your suggestions. We have revised all sections of the manuscript.

3. In sections 2.1 and 2.2, there is some jumping around from instrument to instrument. Please collect into sections for each instrument.

R: Thanks for your comments and suggestions.

We have revised sections 2.1 and 2.2 in lines 92-230 of the revised manuscript and reported here:

"

2 Data and Methods

2.1 Data collection

The AMAZOMIX cruise (Bertrand et al., 2021) was performed over the shelf/slope areas off the AROC during August-October 2021 aboard the IRD vessel RV *ANTEA*. At each designated site, 12-hour stations were set up, with repeated casts (4-5 casts per site) of Conductivity-Temperature-Depth-Oxygen (CTD-O_2)/Lowered Acoustic Doppler Current Profiler (LADCP) and Velocity Microstructure Profiler (VMP) to measure the TKE dissipation rates over a complete tidal (M2) cycle, allowing the separation of the tidal component from the total current. A high-resolution (1/36°) NEMO (Nucleus for European Modeling of the Ocean) model (Madec et al., 2019) was used to determine station locations based on realistic IT generation and propagation maps (Tchilibou et al., 2022; Assene et al., 2024) and to estimate the mean background stratification.

Stations (Fig. 1a and 1c) were located inside the ITs fields, named "IN-ITs" (sites Aa, Ab and D: S2 to S14; site E: S19 to S21), and outside the ITs fields (S24 and S25), named "OUT-ITs", on the shelf-break generation (sites Aa, Ab, D and F) and propagation along 5 transects (Aa, Ab, D, G, and E; Fig. 1).

CTD-O_2 measurements were obtained using a Seabird 911 Plus with dual sensors mounted in the rosette. The 24 Hz CTD-O_2 sensors were calibrated before and after the cruise. The standard deviation of temperature (salinity; oxygen) was 0.003 °C (0.003 PSU; 0.05 ml l^{-1}) according to adjusted data. CTD-O_2 data were averaged over 1-m bins to filter out spikes and missing points, and aligned in time to correct the lag effects.

Two 300 kHz RDI LADCPs were mounted on the rosette to provide vertical current profiles with 8 m resolution, supplemented by 75 kHz shipboard ADCP (SADCP) profiles recorded continuously during the cruise. Vertical resolution of SADCP was adjusted according to bottom depth, e.g., 8 m for depths >150 m (at S6, S7, S10-S14, S20, S21, and S24) and 4 m for other depths. . Data processing and quality control followed GO-SHIP Repeat Hydrography Manual protocols. In total, 71 CTD-O_2/LADCP profiles were collected during the AMAZOMIX cruise.

To characterize mixing, the TKE microstructure profiles were obtained from high-frequency (~ 2 mm resolution) measurements of temperature and velocity shear using a VMP-250 profiler (Rockland Scientific International, Inc.) capable of reaching depths up to 1000 m. The VMP-250 features two high-resolution thermistors (FP07) and two high-resolution velocity shear probes (probe 1 and 2; with 5% signal accuracy), with

a sampling rate of 1024 Hz. The profiler was deployed and retrieved via an electric winch and rope tether, with alternating deployments between the CTD-O_2/LADCP profiles at 33 stations,yielding a total of 202 profiles. For this study, data from 18 stations (S2-S14, S19-S21, S24, and S25) comprising SADCP data, 109 VMP profiles and 54 CTD-O2/LADCP profiles will be analyzed.

2.2 Methods

TKE dissipation rates

The VMP data are processed using ODAS Matlab library (developed by Rockland Scientific International, Inc) to infer the TKE dissipation rate (ε). The processing methods for the VMP data are briefly described here and adhere to the recommendations of ATOMIX (Analyzing ocean turbulence observations to quantify mixing), as reported by Lueck et al. (2024), and have been validated against the benchmark estimates (presented in Fer et al., 2024).

First, the VMP data are converted into physical shear units, and the time series are prepared. Continuous sections of the time series are selected for dissipation estimation. Before spectral estimation, the aberrant shear signals caused by vessel wake contamination are removed. Collisions of the shear probe with plankton and other particles are removed using the de-spiking routine. The records from each section are then high-pass filtered (e.g., at station S6 and S10; Fig. 2a, and Fig. A1, Appendix).

Shear spectra are estimated using record lengths (L) and Fast Fourier Transform segments of 2 s, which are cosine windowed and overlapped by 50% (e.g., at station S6 and S10; Fig. 2b, and Fig. A1, Appendix). Additionally, vibration-coherent noise is removed. Different L and overlap (O) settings were selected and tested based on the environment (e.g., deep vs. shallow water), following Fer et al. (2024). For shallow stations, L (O) was shortened to 5 s (2.5 s), in contrast to the 8 s (4 s) used for deeper stations, due to evidence of overturns observed in AMAZOMIX acoustic measurements at deeper stations (Koch-Larrouy et al., 2024; in preparation). This adjustment helped to optimize the spatial resolution of dissipation estimates in shallow water stations.

Finally, ε is determined using the spectral integration method and by comparison with the Nasmyth empirical spectrum (Nasmyth, 1970). Quality assurance tests are carried out in accordance with ATOMIX's recommendations (Lueck et al., 2024). A figure of merit < 1.4 is used to exclude bad data (e.g., at station S6 and S10; Fig. 2b, and Fig. A1, Appendix), and the fraction of data affected by de-spiking is < 0.05.

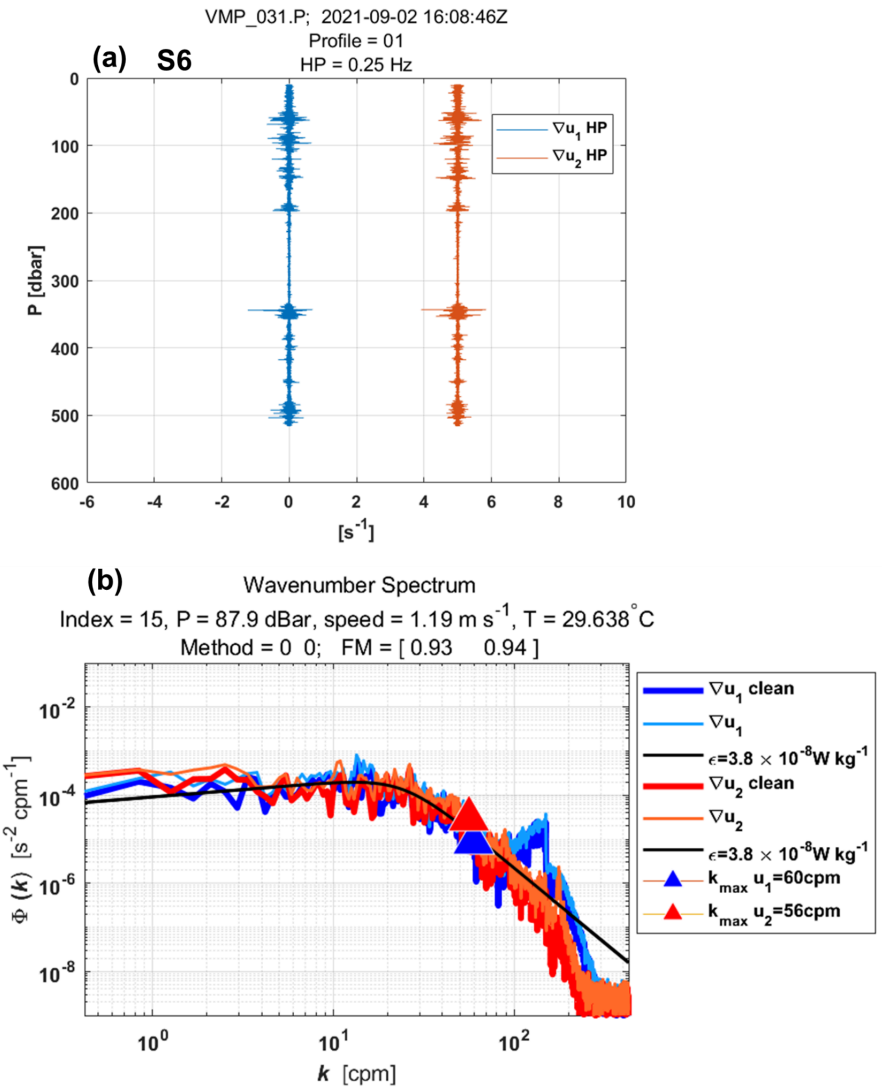

Figure 2: Example of wavenumber spectra from a dissipation structure segment used to determine the dissipation rate at station S6 at a pressure of 87.9 dBar. (a) Cleaned and high-pass filtered signals from shear probe 1 (blue) and shear probe 2 (red, offset by 5 s^{-1}). (b) Wavenumber spectra for shear probes 1 and 2. Thick lines (blue for probe 1, red for probe 2) show shear spectra with coherent noise correction, while thin lines (sky blue for probe 1, orange for probe 2) show spectra without correction. Triangles mark the maximum wavenumber used for dissipation rate estimation. Black lines represent Nasmyth reference spectra for estimated dissipation rate of 3.8 x 10^{-8} W kg^{-1} for both shear probes. Dissipation rate estimates for shear probe 1 and shear probe 2 at a pressure of 87.9 dBar yielded a figure of merit of 0.93 and 0.94, respectively.

The vertical eddy diffusivity coefficient

The efficiency of turbulence in redistributing energy is assessed through the calculation of the vertical eddy diffusivity coefficient (K_z). This coefficient is particularly significant in regions such as pycnoclines, where stratification suppresses mixing, making turbulence-driven mixing a key mechanism for vertical energy transport (Thorpe, 2007).

K_z is calculated from ε following the formulation of Osborn (1980), given by $K_z = \varepsilon\ \Gamma\ N^{-2}$. Here, N^2 is the buoyancy frequency squared, which is calculated using the sorted potential density profiles (σ_θ) obtained from CTD-O_2 data. It is given by $N^2 = -(g/\rho_0)(d\sigma_\theta/dz)$, where ρ_0 is a reference density (1025 kg m^{-3}) and g is the gravitational acceleration. Γ is the mixing efficiency, defined as the ratio between the buoyancy flux and the energy dissipation, and is typically set to 0.2, which corresponds to the critical Richardson number Ri = 0.17 (Osborn, 1980). ε is linearly interpolated into the depths of N^2.

Turbulence within the pycnocline can reduce stratification and increase vertical eddy diffusivity below the mixing layer (Thorpe, 2007). Subsurface mixing, driven by the breaking of ITs and shear instabilities, plays a particularly important role below the mixed layer, especially in equatorial waters (Gregg et al., 2003).

There are several criteria for defining the Mixed Layer Depth (MLD). In this study, we use the commonly accepted density threshold criterion of 0.03 kg m^{-3}, as defined by de Boyer Montégut et al. (2004) and Sutherland et al. (2014), to estimate the MLD for each CTD-O_2 profile. Notably, comparisons with density thresholds of 0.01 and 0.02 kg m^{-3} revealed no major differences in MLD across the AMAZOMIX stations and transects (Fig. A2, Appendix).

The miXing Layer Depth (XLD) is defined as the depth at which ε decreases to a background level (Sutherland et al., 2014). Previous studies have applied various thresholds for background dissipation levels, such as such as 10^{-8} and 10^{-9} W kg^{-1} in higher latitudes based on in situ observations (Sutherland et al., 2014; Lozovatsky et al., 2006; Cisewski et al., 2008; Brainerd and Gregg, 1995) and 10^{-5} m^2 s^{-1} using an ocean general circulation model (Noh and Lee, 2008). In this study, XLD is specified as the depth where ε drops from its first minimum value. This aligns with previous dissipation thresholds and ensures that mixing is captured independently of surface influences. The Upper (UTD) and Lower (LTD/LPD) Thermocline/Pycnocline Depth are delimited as defined by Assunçao et al (2020). UTD corresponded to the depth where the vertical temperature gradient $\partial\theta/\partial z$ = 0.1 ℃ m^{-1}, while LTD/LPD were the last depth below the UTD at which $N^2 \geq 10^{-4}$ s^{-2}.

Baroclinic currents

To analyze the processes explaining dissipation and mixing, particularly along internal tidal (IT) paths, we estimate shear instabilities associated with the semi-diurnal (M2) ITs and mean circulation, as well as their contributions to mixing.

The M2 tidal component of the tidal current is derived by calculating the baroclinic (semi-diurnal) tidal velocity $[u'', v'']$ (Fig. A3, Appendix), following these equations:

$$[u', v'] = [u, v] - [u_{bt}, v_{bt}], \quad (1)$$

$$[u_{bt}, v_{bt}] = \frac{1}{H}\int_{-H}^{0} [u, v]dz, \quad (2)$$

$$[u'', v''] = [u', v'] - [\overline{u'}, \overline{v'}]. \quad (3)$$

Here, $[u, v]$ represent total horizontal velocities (Fig. A3, Appendix) obtained from SADCP data. The components $[u', v']$ and $[u_{bt}, v_{bt}]$ represent baroclinic and barotropic components of horizontal velocities, respectively (Fig. A3, Appendix). H is water depth. The baroclinic mean velocities $[\overline{u'}, \overline{v'}]$ (Fig. A3, Appendix),

calculated to estimate mean circulation along IT paths, are decomposed into along-shore $\overline{u'}_l$ and cross-shore $\overline{u'}_c$ velocities. The overbar denotes the average over a M2 tidal period.

Note that continuously collected SADCP for some stations (e.g., S11) are not sufficiently resolved due to gaps filled by interpolating between time points. The similar processing are applied to the CTD-O_2 data collected alternately. SADCP time series data are less than 17 hours at all long stations, except for S14, which spans 42 hours. As a result, the diurnal and semidiurnal period fittings are not formally distinct (except at S14; Figs. A4 and A5, Appendix), and the inertial period (at least 5 days) cannot be resolved in our dataset. This limits our ability to separate currents by frequency and examine the associated dissipation.

The velocity profiles from LADCP are glued into our SADCP time series data below ~ 500 m depth at long stations.

To evaluate shear instabilities associated with ITs and the mean background circulation, we compute the baroclinic tidal vertical shear squared ($S^{2''}$) and mean shear squared ($\overline{S^{2'}}$) (Fig. A3, Appendix), as follows:

$$S^{2''} = (\partial u''/\partial z)^2 + (\partial v''/\partial z)^2, \quad (4)$$

$$\overline{S^{2'}} = (\partial \overline{u'}/\partial z)^2 + (\partial \overline{v'}/\partial z)^2. \quad (5)$$

To evaluate the impact of bottom friction on mixing, we calculate kinetic energy $\varepsilon_f = \frac{1}{2}\rho_s(u_f^2)$ near the bottom boundary layer at shallow stations using friction velocity $u_f = u_b\sqrt{C_d}$, where C_d=2.5 x 10^{-3} is a drag coefficient obtained from the NEMO model. Huang et al. (2019) showed that the bottom boundary layer thickness spatially varies between 15-123 m in the Atlantic Ocean, with a median of ~ 30-40 m in the North Atlantic. We define bottom layer thicknesses in our study area based on measured bathymetry from CTD-O_2 and near-bottom currents from ADCP. Here, u_b is the total velocity averaged over a thickness of 20 m above the seabed for shallow stations and 40 m for deep stations.

The individual contributions of semi-diurnal ITs and mean circulation are then expressed as follows: $E''/(\overline{E'} + E'')$ for tidal contribution and $\overline{E'}/(\overline{E'} + E'')$ for mean circulation contribution. Here, $E = N^2S$. N is the buoyancy frequency and S is vertical shear. S can be substituted by $S^{2''}$ and $\overline{S^{2'}}$.

Ray tracing calculation

Analyzing both the mean currents and the spatial dimension along the IT pathways offers another insight into the mechanisms responsible for observed mixing (Rainville and Pinkel, 2006). IT energy rays are generated in regions with steep topography, such as the shelf break, where IT slope matches with the bottom slope (i.e., critical slopes) before propagating within the ocean interior.. These rays, moving both downward and upward, encounter the seasonal pycnocline, resulting in beam scattering and the formation of large IT oscillations. As these oscillations steepen, they disintegrate into nonlinear ISWs, a process known as "local generation" of ISWs (New and Pingree, 1992). To explore IT paths, ray-tracing techniques are employed, as previously used by New and Da Silva (2002) and Muacho et al. (2014), to investigate the effectiveness and expected pathways of the IT beams off the Amazon shelf. One main assumption in our linear-theory-based hypothesis is that stratification

remains horizontally uniform along the IT propagation path, although in reality, it may vary due to submesoscale and mesoscale variability. This limitation makes the ray tracing approach less realistic but still useful as a first-order estimate of energy distribution. The IT ray-tracing calculation assumes that in a continuously stratified fluid, ITs energy can be described by characteristic pathways of beams (or rays) with a slope c to the horizontal:

$$c = \pm\left(\frac{\sigma^2 - f^2}{N^2 - \sigma^2}\right)^{1/2}, \quad (6)$$

where σ is the M2 tidal frequency (1.4052×10^{-4} rad s^{-1}), and f is the Coriolis parameter. N^2 are obtained from time-averaged AMAZOMIX CTD-O_2, glued with monthly N^2 profiles from Amazon36 (NEMO model outputs, 2012-2016) below 1000 m depth. Amazon36 is a NEMO configuration, specifically designed to cover the western tropical Atlantic from the mouth of the Amazon River to the open sea (see Tchilibou et al., 2022; Assene et al., 2024; for configuration details and model description). IT ray-tracing diagrams are performed along the transects. Seasonal sensitivity tests of rays (August, September, October, and April) are conducted by varying the critical slope positions and N^2 to explore its influence and generate a set of ray paths consistent with characteristics of IT pathways (Figs. A6 and A7, Appendix).

”

4. MacKinnon and Gregg (2003) provided validation in their paper. There needs to be some explanation of the advantages/conditions for this parameterization over those following from Gregg 1989. Gregg (2003) describe how latitude affects these mixing parameterizations. I saw no mention of this.

R: Thanks for your comments.

Please see the previous response to your comment n°7.

5. It is unclear how mixing layer depth is chosen. There is a statement about choosing a minimum but the profiles show a lot of variance.

R: Thanks for your remarks.

Mixed layer definitions are very sensitive depending on the criteria we adopt and the region of interest (e.g., Thomson and Fine, 2003; de Boyer Montégut et al., 2004; Cisewski et al., 2008; Noh and Lee 2008). We have performed a lot of tests and present them in the revision figure RC1.15.

In our study, we decided, since we have access to the direct microstructure profiles to calculate the mixing layer depth (XLD) defined as the depth at which dissipation estimates decrease from its first minimum value, ensuring that mixing is captured below the influence of surface dynamics. This definition of XLD is consistent with previous studies (e.g., Lozovatsky et al., 2006; Cisewski et al., 2008; Noh and Lee, 2008). As you mentioned, the dissipation profiles show a lot of variance, as does the XLD and the classical MLD (figure RC1.15). In the final manuscript we revised more carefully the definition of the XLD and the MLD and provided a new figure of comparison to show the sensitivity of all these layers.

We have revised the manuscript to clarify in section “methods/The vertical eddy diffusivity coefficient”, in lines 153–177 of the revised manuscript and reported here:

“

The vertical eddy diffusivity coefficient

The efficiency of turbulence in redistributing energy is assessed through the calculation of the vertical eddy diffusivity coefficient (K_z). This coefficient is particularly significant in regions such as pycnoclines, where stratification suppresses mixing, making turbulence-driven mixing a key mechanism for vertical energy transport (Thorpe, 2007).

K_z is calculated from ε following the formulation of Osborn (1980), given by $K_z = \varepsilon\ \Gamma\ N^{-2}$. Here, N^2 is the buoyancy frequency squared, which is calculated using the sorted potential density profiles (σ_θ) obtained from CTD-O_2 data. It is given by $N^2 = -(g/\rho_0)(d\sigma_\theta/dz)$, where ρ_0 is a reference density (1025 kg m^{-3}) and g is the gravitational acceleration. Γ is the mixing efficiency, defined as the ratio between the buoyancy flux and the energy dissipation, and is typically set to 0.2, which corresponds to the critical Richardson number Ri = 0.17 (Osborn, 1980). ε is linearly interpolated into the depths of N^2.

Turbulence within the pycnocline can reduce stratification and increase vertical eddy diffusivity below the mixing layer (Thorpe, 2007). Subsurface mixing, driven by the breaking of ITs and shear instabilities, plays a particularly important role below the mixed layer, especially in equatorial waters (Gregg et al., 2003).

There are several criteria for defining the Mixed Layer Depth (MLD). In this study, we use the commonly accepted density threshold criterion of 0.03 kg m^{-3}, as defined by de Boyer Montégut et al. (2004) and Sutherland et al. (2014), to estimate the MLD for each CTD-O_2 profile. Notably, comparisons with density thresholds of 0.01 and 0.02 kg m^{-3} revealed no major differences in MLD across the AMAZOMIX stations and transects (Fig. A2, Appendix).

The miXing Layer Depth (XLD) is defined as the depth at which ε decreases to a background level (Sutherland et al., 2014). Previous studies have applied various thresholds for background dissipation levels, such as such as 10^{-8} and 10^{-9} W kg^{-1} in higher latitudes based on in situ observations (Sutherland et al., 2014; Lozovatsky et al., 2006; Cisewski et al., 2008; Brainerd and Gregg, 1995) and 10^{-5} m^2 s^{-1} using an ocean general circulation model (Noh and Lee, 2008). In this study, XLD is specified as the depth where ε drops from its first minimum value. This aligns with previous dissipation thresholds and ensures that mixing is captured independently of surface influences. The Upper (UTD) and Lower (LTD/LPD) Thermocline/Pycnocline Depth are delimited as defined by Assunçao et al (2020). UTD corresponded to the depth where the vertical temperature gradient $\partial\theta/\partial z = 0.1$ ℃ m^{-1}, while LTD/LPD were the last depth below the UTD at which $N^2 \geq 10^{-4}$ s^{-2}.

“

6. It is stated the mixing layer depth is always less than the mixed layer depth. This seems like it cannot be true by definition- you need mixing to make a mixed layer. Maybe the mixed layer depth criterion is too small. How about 0.1 kg m-3?

R: Thanks for your comments.

Indeed, you need mixing to make a mixed layer. There are several criteria for defining the mixed layer depth (MLD). We have tested different density threshold criterion from 0.01 to 0.03 kg m−3 , which are the commonly accepted density threshold used in previous studies (e.g., Thomson and

Fine, 2003; de Boyer Montégut et al., 2004; Cisewski et al., 2008; Noh and Lee 2008) as well the less used threshold and from 0.1 to 0.3 kg m−3 (e.g., Brainerd and Gregg, 1995). We have provided on figure RC1.15 and RC1.16, a calculation of these layers for each station. We can see that the XLD is typically deeper than the MLD, which is calculated using a density threshold 0.01-0.03 kg m-3, except for stations 8,10 and 25. This is consistent with regions exhibiting strong subsurface shear, such as the equatorial ocean and western boundary current areas (Noh and Lee, 2008). In contrast, XLD can be lesser than MLD during early restratification and at high latitudes during convective cooling (Noh and Lee, 2008). In our case, the exception for stations 8,10 and 25 (MLD>XLD) might be attributed to shelf break dynamics, including internal tides.

We have added the figure RC1.15 in Appendix of manuscript and pointed out in lines 257-259 and 461-464 of the revised manuscript and reported here:

Lines 257-259:

“

It is important to note that the XLD is typically deeper than the MLD at all stations (except at S8, S10, and S25), which is calculated using a density threshold 0.01, 0.02 or 0.03 kg m^{-3} (Fig. A2, Appendix).

“

Lines 461-464:

“

The XLD was found to be considerably larger than the MLD at all stations, except at S8, S10, and S25. This is consistent with regions exhibiting strong subsurface shear, such as the equatorial ocean and western boundary current areas (Noh and Lee, 2008). The exception observed at other stations may reflect larger mixing events that were not captured by the VMP measurements.

“

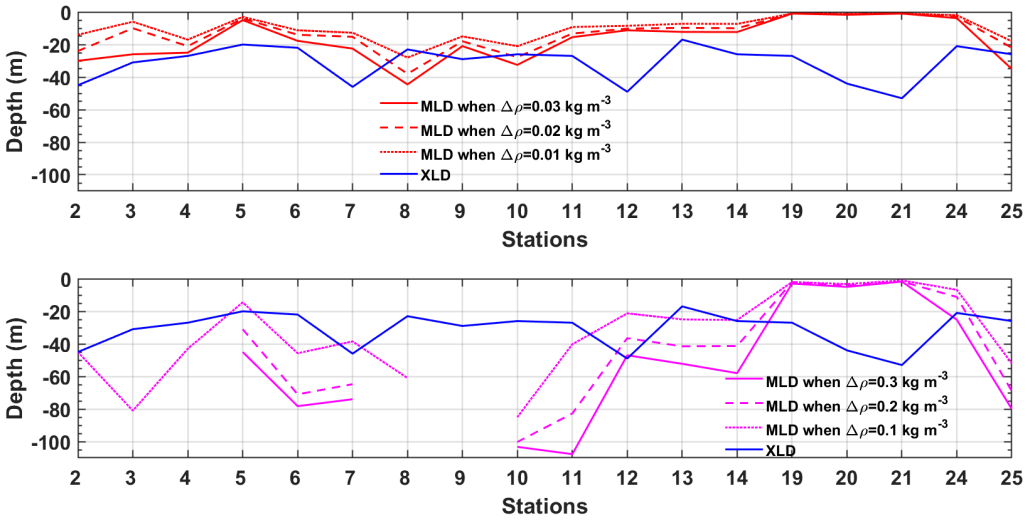

Figure RC1.15: *Comparison of Mixing Layer Depths (XLD, blue line) with Mixed Layer Depths (MLD) defined using (a) larger and (b) smaller density thresholds ($\Delta\rho$). In panel (a), dotted, dashed, and solid red lines represent MLDs defined by $\Delta\rho$ = 0.01, 0.02, 0.03 kg m^{-3}, respectively. In panel (b), dotted, dashed, and solid magenta lines represent MLDs defined by $\Delta\rho$ = 0.1, 0.2, 0.3 kg m^{-3}, respectively.*

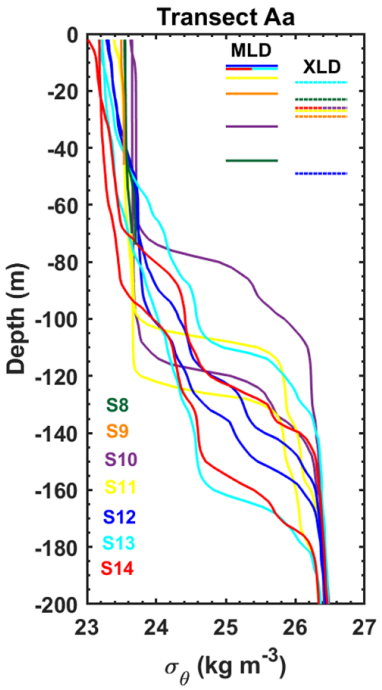

Figure RC1.16: Density profiles at selected stations (S8 to S14) overlaid MLD (in colored solid lines) and XLD (colored dashed lines). Distinct colors are used to represent each station.

7. Figure caption does not correspond to what is plotted. Shear is missing? Figure labelling: how about (a), (b), … instead 4.a.1? There are also faint grey lines around the figures. All the dots in the shear vs N figures are hard to see. Consider binning the results.

R: Thanks for your comments and suggestions.

We have reorganized and revised all the figures and captions (e.g., Figures 5, 6, and 7) in the revised manuscript to make them clearer. We also added the shear (e.g., Figure 6 and 7) in the revised manuscript and reported here in figure RC1.17 and RC1.18 for selected stations (e.g., S10, S11, S14).

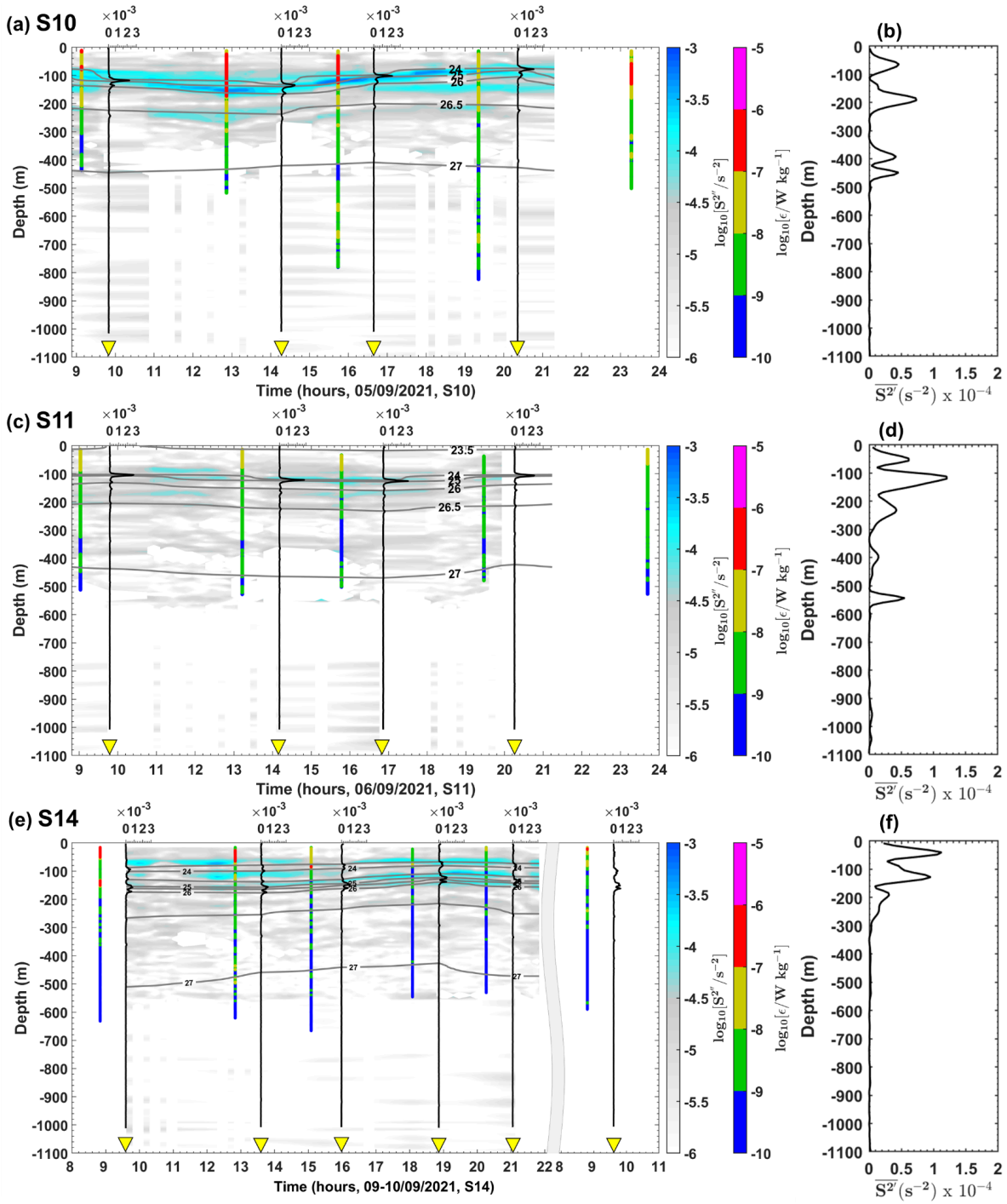

Figure RC1.17: Semi-diurnal baroclinic vertical shear squared (S2”, in m s-1, on a logarithmic scale) for stations (a) S10, (c) S11, and (e) S14. Panels (a), (c), and (e) also display the buoyancy frequency squared (N2, in s-2) represented by vertical black lines, potential density represented by grey contours, and dissipation rate profiles (ε, in W kg-1, on a logarithmic scale) represented by vertical colored bars. Mean baroclinic vertical shear squared (S2', in m s-1) for stations (b) S10, (d) S11, and (f) S14.

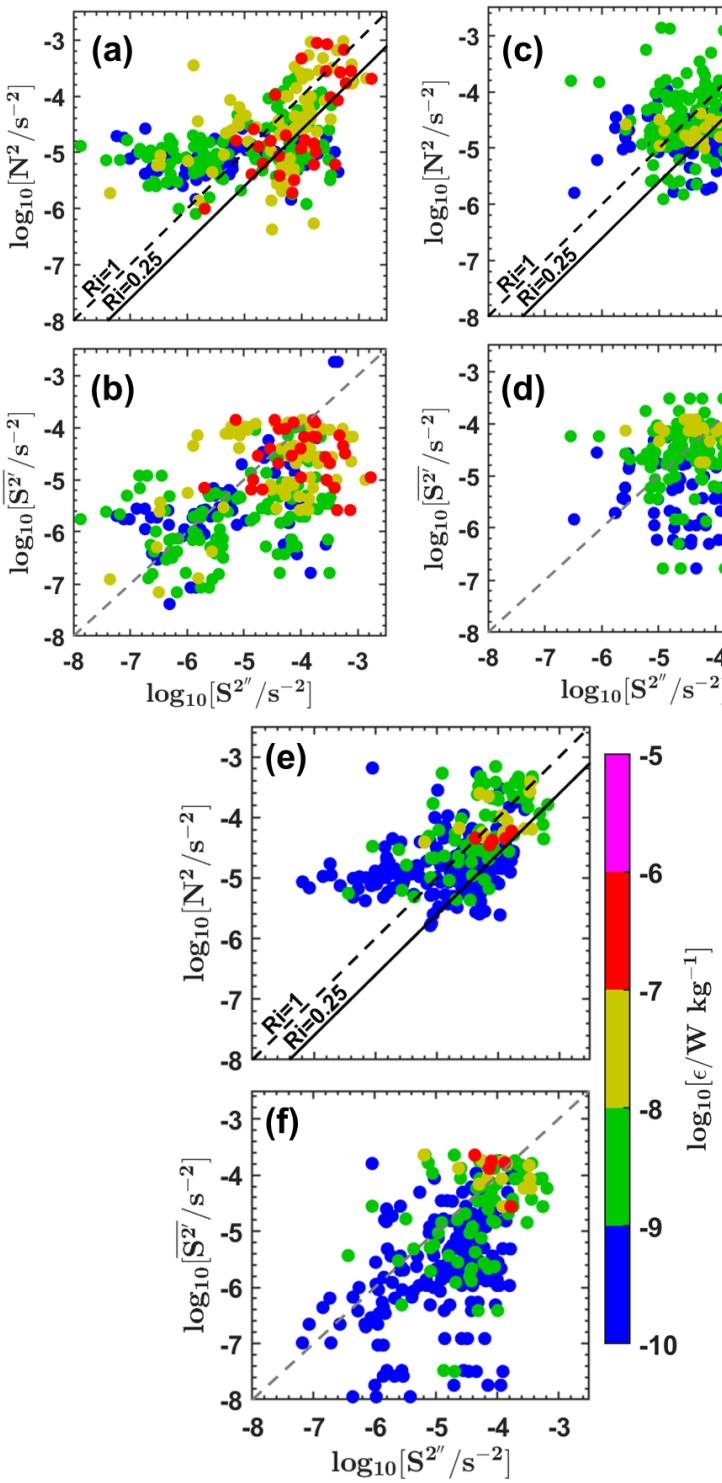

Figure RC1.18: *Dissipation rates (ε, in W kg^{-1}, on a logarithmic scale) below the XLD as a function of the buoyancy frequency squared (N^2, in s^{-2}, on a logarithmic scale) and semi-diurnal baroclinic vertical shear squared ($S^{2''}$, in m s^{-1}, on a logarithmic scale) for stations (a) S10, (c) S11, and (e) S14. Dissipation rates (ε, in W kg^{-1}, on a logarithmic scale) below the XLD as a function of mean baroclinic vertical shear squared ($\overline{S^{2'}}$, in m s^{-1}, on a logarithmic scale) and semi-diurnal baroclinic vertical shear squared ($S^{2''}$, in m s^{-1}, on a logarithmic scale) for stations (b) S10, (d) S11, and (f) S14. N^2 was linearly interpolated into the depths of $S^{2''}$ to have same vertical scales. Panels (a), (c), and (e) also display two solid black lines corresponding to Richardson*

number Ri = 0.25 and Ri = 1, respectively. Dashed grey lines in panels (b), (d), and (f) are included for comparison purposes.

8. There are lots of seemingly correct facts and figures in the text but I am unclear what is the point of them. Take section 3.2.2, for example. Currents are going this way and that at various depths and locations. True. I would suggest a format for each paragraph as follows. “In this paragraph, we examine the flow patterns over the slope to show something [topic sentence]. Here are the relevant facts and skip ones not immediately related to the topic sentence. In summary, we have shown flow is in this direction here which is important for something. Something is described in the next paragraph.”

R: Thanks for your suggestions. All sections of manuscript have been revised.

Comments by line number

19 - twelve hours is the semidiurnal period but not the M2 period = 12.42 hrs

R: Thanks for your remarks. We have corrected it in the revised manuscript in line 18 of the revised manuscript, as shown below:

“

During the AMAZOMIX survey (2021), currents, hydrography, and turbulence were measured over M2 tidal period (12.42h) at numerous sites near the Amazon outflow, where ITs are also generated along the slope.

“.

129 - fft_length, etc. Perhaps you could just give these a symbol if they come up more than once, e.g., L or n. Otherwise skip the variable names in a manuscript.

R: Thanks for your remarks. We have corrected it in the revised manuscript in lines 130-136.

“

Shear spectra are estimated using record lengths (L) and Fast Fourier Transform segments of 2 s, which are cosine windowed and overlapped by 50% (e.g., at station S6 and S10; Fig. 2b, and Fig. A1, Appendix). Additionally, vibration-coherent noise is removed. Different L and overlap (O) settings were selected and tested based on the environment (e.g., deep vs. shallow water), following Fer et al. (2024). For shallow stations, L (O) was shortened to 5 s (2.5 s), in contrast to the 8 s (4 s) used for deeper stations, due to evidence of overturns observed in AMAZOMIX acoustic measurements at deeper stations (Koch-Larrouy et al., 2024; in preparation). This adjustment helped to optimize the spatial resolution of dissipation estimates in shallow water stations.

“

136 - what is the high pass? and the low pass?

R: The high-pass filter was applied to the shear probe data and the low-pass filter was applied to the temperature gradients. We have rewritten this subsection "**TKE dissipation rates** " in the revised manuscript.

150 - mixing layer depth

R: Thanks for your remarks. We have corrected it in the revised manuscript in line 166 of the revised manuscript.

170 - I don't understand. Please rephrase

R: Thanks for your remarks. We have rewritten it in line 193 of the revised manuscript, as shown below:

"

> The velocity profiles from LADCP are glued into our SADCP time series data below ~ 500 m depth at long stations.

"

172 - what is H?

R: Thanks for your remarks.

H is the water depth. We have revised it in the revised manuscript in lines 184-185 of the revised manuscript.

193 - references? Also strong internal tides propagating upward and impinging on the thermocline make ISW. No need for bottom reflections.

R:Thanks for your remarks.

Indeed, strong internal tides propagating upward and impinging on the thermocline generate ISWs. We have revised the subsection "Ray Tracing Calculation" to clarify this, in lines 214–221 of the revised manuscript, as reported here:

"

> These rays, moving both downward and upward, encounter the seasonal pycnocline, resulting in beam scattering and the formation of large IT oscillations. As these oscillations steepen, they disintegrate into nonlinear ISWs…

"

200- You have cross-shore measurements of N. Are those not enough to make a horizontally varying N?

R: Thanks for your comments.

Indeed, we have cross-shore measurements of N. We have varied N2 profiles from stations (e.g., S10, S12, and S14) along transect Aa. Please see the results in figure RC1.19 and RC1.20 below. The sensitivity tests (Figure RC1.19) showed that ray paths align within the packets of rays observed when using mean N2 profiles along transect Aa at different times (e.g., in September and October; Figure RC1.20).

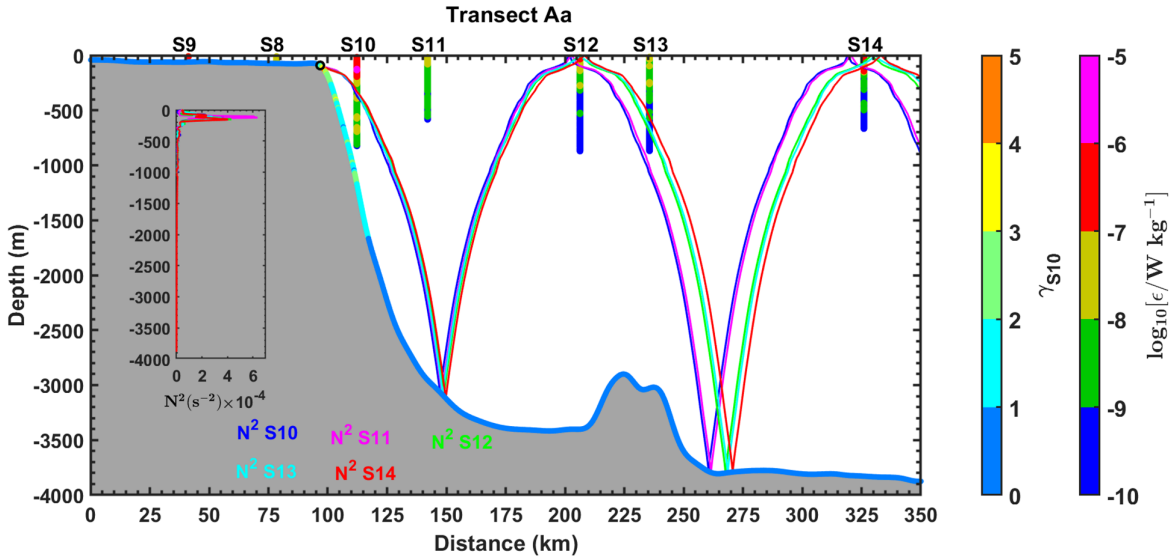

Figure RC1.19: Example of sensitivity tests with different cross-sectional measurements of N^2 along the transect T1 N^2. colors are used to distinguish different cross-shore measurements of N^2 for corresponding stations on T1. Topography steepness (gamma = ray slope / topography slope) for T1 using measured N^2 of S10. Gamma is illustrated by the colored bar (named gamma S10).

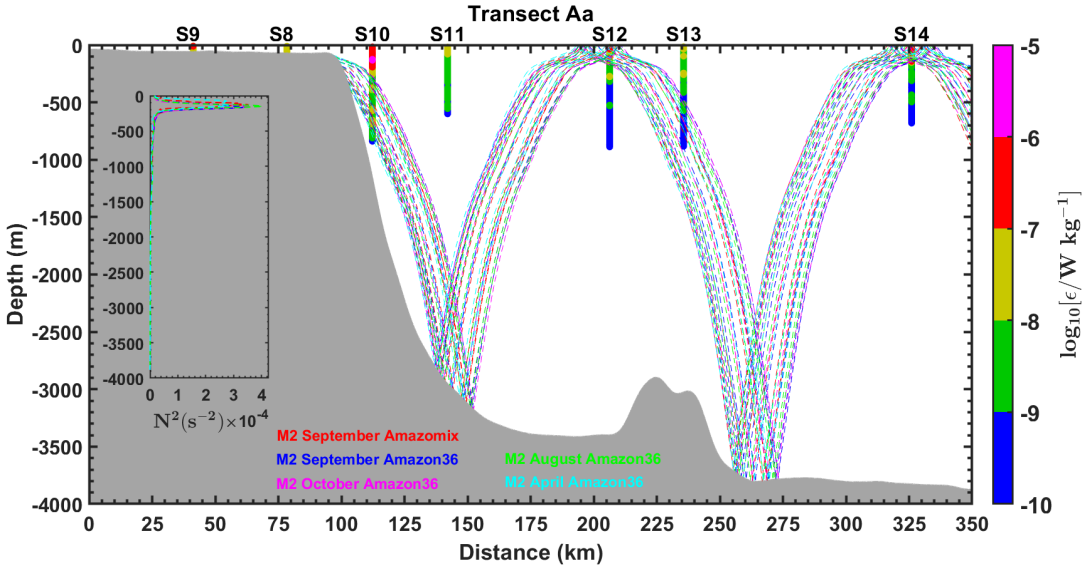

Figure RC1.20: Sensitivity tests of M2 IT ray-tracing along the transects Aa, conducted by varying the location of the critical topography slope. The tests use mean buoyancy frequency squared (N^2, in s^{-2}) obtained from CTD-O_2 data (September 2021) and NEMO-Amazon36 model data (2012-2016). Dashed colored lines represent IT beams calculated for different seasons (April, August, October, and September) and for varying locations of the critical topography slope. Grey areas indicate local topography. Panel also includes dissipation rate profiles (ε, in W kg^{-1}, shown as vertical colored bars on a logarithmic scale) from

the VMP measurements. Subpanels within each panel illustrate the N^2 profiles derived from AMAZOMIX and the NEMO-Amazon36 model, which were used in the ray-tracing calculations. For comparison, sensitivity tests using N^2 measurements from individual stations along the corresponding transect (e.g., at S10) revealed similar ray paths (not shown), consistent with the packet of rays obtained using the mean N^2.

207- there has to be some minimal description of amazon36 here even if it is referenced

R: Thanks for your remarks.

We have added a short description of amazon36 in the revised manuscript (in lines 226-227) and refer to previous studies. We have reported the revision here:

"

Amazon36 is a NEMO configuration, specifically designed to cover the western tropical Atlantic from the mouth of the Amazon River to the open sea (see Tchilibou et al., 2022; Assene et al., 2024; for configuration details and model description).

"

210- sensitivity not sensibility test, although the latter could also be used

R: Thanks for your remarks. We have revised it in line 228 of the revised manuscript.

263- 3-5 not 03-05

R: Thanks for your remarks. We have revised itn lines 301-302 of revised manuscript, as shown below:

"

The baroclinic tidal velocities reveal a superposition of 3-5 tidal modes at IN-ITs stations (Figs. 5a, 5c, and 5e, and Figs. A9 to A15, Appendix).

"

267-272 - Shear obviously varies with N because if shear were bigger than it would have lower Ri and be unstable. It would be more instructive to consider Ri or reduced shear = S2 - 4N2.

R: Thanks for your comments.

Indeed, shear varies noticeably with N at certain stations farther from IT generation sites. However, closer to the generation sites, such as at S10, stronger tidal shears were observed in areas where Ri was lower (<0.25), coinciding with hotspots of mixing.

This is why we specifically considered shear and quantified the contribution of tidal shear to mixing along IT paths. Please refer to the results for reduced shear presented below in figure RC1.21.

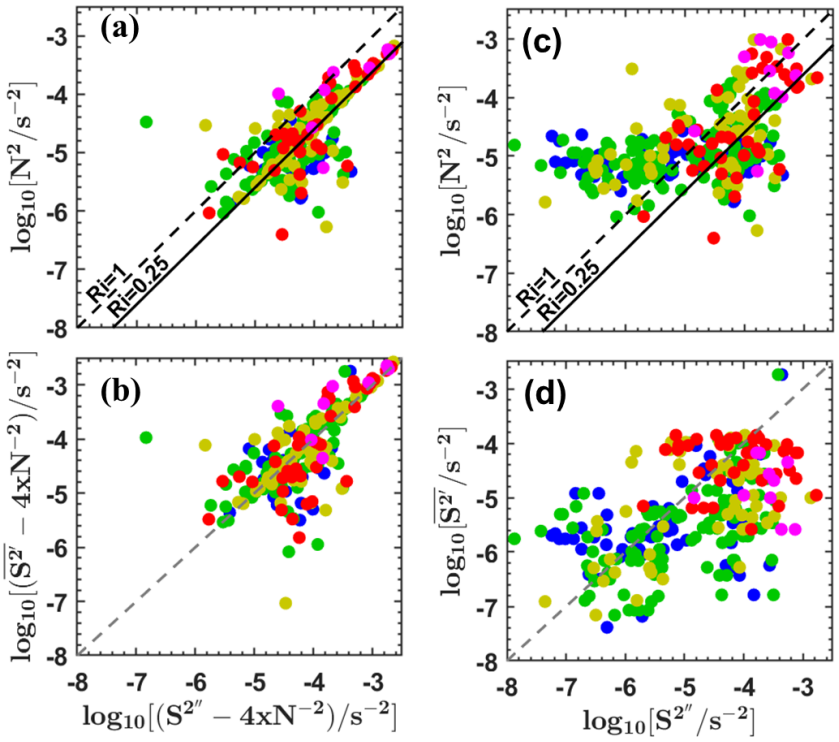

Figure RC1.21: For station S10. *Dissipation rates (ε, in W kg^{-1}, on a logarithmic scale) below the XLD as a function of the buoyancy frequency squared (N^2, in s^{-2}, on a logarithmic scale) and semi-diurnal baroclinic vertical shear squared ($S^{2''}$, in m s^{-1}, on a logarithmic scale), when using (a)-(b) reduced shear. Dissipation rates (ε, in W kg^{-1}, on a logarithmic scale) below the XLD as a function of mean baroclinic vertical shear squared ($\overline{S^{2'}}$, in m s^{-1}, on a logarithmic scale) and semi-diurnal baroclinic vertical shear squared ($S^{2''}$, in m s^{-1}, on a logarithmic scale), when using (c)-(d) no reduced shear. N^2 was linearly interpolated into the depths of $S^{2''}$ to have same vertical scales. Panels (a), (c), and (e) also display two solid black lines corresponding to Richardson number Ri = 0.25 and Ri = 1, respectively. Dashed grey lines in panels (b), (d), and (f) are included for comparison purposes.*

You could use some mean N or interpolated N and see what it looks like.

R: Indeed, several tests were conducted using both mean and interpolated N. Ultimately, we opted to use the time-interpolated N and shear values at all dissipation times (at VMP measurement hours) along IT paths.

If the text talks a lot about shear, it would be helpful to plot shear. In fact the baroclinic vs tidal shear is discussed but there are no plots.

R: Thanks for your remarks. We have added the plots of the shears both in text and appendix.

Fig 4- caption and figure all on same page please. Add tick marks to the x axis to show when your CTD/VMP casts took place. Also this figure seems to include transits and time on station.

In Fig 4b1 there are some strange looking changes in the current. Perhaps it would be better to do your analysis station by station. Or are there artifacts of the SADCP processing going from on station to transit?

R: Thanks for your comments.

We have reorganized the figures and added an x-axis to indicate when CTD/VMP casts were conducted. Please refer to the updated figure in the revised manuscript (figure 5) and reported below in figure RC1.22.

Regarding the updated figure of the revised manuscript (figure 5), we noticed some unusual changes in the current patterns, which have been rechecked. The continuously collected SADCP for some stations (e.g., S11) are not sufficiently resolved due to gaps filled by interpolating between time points (e.g., between 13:30 and 15:30 at S11). Doing this interpolation would introduce potential artifacts in the calculations. The interpolation allowed us to extract some current profiles at the dissipation times to ensure consistency in the analyses.

The analyses were performed separately by station and by transect. For example, Figure RC1.22 shows the semidiurnal current over time at a fixed position for station S11. In contrast, Figure RC1.23 displays the mean alongshore currents along transect Aa, including transit between stations.

We have pointed out in text in lines 187-188 of revised manuscript and reported here

“

> Note that continuously collected SADCP for some stations (e.g., S11) are not sufficiently resolved due to gaps filled by interpolating between time points. The similar processing are applied to the CTD-O_2 data collected alternately.

“

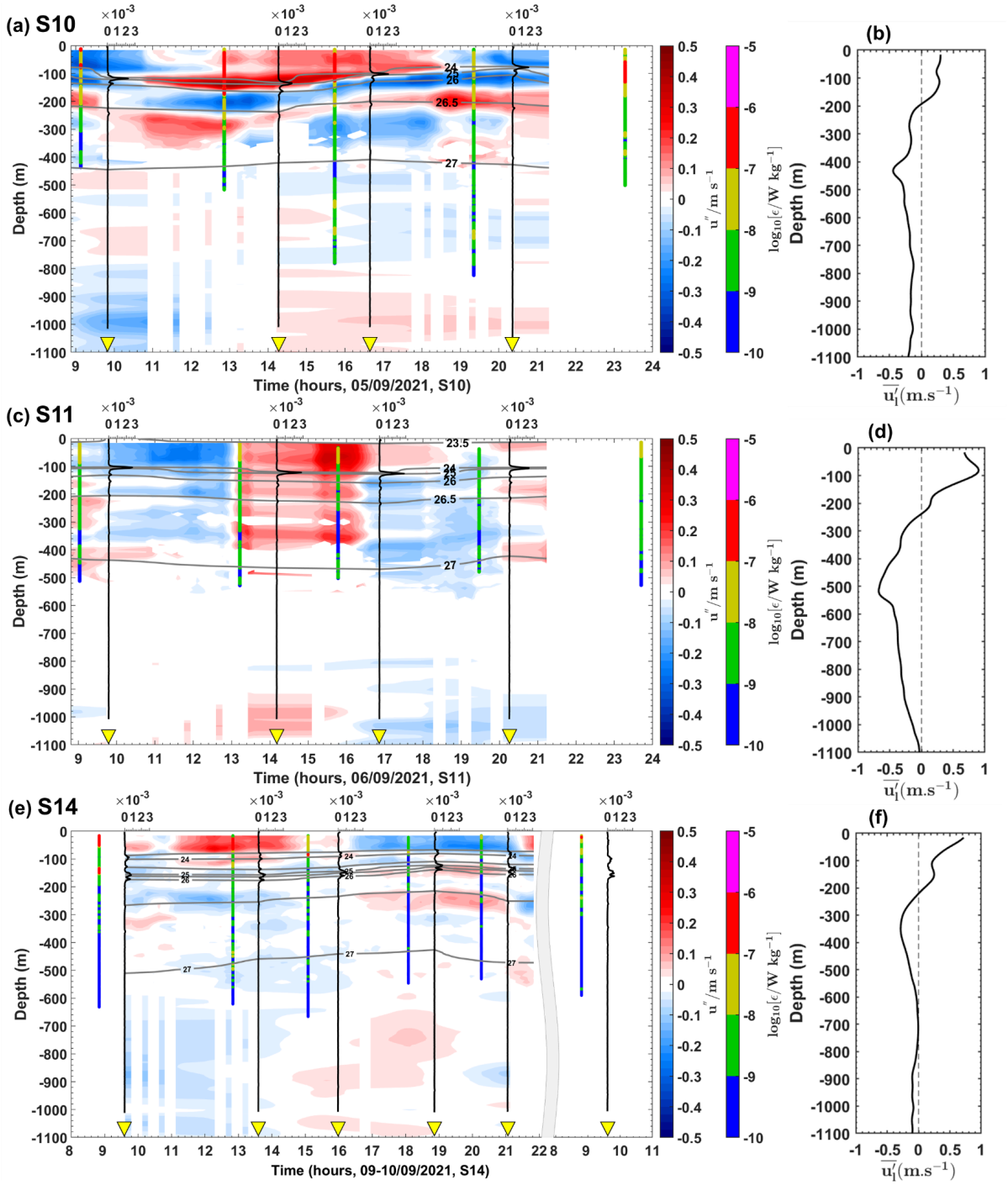

Figure RC1.22: Semi-diurnal baroclinic zonal currents (u", in m s-1) from the ADCP for stations (a) S10, (c) S11, and (e) S14. Panels (a), (c), and (e) also display the buoyancy frequency squared (N2, in s-2) represented by vertical black lines, potential density represented by grey contours, and dissipation rate profiles (ε, in W kg-1, on a logarithmic scale) represented by vertical colored bars. Along-shore mean baroclinic currents (u'l, in m s-1) from the ADCP for stations (b) S10, (d) S11, and (f) S14.

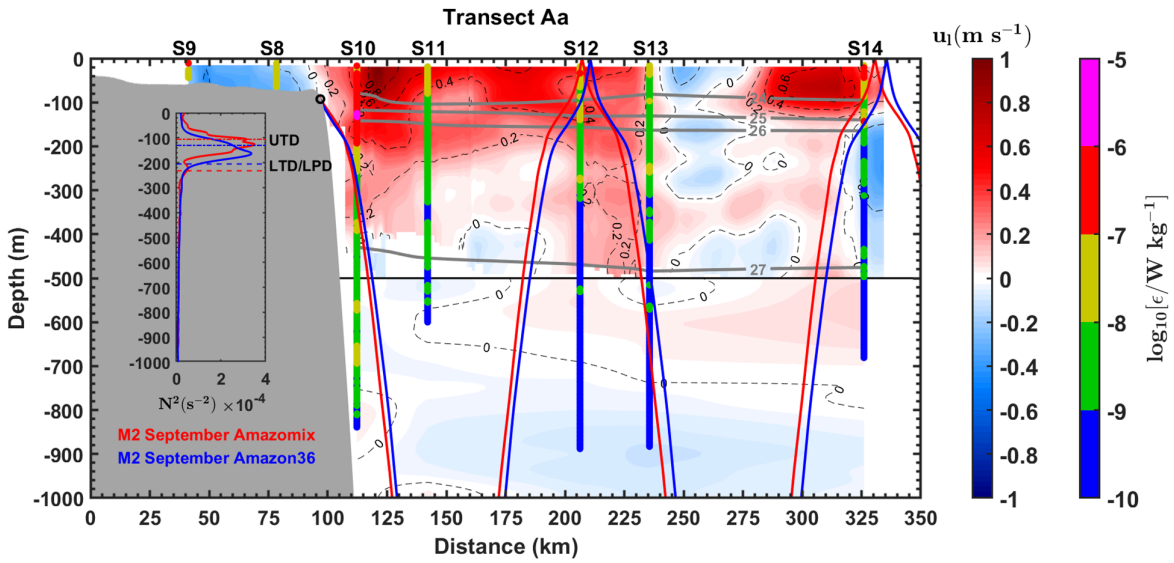

Figure RC1.23: IT ray-tracing diagrams for the M2 tidal constituent along transects Aa. The calculations were performed using the mean buoyancy frequency squared (N^2, in s^{-2}) obtained from CTD-O_2 data (ray in red) and NEMO-Amazon36 model data (ray in blue) for September. Grey areas represent local topography and black circles indicate the critical topography slope (ray generation sites). Panel also show along the transects Aa: along-shore mean total currents (u_l, in m s^{-1}) from ADCP (Dashed black lines), potential density from CTD-O_2 (grey contours), and dissipation rate profiles (ε, in W kg^{-1}, on a logarithmic scale) from the VMP (vertical colored bars). Subpanels within each panel illustrate the N^2 profiles from AMAZOMIX (red line) and the NEMO-Amazon36 model (blue line) used for ray-tracing calculations. Upper Thermocline Depth (UTD, dotted lines) and Lower Thermocline/Pycnocline Depth (LTD/LPD, dashed lines) are also indicated.

301- what sort of of mean? time, depth, etc

R: Thanks for your remarks. It is time-mean. We have revised it in line 355 of the revised manuscript

312-314- More explanation is needed here.

R: These have been removed during the revision of the manuscript.

Fig 5- the tidal rays look to have shallower slope than the topography. It would be helpful to plot ray slope vs topographic slope to verify. The dissipation seems unrelated to the ray paths as far as I can tell. Perhaps it is not 2D. There appear to be 2 sources at least, which can constructively interfere. Rays may propagate at an angle to the coast.

R: Thanks for your comments.

We attempted to verify our analysis by plotting the ray slope against the topographic slope. Using our bathymetry data from the NEMO-AMAZON36 model or GEBCO, the tidal rays did not appear to have a shallower slope (around 225 km) than the topography in any of the sensitivity tests, as illustrated in Figure RC1.24 (with topography steepness "gamma") below. These results may differ if using alternative bathymetric products.

Following the ray tracing, we observed that some dissipation hotspots are located along the ray paths, particularly above the generation sites and during ray propagation.

Interestingly, there seem to be at least two sources that could constructively interfere, potentially explaining the high dissipation observed at S14. This wave-wave interference is being explored further in a separate study to confirm these findings.

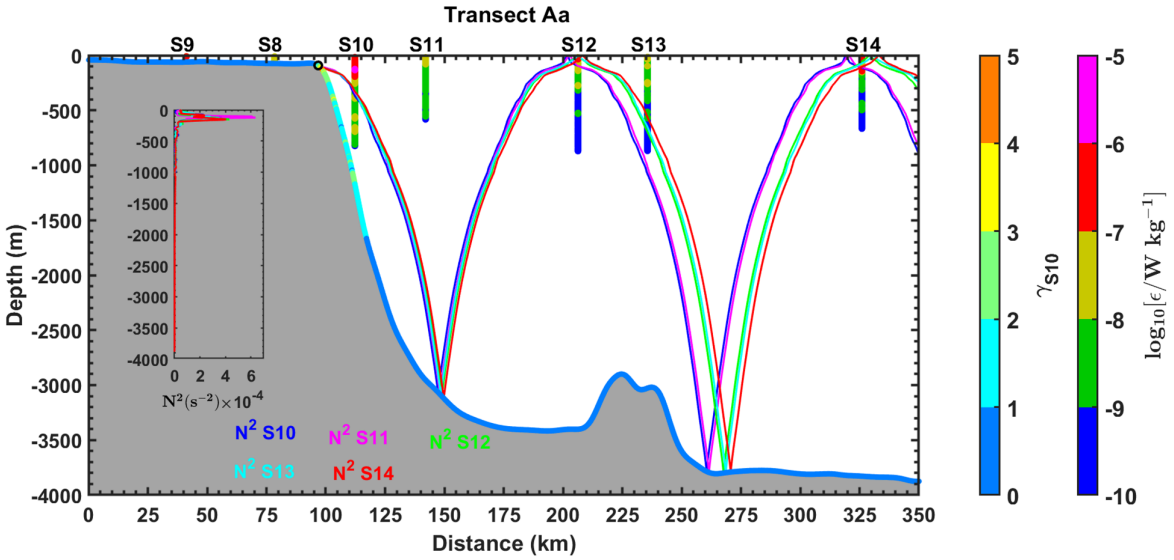

Figure RC1.24: Example of sensitivity tests with different cross-sectional measurements of N^2 along the transect T1 N^2. colors are used to distinguish different cross-shore measurements of N^2 for corresponding stations on T1. Topography steepness (gamma = ray slope / topography slope) for T1 using measured N^2 of S10. Gamma is illustrated by the colored bar (named gamma S10).

384 - “for the first time” How sure are you of this? It would be conservative to add: to the best of our knowledge

R: Thanks for your remarks.

We have corrected the sentence of the text in line 427 of the revised manuscript, as follows:

“

To the best of our knowledge, the AMAZOMIX 2021 cruise provided, for the first time, direct measurements of turbulent dissipation using a velocity microstructure profiler….

”

End

……

For Reviewer comments 2 RC2

We thank this Reviewer for thoughtful and constructive comments on our manuscript. We appreciate the time s/he invested in the review. We believe that our revised manuscript addresses all the comments. In this regard, we have revised and rewritten a few sections such as Abstract, method, results, discussion and conclusion in the revised manuscript. Quality control and revision of dissipation estimates, as well as current calculations were also done to ensure the validity of our results. We thought it useful to point out its detailed revisions (lines and sections) in the reply to your comments. Below (highlighted in blue and magenta) is an itemized response to the different issues raised in the review.

Review of "Turbulent dissipation from AMAZOMIX off the Amazon shelf along internal tides paths", by Kouogang et al. Submitted to EGUsphere.

By Kouogang et al.

The paper reports oceanographic observations in the tropical Atlantic ocean within the framework of project AMAZOMIX, which aims to quantify mixing, identify the associated processes, and investigate their impact on nutrient fluxes off the Amazon shelf. The observations were collected during a field campaign in August-October 2021, on board the RV ANTEA with a dedicated satellite coverage (reported elsewhere). The region is well known for large amplitude internal tides and Internal Solitary Waves (ISWs), that were first measured and reported in Brandt et al., 2002, with wave amplitudes exceeding 100 m. Those large amplitude ISWs are clearly seen in Synthetic Aperture Radar (SAR) satellite images, as illustrated in the author's Figure 1. Clearly, the cruise measurements were carefully planned in advance based on the knowledge provided by the SAR image archive. The most relevant aspect reported in the paper is the relative increase of mixing found about 225 km away from two distinct generation sites of internal tidal waves at the shelf break. The site where the relative mixing increases coincides with the surfacing of Internal Tidal (IT) rays emanating from different sites at the shelf break. But it also coincides with the appearance of large amplitude ISWs seen in the satellite record. While the constructive interference of IT rays has been suggested, and indeed is consistent with ocean colour images, in the central region of the Bay of Biscay (Western Europe), this aspect has not been documented elsewhere until now. It is therefore remarkable the association made by the authors between enhanced mixing and IT interference.

Thanks for this very concise and precise summary. We took the liberty of using some of your wording to improve our abstract and our conclusion.

However, a more comprehensive comment should be made concerning the presence of ISWs near Station S14, and its possible relation with the measured increased mixing.

R: This is a very interesting question. We have a specific point on the discussion (in lines 556-567 of the revised manuscript) on that matter, and we agree that this funding is quite important. Please find the revised section "**Discussion on the strong mixing at S14**" below:

"

Discussion on the strong mixing at S14

Along the IT paths, elevated remote dissipation rates (within $[10^{-7}, 10^{-6}]$ W kg^{-1}) were identified ~ 230 km from the shelf-break at S14.

This region is well known for intense IT dissipation, as shown by a realistic model (Tchilibou et al., 2022; Assene et al., 2024), and for the highest occurrences of ISWs generated by ITs (Fig. 1a; de Macedo et al., 2023), with large-amplitude ISWs exceeding 100 m clearly visible in satellite records (Brandt et al., 2002).

At station S14, where relative mixing increases, IT rays surfacing from two distinct IT generation sites coincide with the appearance of ISWs and mark the location where the NBC vanishes.

This region of wave-wave interactions can lead to the constructive interference of IT rays, potentially facilitating the emergence of higher tidal modes (New & Pingree, 1992; Silva et al., 2015; Barbot et al., 2022; Solano et al., 2023). These higher modes, in turn, could enhance the generation of nonlinear ISWs (e.g., Jackson et al., 2012) and contribute to the elevated dissipation rates (Xie et al., 2013), as observed at this station.

"

This question is so interesting that we are dealing with an additional paper. Indeed, AMAZOMIX provides acoustic data that clearly shows ISW and overturn associated with it at station 14, and a paper is in construction on this matter. Furthermore, their signature at the surface was studied in Macedo et al., 2023 in the region. The mixing hotspots observed at this station could be related to their presence, but more work is needed to establish it with more confidence

The authors calculate the turbulent kinetic energy (TKE) dissipation rates and vertical diffusivities making use of microstructure and hydrography data collected at a series of stations and transects in a vast study region, being able to compare these values within internal tide pathways, and away from those paths. The observations also reveal a great deal of mixing at the shelf break, as expected. **Baroclinic shear currents were calculated from ADCP data collected between stations and transects. It was then possible to estimate the ratio contribution to mixing between IT and Baroclinic Currents (BC). Interestingly, ITs dominate the ratio for IT/BC near the generation sites of ITs at the shelf break (65%/35%) and also at Station S14, 225 km away from the shelf break, admittedly where the IT beams coming from different sites may interfere (60%/40%).** Although this fact is suggestive of the IT rays interference being capable of impacting mixing well away from the shelf break, the authors do not attempt comparison with the impact ISWs alone would have, on mixing.

R: Thank you for your comment.

Indeed, ISWs may influence mixing. While our study did not quantify the specific contribution of ISWs, we suggest that their presence, likely resulting from IT decay, could

play a role in the mixing process at S14. In order to explore further the difference between ITs mixing compared to ISWs mixing a non hydrostatic model at very fine resolution should be runned such as in da Silva et al. (2015) and Solano et al. (2023). It would be very interesting to compare the AMAZOMIX data to such model.

The manuscript is reasonably written (with some minor pitfalls indicated below), and the data analysis certainly merits publication at EGUsphere. The hypotheses tested in the paper are well explained and presented, representing a milestone in the oceanography of the study region. The paper also includes an extensive appendix with auxiliary results. This reviewer recommends publication after some minor corrections (please see list below).

Minor comments:

Introduction:

Line 46 – 47: “They can dissipate where the energy beam reflects at the bottom, at the surface or at the thermocline levels…”; The authors start describing bottom reflection of IT beams etc. without first explaining how those beams form and propagate in the vertical. A reader may like to read first how these beams are formed and why they propagate following rays that are determined by the well known formula that gives the angle to the horizontal. There should be a more comprehensive explanation about tidal beams before this point in the text. It may be worth referring to the work of Theo Gerkema (Gerkema, 2001 and Gerkema and Zimmerman, 2008).

R: Thanks for your comments and suggestions. We have rewritten to make it clearer in the text as you suggested. The revisions can be found in lines 34-82, as shown below:

“

1 Introduction

Turbulent mixing in the ocean plays an important role in sustaining the thermohaline and meridional overturning circulation and in closing the global ocean energy budget (Kunze, 2017). These processes have strong implications for the climate, influencing heat and carbon transport, as well as nutrients supply for photosynthesis (Huthnance, 1995; Munk and Wunsch, 1998). Mixing processes can result from wind in the surface waters layer, internal waves and shear instability in the ocean interior, and bottom friction near the bottom layer (Miles, 1961; Thorpe, 2018; Ivey et al., 2020; Inall et al., 2021). Barotropic tides interacting with steep shelf-break topography trigger internal waves at tidal frequencies and harmonics, known as internal tides (ITs), which can propagate and produce mixing. These ITs can be expressed by large vertical displacements (up to tens of meters) of water masses (Garrett and Kunze, 2007). After their generation on the shelf-break, the (more unstable) higher modes of ITs may dissipate locally, while the lower modes can propagate far away (Zhao et al., 2016). IT beams (generated where the slope of the ITs and the topography match together on the shelf-break) can propagate vertically, resulting in reflection, scattering and dissipation of ITs at the bottom, surface waters, or thermocline levels (New and Da Silva, 2002; Gerkema and Zimmerman, 2008; Bordois, 2015; Zhao et al. 2016). They can also dissipate when energy fluxes interfere (Zhao et al., 2012) or interact with strong baroclinic eddies or currents (Rainville and Pinkel, 2006; Whalen et al., 2012). Furthermore, ITs may disintegrate into packets of

higher-mode nonlinear internal solitary waves (ISWs), which can propagate and dissipate offshore (Jackson et al., 2012).

Previous and recent studies have shown that ITs-induced turbulent mixing can affect the surface, such as sea surface temperature (Ray and Susanto, 2016; Nugroho et al., 2018; Assene et al., 2024), chlorophyll content (Muacho et al., 2014; M'Hamdi et al., 2024; in preparation), marine ecosystems (Wang et al., 2007; Zaron et al., 2023), and atmospheric convection and the rainfall structure (Koch-Larrouy et al., 2010, Sprintall et al. 2014).

In the western tropical Atlantic, the Amazon River-Ocean Continuum (AROC) constitutes a key region of the global oceanic and climate system (Araujo et al., 2017; Varona et al., 2018). This region (Fig. 1a) is characterized by a system of western boundary currents, including North Brazil Current (NBC). NBC, which flows northwestward, has its core velocities (~ 1.2 m s^{-1}) that remain stable from the surface to a depth of 100 m (Johns et al., 1998; Bourlès et al., 1999; Barnier et al., 2001; Neto and Silva, 2014). This region also experiences highly variable dynamics due to the Amazon River Plume. During the rainy season (May-July), peak discharge can extend the plume over 1500 km offshore, northwest along the NBC. In the dry season (September-November), reduced discharge and stronger saline intrusion may confine the plume to less than 500 km offshore, near the Amazon Shelf, with some eastward dispersion (Coles et al., 2013). The Amazon plume can generate vertical shear in underlying currents, enhancing mixing. Additionally, a system of Amazonian Lenses of water (AWL), influenced by continental inputs, may affect both the boundary layer and mixed layer patterns (Silva et al., 2005; Prestes et al., 2018).

In the AROC region, the Amazon shelf-break is a hotspot for the generation, propagation and dissipation of ITs and ISWs as a result of non-linear processes (Geyer, 1995; Brandt et al., 2002; Magalhães et al., 2016; Ruault et al., 2020; Tchilibou et al., 2022; Fig 1). Previous studies using Synthetic Aperture Radar (SAR) satellite images (Magalhaes et al., 2016) identified ISWs along the path of ITs propagating from two sites (i.e., sites Aa and Ab; Fig. 1a). Conversely, other sites showed no ISWs propagation (i.e., sites E and D; Fig. 1a, 1b and 1c) (see Magalhaes et al., 2016 for definition). Using numerical modeling, Tchilibou et al. (2022) showed that about 30 % of the M2 (dominant tidal component; Le Bars et al. 2010) ITs energy is dissipated locally (for higher-modes ITs) at sites E, Aa, Ab and D (Fig. 1a), while the remaining lower-modes ITs energy can be dissipated remotely. Dissipation away from the generation sites (E, Aa, Ab and D; Fig. 1a) can result from the shear instabilities caused by ITs-ITs and/or ITseddy/current interactions. Despite the presence of ITs, no direct measurements of dissipation rates have been conducted to our knowledge.

The mixing induced by these internal waves in the region was observed during the AMAZOMIX cruise (Bertrand et al., 2021). The cruise was designed with stations/transects inside and outside ITs fields (Fig. 1a and 1c) to measure ITs dissipation and study their impact on the AROC ecosystem. Direct microstructure measurements of temperature, salinity and velocity were conducted at the different repeated stations/transects over a M2 tidal cycle (~ 12.42 h). These cruise measurements offer an opportunity to explore whether ITs play a role in mixing within the AROC region. In this study, we will quantify mixing and identify the associated processes off the Amazon shelf. We will calculate turbulent kinetic energy (TKE) dissipation rates, vertical displacements of isopycnal surfaces and vertical eddy diffusivities using in situ microstructure and hydrography data. Finally, the baroclinic shear of currents and their contributions to mixing will be calculated from current data collected between stations and transects.

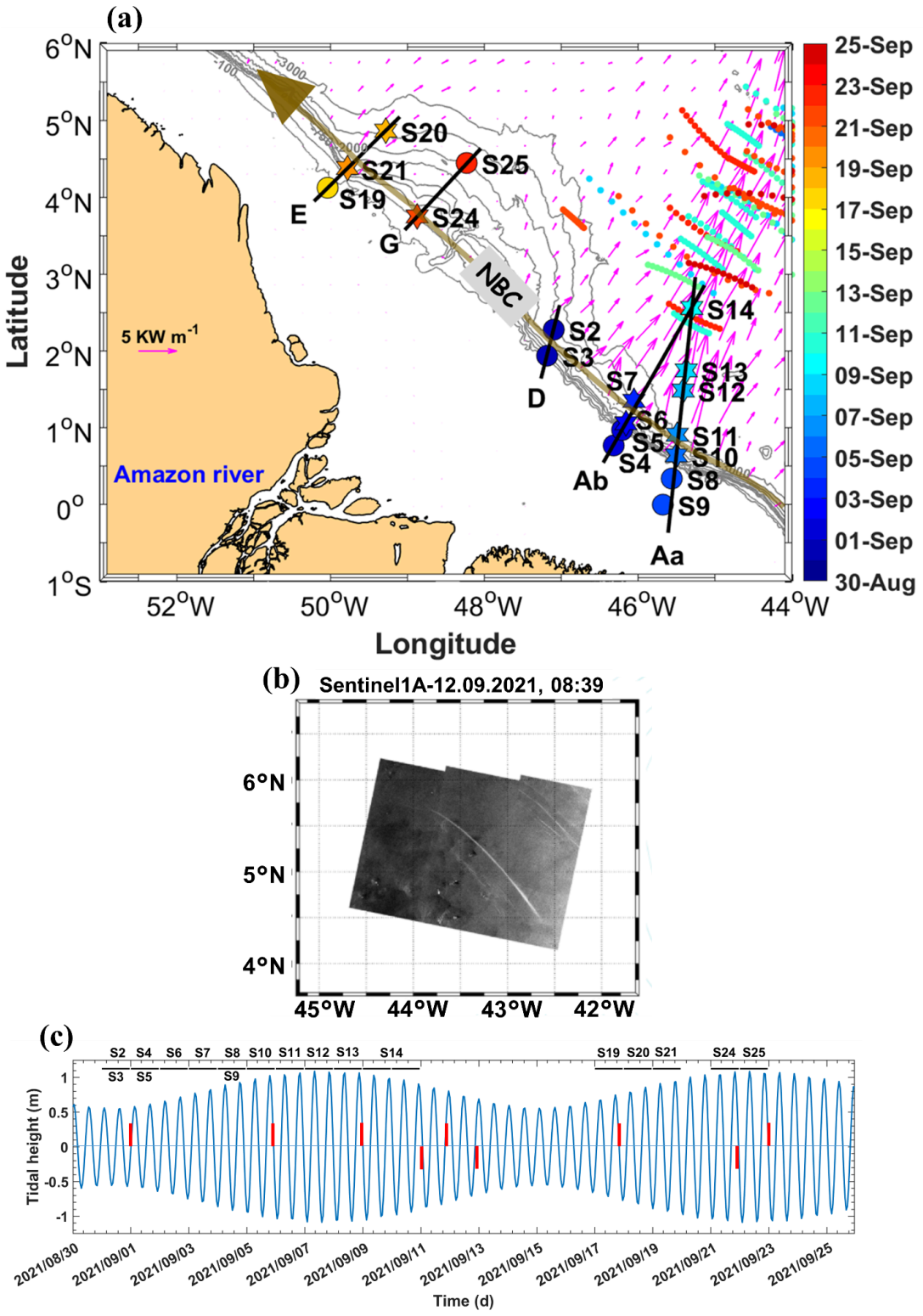

Figure 1: a) Map of a part of the AMAZOMIX 2021 cruise off the Amazon shelf, showing bathymetric contours (100 m, 750 m, 2000 m, and 3000 m isobaths) in gray. Colored circles and stars indicate short and long CTD-O2/L-S-ADCP stations, respectively, with the corresponding sampling dates represented by the color bar. Solid black lines depict SADCP transects (for Aa, Ab, D, G, and E). Magenta arrows show the 25-hour mean depth-integrated baroclinic IT energy flux (September 2015, from the NEMO model) originating from IT generation sites (Aa, Ab, D, and E) along the shelf break. The solid brown line represents the NBC pathways

illustrating background circulation. Shattered colored lines highlight ISW signatures. b) 1A Sentinel image acquired on 12th September 2021, showing ISW signatures. c) Tidal range at AMAZOMIX stations, with ISW signature dates marked by red bars.

"

Line 53: The reference Muacho et al, 2014 should be referred earlier, together with M'Hamdi et al., 2024, in preparation)

R: Thanks for your suggestions. We have rewritten to make it clearer in the text as you suggested. The revisions can be found in lines 50-51 of the revised manuscript, as shown in your previous comment.

Line 62: Please include reference Brandt et al., 2002 in JPO about ISW in situ observations.

R: we could not find this reference in JPO. Could you please share the link to this article, if you have it ?.

Line 69: "…no direct measurements of dissipation rates have been conducted.". Do you mean before the present paper?

R: We have corrected the sentence of the text in lines 71-72 of the revised manuscript. I meant that:

"

Despite the presence of ITs, no direct measurements of dissipation rates have been conducted to our knowledge.

"

Methods:

Line 170: "…time series with LADCP profiles glued below ~500m…". later, in line 209 (page 8), the word "stitched" is used with a similar meaning? Could the authors use jargon more carefully, and consistently, please.

R: Thanks for your remarks. We have rewritten to make it clearer as you suggested in lines 121-230 of the revised manuscript. The revision of section "methods" can be found below:

"

2.2 Methods

TKE dissipation rates

The VMP data are processed using ODAS Matlab library (developed by Rockland Scientific International, Inc) to infer the TKE dissipation rate (ε). The processing methods for the VMP data are briefly described here and adhere to the recommendations of ATOMIX (Analyzing ocean turbulence observations to quantify mixing), as reported by Lueck et al. (2024), and have been validated against the benchmark estimates (presented in Fer et al., 2024).

First, the VMP data are converted into physical shear units, and the time series are prepared. Continuous sections of the time series are selected for dissipation estimation. Before spectral estimation, the aberrant shear signals caused by vessel wake contamination are removed. Collisions of the shear probe with plankton and other particles are removed using the de-spiking routine. The records from each section are then high-pass filtered (e.g., at station S6 and S10; Fig. 2a, and Fig. A1, Appendix).

Shear spectra are estimated using record lengths (L) and Fast Fourier Transform segments of 2 s, which are cosine windowed and overlapped by 50% (e.g., at station S6 and S10; Fig. 2b, and Fig. A1, Appendix). Additionally, vibration-coherent noise is removed. Different L and overlap (O) settings were selected and tested based on the environment (e.g., deep vs. shallow water), following Fer et al. (2024). For shallow stations, L (O) was shortened to 5 s (2.5 s), in contrast to the 8 s (4 s) used for deeper stations, due to evidence of overturns observed in AMAZOMIX acoustic measurements at deeper stations (Koch-Larrouy et al., 2024; in preparation). This adjustment helped to optimize the spatial resolution of dissipation estimates in shallow water stations.

Finally, ε is determined using the spectral integration method and by comparison with the Nasmyth empirical spectrum (Nasmyth, 1970). Quality assurance tests are carried out in accordance with ATOMIX's recommendations (Lueck et al., 2024). A figure of merit < 1.4 is used to exclude bad data (e.g., at station S6 and S10; Fig. 2b, and Fig. A1, Appendix), and the fraction of data affected by de-spiking is < 0.05.

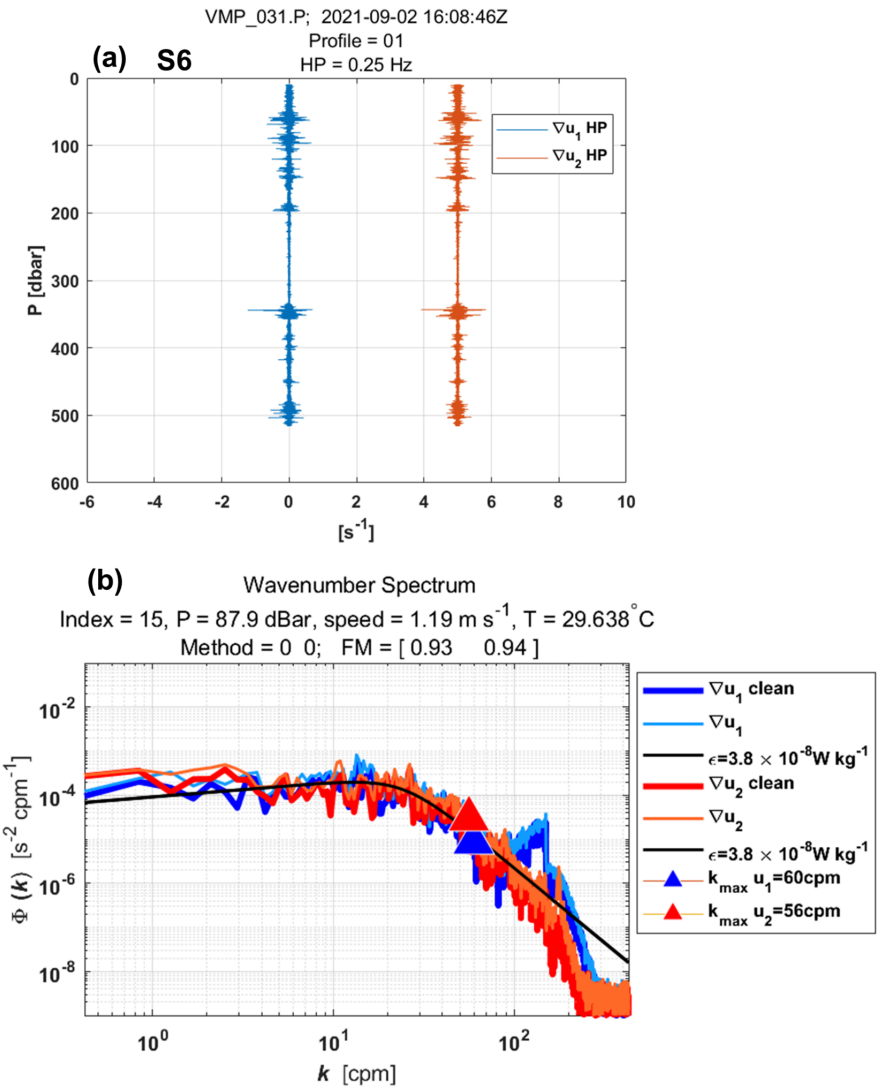

Figure 2: Example of wavenumber spectra from a dissipation structure segment used to determine the dissipation rate at station S6 at a pressure of 87.9 dBar. (a) Cleaned and high-pass filtered signals from shear probe 1 (blue) and shear probe 2 (red, offset by 5 s^{-1}). (b) Wavenumber spectra for shear probes 1 and 2. Thick lines (blue for probe 1, red for probe 2) show shear spectra with coherent noise correction, while thin lines (sky blue for probe 1, orange for probe 2) show spectra without correction. Triangles mark the maximum wavenumber used for dissipation rate estimation. Black lines represent Nasmyth reference spectra for estimated dissipation rate of 3.8 x 10^{-8} W kg^{-1} for both shear probes. Dissipation rate estimates for shear probe 1 and shear probe 2 at a pressure of 87.9 dBar yielded a figure of merit of 0.93 and 0.94, respectively.

The vertical eddy diffusivity coefficient

The efficiency of turbulence in redistributing energy is assessed through the calculation of the vertical eddy diffusivity coefficient (K_z). This coefficient is particularly significant in regions such as pycnoclines, where stratification suppresses mixing, making turbulence-driven mixing a key mechanism for vertical energy transport (Thorpe, 2007).

K_z is calculated from ε following the formulation of Osborn (1980), given by $K_z = \varepsilon\ \Gamma\ N^{-2}$. Here, N^2 is the buoyancy frequency squared, which is calculated using the sorted potential density profiles (σ_θ) obtained from CTD-O_2 data. It is given by $N^2 = -(g/\rho_0)(d\sigma_\theta/dz)$, where ρ_0 is a reference density (1025 kg m^{-3}) and g is the gravitational acceleration. Γ is the mixing efficiency, defined as the ratio between the buoyancy flux and the energy dissipation, and is typically set to 0.2, which corresponds to the critical Richardson number Ri = 0.17 (Osborn, 1980). ε is linearly interpolated into the depths of N^2.

Turbulence within the pycnocline can reduce stratification and increase vertical eddy diffusivity below the mixing layer (Thorpe, 2007). Subsurface mixing, driven by the breaking of ITs and shear instabilities, plays a particularly important role below the mixed layer, especially in equatorial waters (Gregg et al., 2003).

There are several criteria for defining the Mixed Layer Depth (MLD). In this study, we use the commonly accepted density threshold criterion of 0.03 kg m^{-3}, as defined by de Boyer Montégut et al. (2004) and Sutherland et al. (2014), to estimate the MLD for each CTD-O_2 profile. Notably, comparisons with density thresholds of 0.01 and 0.02 kg m^{-3} revealed no major differences in MLD across the AMAZOMIX stations and transects (Fig. A2, Appendix).

The miXing Layer Depth (XLD) is defined as the depth at which ε decreases to a background level (Sutherland et al., 2014). Previous studies have applied various thresholds for background dissipation levels, such as such as 10^{-8} and 10^{-9} W kg^{-1} in higher latitudes based on in situ observations (Sutherland et al., 2014; Lozovatsky et al., 2006; Cisewski et al., 2008; Brainerd and Gregg, 1995) and 10^{-5} m^2 s^{-1} using an ocean general circulation model (Noh and Lee, 2008). In this study, XLD is specified as the depth where ε drops from its first minimum value. This aligns with previous dissipation thresholds and ensures that mixing is captured independently of surface influences. The Upper (UTD) and Lower (LTD/LPD) Thermocline/Pycnocline Depth are delimited as defined by Assunçao et al (2020). UTD corresponded to the depth where the vertical temperature gradient $\partial\theta/\partial z$ = 0.1 ℃ m^{-1}, while LTD/LPD were the last depth below the UTD at which $N^2 \geq 10^{-4}$ s^{-2}.

Baroclinic currents

To analyze the processes explaining dissipation and mixing, particularly along internal tidal (IT) paths, we estimate shear instabilities associated with the semi-diurnal (M2) ITs and mean circulation, as well as their contributions to mixing.

The M2 tidal component of the tidal current is derived by calculating the baroclinic (semi-diurnal) tidal velocity $[u'', v'']$ (Fig. A3, Appendix), following these equations:

$$[u', v'] = [u, v] - [u_{bt}, v_{bt}], \quad (1)$$

$$[u_{bt}, v_{bt}] = \frac{1}{H}\int_{-H}^{0} [u, v]dz, \quad (2)$$

$$[u'', v''] = [u', v'] - [\overline{u'}, \overline{v'}]. \quad (3)$$

Here, $[u, v]$ represent total horizontal velocities (Fig. A3, Appendix) obtained from SADCP data. The components $[u', v']$ and $[u_{bt}, v_{bt}]$ represent baroclinic and barotropic components of horizontal velocities, respectively (Fig. A3, Appendix). H is water depth. The baroclinic mean velocities $[\overline{u'}, \overline{v'}]$ (Fig. A3, Appendix),

calculated to estimate mean circulation along IT paths, are decomposed into along-shore $\overline{u'}_l$ and cross-shore $\overline{u'}_c$ velocities. The overbar denotes the average over a M2 tidal period.

Note that continuously collected SADCP for some stations (e.g., S11) are not sufficiently resolved due to gaps filled by interpolating between time points. The similar processing are applied to the CTD-O_2 data collected alternately. SADCP time series data are less than 17 hours at all long stations, except for S14, which spans 42 hours. As a result, the diurnal and semidiurnal period fittings are not formally distinct (except at S14; Figs. A4 and A5, Appendix), and the inertial period (at least 5 days) cannot be resolved in our dataset. This limits our ability to separate currents by frequency and examine the associated dissipation.

The velocity profiles from LADCP are glued into our SADCP time series data below ~ 500 m depth at long stations.

To evaluate shear instabilities associated with ITs and the mean background circulation, we compute the baroclinic tidal vertical shear squared ($S^{2''}$) and mean shear squared ($\overline{S^{2'}}$) (Fig. A3, Appendix), as follows:

$$S^{2''} = (\partial u''/\partial z)^2 + (\partial v''/\partial z)^2, \quad (4)$$

$$\overline{S^{2'}} = (\partial \overline{u'}/\partial z)^2 + (\partial \overline{v'}/\partial z)^2. \quad (5)$$

To evaluate the impact of bottom friction on mixing, we calculate kinetic energy $\varepsilon_f = \frac{1}{2}\rho_s(u_f^2)$ near the bottom boundary layer at shallow stations using friction velocity $u_f = u_b\sqrt{C_d}$, where C_d=2.5 x 10^{-3} is a drag coefficient obtained from the NEMO model. Huang et al. (2019) showed that the bottom boundary layer thickness spatially varies between 15-123 m in the Atlantic Ocean, with a median of ~ 30-40 m in the North Atlantic. We define bottom layer thicknesses in our study area based on measured bathymetry from CTD-O_2 and near-bottom currents from ADCP. Here, u_b is the total velocity averaged over a thickness of 20 m above the seabed for shallow stations and 40 m for deep stations.

The individual contributions of semi-diurnal ITs and mean circulation are then expressed as follows: $E''/(\overline{E'} + E'')$ for tidal contribution and $\overline{E'}/(\overline{E'} + E'')$ for mean circulation contribution. Here, $E = N^2S$. N is the buoyancy frequency and S is vertical shear. S can be substituted by $S^{2''}$ and $\overline{S^{2'}}$.

Ray tracing calculation

Analyzing both the mean currents and the spatial dimension along the IT pathways offers another insight into the mechanisms responsible for observed mixing (Rainville and Pinkel, 2006). IT energy rays are generated in regions with steep topography, such as the shelf break, where IT slope matches with the bottom slope (i.e., critical slopes) before propagating within the ocean interior. These rays, moving both downward and upward, encounter the seasonal pycnocline, resulting in beam scattering and the formation of large IT oscillations. As these oscillations steepen, they disintegrate into nonlinear ISWs, a process known as "local generation" of ISWs (New and Pingree, 1992). To explore IT paths, ray-tracing techniques are employed, as previously used by New and Da Silva (2002) and Muacho et al. (2014), to investigate the effectiveness and expected pathways of the IT beams off the Amazon shelf. One main assumption in our linear-theory-based hypothesis is that stratification

remains horizontally uniform along the IT propagation path, although in reality, it may vary due to submesoscale and mesoscale variability. This limitation makes the ray tracing approach less realistic but still useful as a first-order estimate of energy distribution. The IT ray-tracing calculation assumes that in a continuously stratified fluid, ITs energy can be described by characteristic pathways of beams (or rays) with a slope c to the horizontal:

$$c = \pm\left(\frac{\sigma^2 - f^2}{N^2 - \sigma^2}\right)^{1/2}, \quad (6)$$

where σ is the M2 tidal frequency (1.4052×10^{-4} rad s^{-1}), and f is the Coriolis parameter. N^2 are obtained from time-averaged AMAZOMIX CTD-O_2, glued with monthly N^2 profiles from Amazon36 (NEMO model outputs, 2012-2016) below 1000 m depth. Amazon36 is a NEMO configuration, specifically designed to cover the western tropical Atlantic from the mouth of the Amazon River to the open sea (see Tchilibou et al., 2022; Assene et al., 2024; for configuration details and model description). IT ray-tracing diagrams are performed along the transects. Seasonal sensitivity tests of rays (August, September, October, and April) are conducted by varying the critical slope positions and N^2 to explore its influence and generate a set of ray paths consistent with characteristics of IT pathways (Figs. A6 and A7, Appendix).

”

Line 174: “… with overbar the average…”. A word seems to be missing between “overbar” and “the average”.

R: Thanks for your remarks. We have rewritten it in line 186 of the revised manuscript, as shown in your previous comment.

Line 183: “… for M2 semi-diurnal baroclinic energy)…”. The parenthesis after the word “energy” appears to be unnecessary!
R: Thanks for your remarks. We have rewritten the subsection “Baroclinic currents” in lines 176-186 of the revised manuscript, as shown in your previous comment.

Line 187: “Previous study of Huang et al. (2019) shown…”. Please revise grammar.

R: Thanks for your remarks. We have revised grammar in lines 202-203 of the revised manuscript, as shown in your previous comment.

Line 188: “… between 15-123 m in Ocean Atlantic”. Do you mean “Atlantic Ocean”?

R: Yes, thanks for your remarks. We have rewritten it in line 202 of the revised manuscript, as shown in your previous comment.

Line 209: “ and stitched…”. Please be consistent with jargon language.

R: Thanks for your remarks. We have rewritten it in line 193 of the revised manuscript, as shown in previous replies.

Results:

Line 218: "… . They are thicker along the IN-ITs…". If you are referring to the "step-like" structures from the previous line, consider using another word for "thicker", e.g. "larger".

R: Thanks for your remarks. We have rewritten it in lines 234-247 of the revised manuscript. The revision of section "Results" can be found below:

"

3.1.1 Thermohaline and IT features

In this subsection, we analyze the density profiles to gain insight into mixing processes and/or wave propagation. Step-like features are observed in the density profiles (Figs. 3a and 3b). During the M2 tidal period, step-like structures ~20-40 m in length occur at depths ranging from 80 to 160 m at stations S10, S12, S13, and S14 (Fig. 3a). These features are more pronounced along the IN-ITs transect Aa and Ab compared to the other transects (e.g., E and G; Figs. A8.a and A8.b, Appendix).

In this layer (between 60 and 170 m depth), significant vertical displacements, ranging from 20 to 60 m, are detected along transects Aa, Ab, and E (e.g., 40 m at S10, 48 m at S6, 52 m at S13, and 32 m at S14; Figs. 3a and 3b). The smallest displacements (~8 m at S25) are observed along the OUT-ITs transect G (Fig. A8.b, Appendix). These vertical displacements are also evident in the variability of the mixed layer depth (MLD), which fluctuates between 18 and 84 m over a semi-diurnal cycle (figure not shown).

In conclusion, the presence of step-like structures and isopycnal displacements suggests strong mixing in the water column, and supports the hypothesis of ITs propagating, with stronger energy along transects Aa and Ab, weaker energy along D and E, and almost absent along G (Fig. 1a).

"

In Figure 3 the choice of colours for dissipation rates (epsilon) is somewhat difficult to grasp. The colours "red" and "magenta" are sometimes confusing, particularly in the vertical profiles in Figs. 3b to 3e. Could the "red" colour be changed to a "light Orange", or similar?

R: Thank you for your comments and suggestions. The light orange color was already used in Figure 3 (as shown below for example) and is sometimes referenced in subsequent figures for analysis. We have changed the magenta color to purple to enhance visual clarity and make it more noticeable.

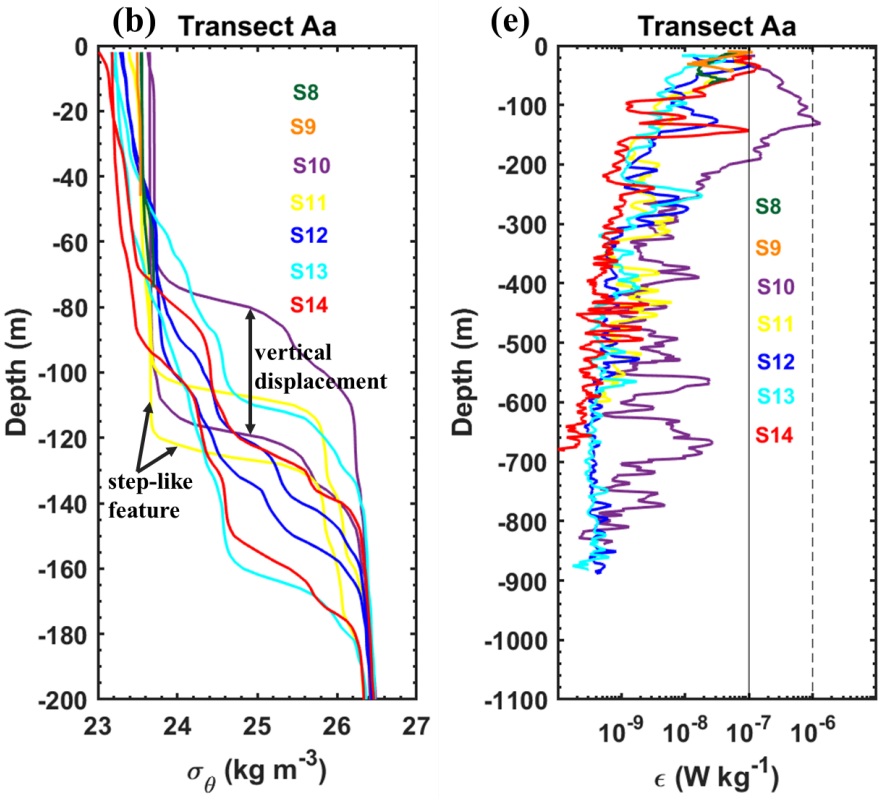

Figure RC3.1: *(b) Density profiles (σ_θ, kg m^{-3}) obtained from CTD-O_2 measurements during the AMAZOMIX 2021 cruise for stations S8 to S14 along transects Aa, located within IT fields. For long stations (S10-S14), two density profiles are shown to highlight step-like structures and isopycnal vertical displacements (illustrated by black arrows) along the transects. Distinct colors are used to represent each station within each transect. The density values for stations S8, and S9 range between 23.4 and 23.8 kg m^{-3}. (e) Vertical dissipation profiles for stations along transects Aa. Distinct colors are used to represent each station within each transect. Dashed and solid black lines in panel (e) are included for comparison purposes.*

Line 236: “Now, ….”; Unnecessary use of word “Now”.

R: Thanks for your remarks. We have rewritten it in line 256 of the revised manuscript.

Line 246: “….are found almost anywhere at S14…”; is there a better word than “anywhere” to be used in this sentence. Perhaps the words “at any depth” would be more appropriate?

R: Thanks for your remarks. We have rewritten it in lines 256-282 of the revised manuscript.

Line 247: “…shelf stations in the ITs regions, S3 and S5, ….” ; the vertical profile of station S3 does not appear in Fig. 3. (it appears only in Fig. A1.c). Please refer to where it appears.

R: Thanks for your remarks. We have rewritten it in lines 270-271 of the revised manuscript, as shown below:

“

For shelf/shallow stations within the ITs regions (S3 and S5; Fig. 4c, and Fig. A8.c, Appendix), mixing is more pronounced, between [10^{-6}, 10^{-5}] W kg^{-1}, near the bottom layer.

“.

Line 271: “… dissipation rates (epsilon) already presented in section 3.1.2, IS….”; do you mean “ARE also reported in Fig. 3”?

R: Yes, thanks for your remarks. We have rewritten it in lines 310-311 of the revised manuscript, as reported here:

“

Dissipation rates, previously presented in subsection 3.1.2 and shown in Fig. 4, are found to be 2-3 orders of magnitude higher in the pycnocline compared at greater depths.

“

In Figure 4b, the baroclinic tidal currents at S11 are less clear. Do you have any reason to suggest for this fact?

R: Thanks for your remarks.
This issue could be related to the temporal interpolation of the SADCP data. Continuous SADCP measurements revealed missing values (e.g., between 13:30 and 15:30) at S11. Interpolation allowed us to estimate current data corresponding to the dissipation times.

Line 287: “Now, …”; Unnecessary use of word “Now”.

R: Thanks for your remarks. We have rewritten it in line 329 of the revised manuscript.

Line 331: “IT ray paths were observed reflecting at the surface….”; The words “were observed” are not the best choice here, as you are talking about a model calculation; This reviewer suggests the use of the words “are expected to reflect” or “were predicted to reflect”.

R: Thanks for your remarks. We have rewritten it in lines 399-400 of the revised manuscript, as shown below:
“

After bottom reflection and subsequent interaction with the pycnocline, the rays are expected to reflect seaward at the surface, typically at distances between 115-400 km.

“.

Line 335: “flow becomes unstable beyond ….”; use the word “below” or beneath” instead of beyond?

R: Thanks for your remarks. We have rewritten it in lines 404-406 of the revised manuscript.

Line 336: “Large epsilon are encountered where IT rays presumably interfere between them or….”

This reviewer does not see “IT ray path interference, since the different ray tracing computations (in red and blue colours) are a matter of different stratification choices, and hence you either have a “blue” ray or a “red” ray.

R: Thanks for your comments.
Our IT interference hypothesis is based on ray-tracing calculations using various stratification scenarios and sensitivity tests, which revealed a packet of rays (see Fig. A19 of paper, Appendix, for example) as shown below in figure RC3.2. To explain the persistent high mixing observed at S14 in the open ocean, we also proposed constructive interference of IT rays originating from two generation sites, Aa and Ab, as discussed in lines 556-567 of the revised manuscript. This hypothesis will be further investigated in a subsequent study.

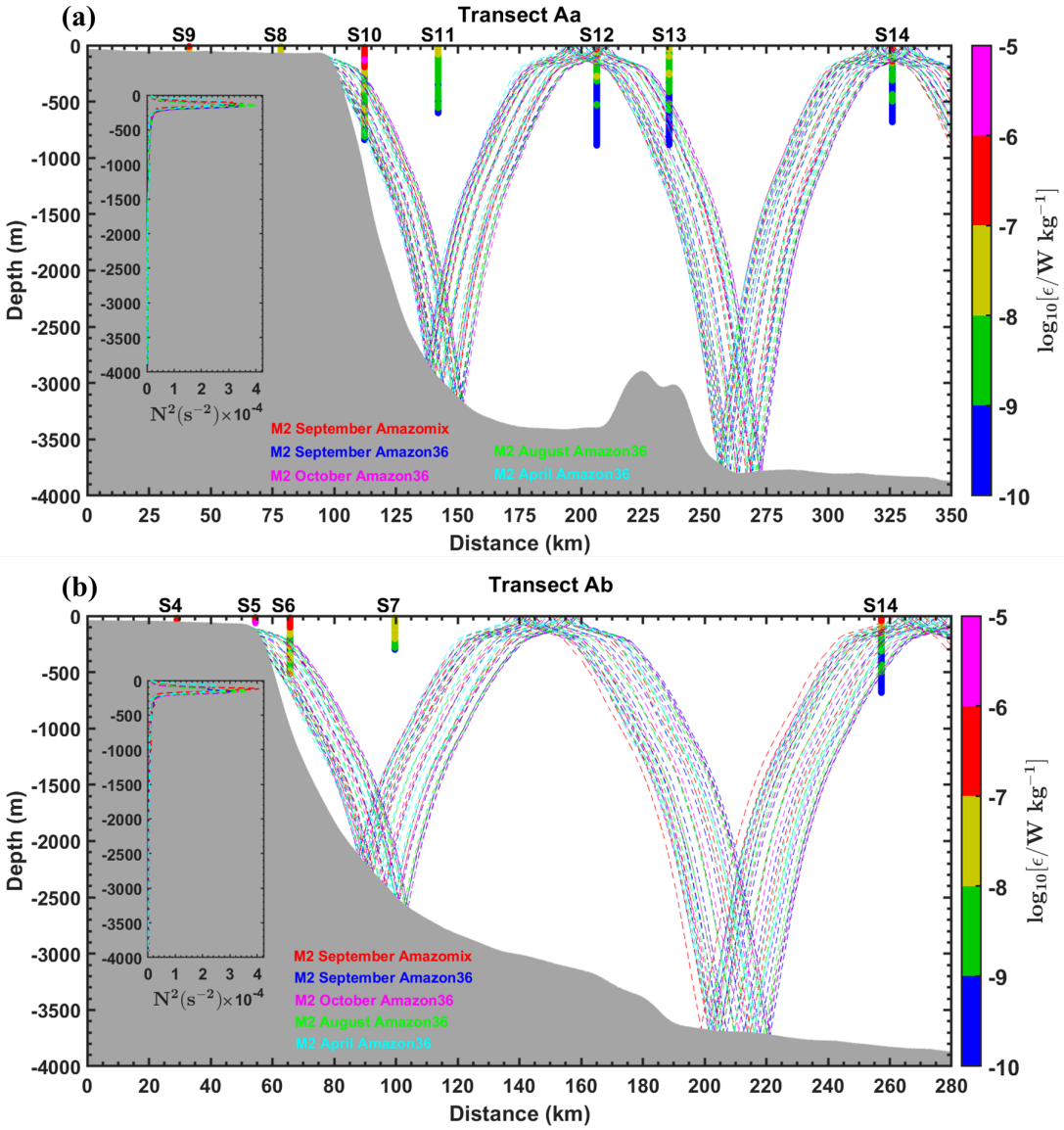

Figure RC3.2: *Sensitivity tests of M2 IT ray-tracing along the transects (a) Aa and (b) Ab, conducted by varying the location of the critical topography slope. The tests use mean buoyancy frequency squared (N^2, in s^{-2}) obtained from CTD-O_2 data (September 2021) and NEMO-Amazon36 model data (2012-2016). Dashed colored lines represent IT beams calculated for different seasons (April, August, October, and September) and for varying locations of the critical topography slope. Grey areas indicate local topography. Panels (a) and (b) also include dissipation rate profiles (ε, in W kg^{-1}, shown as vertical colored bars on a logarithmic scale) from the VMP measurements. Subpanels within each panel illustrate the N^2 profiles derived from AMAZOMIX and the NEMO-Amazon36 model, which were used in the ray-tracing calculations. For comparison, sensitivity tests using N^2 measurements from individual stations along the corresponding transect (e.g., at S10) revealed similar ray paths (not shown), consistent with the packet of rays obtained using the mean N^2.*

Line 338-339: “Some large epsilon are observed where IT rays radiated at the surface (e.g. at S12, S14 and S20)…..”; Large epsilon values are a common feature to all turbulence

profiles of dissipation rates near the surface. It looks more like the effect of wind mixing, rather than surfacing and reflection of IT rays.

R: Thanks for your comments.
Indeed, the mixing on the surface would also be linked to the effect of the wind.
Our study focuses more on the mixing observed outside of surface influence along IT paths, and the contribution of IT compared to other processes.

Line 353: “The next steps of our study IS…”; either use singular (“step”) or use correct tense (“ARE”).

R: Thanks for your remarks. We have rewritten it.
Ultimately, we decided to remove and reserve all sections on “Nutrients fluxes” for a separate paper in progress.

Discussion and Conclusion.

Line 398: “…., both large (up to 60 m length) isopycnal displacements…”; perhaps the wording “…, both large (up to 60 m) AMPLITUDE isopycnal displacements…” is more apropriate?

R: Yes. Thanks for your remarks. We have rewritten it in line 440 of the revised manuscript.

Revisions of section “Discussion and Conclusion” can be found below:

.
“

4 Discussion and Conclusion

The AMAZOMIX 2021 cruise provided, to the best of our knowledge, for the first time, direct measurements of turbulent dissipation using a velocity microstructure profiler (VMP) at multiple stations both inside and outside the influence of ITs. These measurements enabled the study of mixing processes at the Amazon Shelf break and the adjacent open ocean. To capture a full tidal cycle, data on turbulent dissipation rates, hydrography, and currents were collected alternately over 12 hours, with 4 to 5 profiles taken per station (see section 2). The locations of the 12-hour sampling stations were selected based on modeling results that provided realistic maps of IT generation, propagation and dissipation (Fig. 1a; Tchilibou et al., 2022). Stations were located in the most energetic regions of IT, specifically at sites Aa, Ab, and D, covering stations S2 to S14, as identified in previous studies (Magalhaes et al., 2016; Tchilibou et al., 2022; Assene et al., 2024). Stations S19 to S21 were positioned in less energetic IT generation areas at site E, while stations S24 and S25 were located outside the influence of the IT fields (site G). Stations were distributed across different areas, including the shelf (e.g., S4, S9, and S19), the shelf-break (e.g., S3, S6, and S10), and the open ocean (e.g., S14, S24, and S20).

Vertical Displacement, homogeneous layers

The results revealed that, over a semi-diurnal tidal cycle, relevant amplitudes of vertical displacements (up to 60 m in length) and pronounced step-like structures (up to 40 m thick) were observed along transects Aa and

Ab. In contrast, smaller and thinner structures were identified along other transects, such as E. These differences are likely related to the propagation of ITs, which induce vertical displacements at tidal frequencies and promote mixing by creating homogeneous layers visible as step-like features in the density structure. The isopycnal displacements and step-like structures observed within the pycnocline are consistent with findings from other IT regions (e.g., Stansfield et al., 2001; Simpson and Sharples, 2012; Bordois, 2015; Koch-Larrouy et al., 2015; Zhao et al., 2016; Bouruet-Aubertot et al., 2018; Xu et al., 2020). Furthermore, IT propagation appears to have stronger energy along transects Aa and Ab compared to others, consistent with prior modeling studies (Tchilibou et al., 2022; Assene et al., 2024).

Direct measurements of dissipation rate

Dissipation rates measured with the VMP ranged from between [10^{-10}, 10^{-5}] W kg^{-1} below the XLD, spanning from the continental shelf to the open ocean.

The highest dissipation rates, within [10^{-6}, 10^{-5}] W kg^{-1}, were observed primarily at generation sites Aa, Ab, and D (e.g., at stations S6, S10, and S3), as represented for A region in Fig. 9 (red zigzags). Slightly lower but still substantial dissipation rates, ranging from 10^{-8} to 10^{-7} W kg^{-1}, occurred a few kilometers (~40 km) from these generation sites (e.g., at S11 and S7), along IT pathways (e.g., at S12, S13, and S20), and even in regions farther from IT influence (e.g., at S24). Interestingly, dissipation rates were higher within [10^{-7}, 10^{-6}] W kg^{-1} in the open ocean, such as at station S14, located ~230 km from generation site Aa, as summarized in Fig. 9 (orange zigzags).

Using dissipation measurements, we calculated the XLD, defined as the depth where the dissipation rate drops from its first minimum value. The XLD was found to be greater than the MLD at all stations except S8, S10, and S25. This exception may reflect larger mixing events at those stations that were not captured during the VMP deployment. For the other, it is consistent with regions exhibiting strong subsurface shear, such as the equatorial ocean and western boundary current areas (Noh and Lee, 2008).

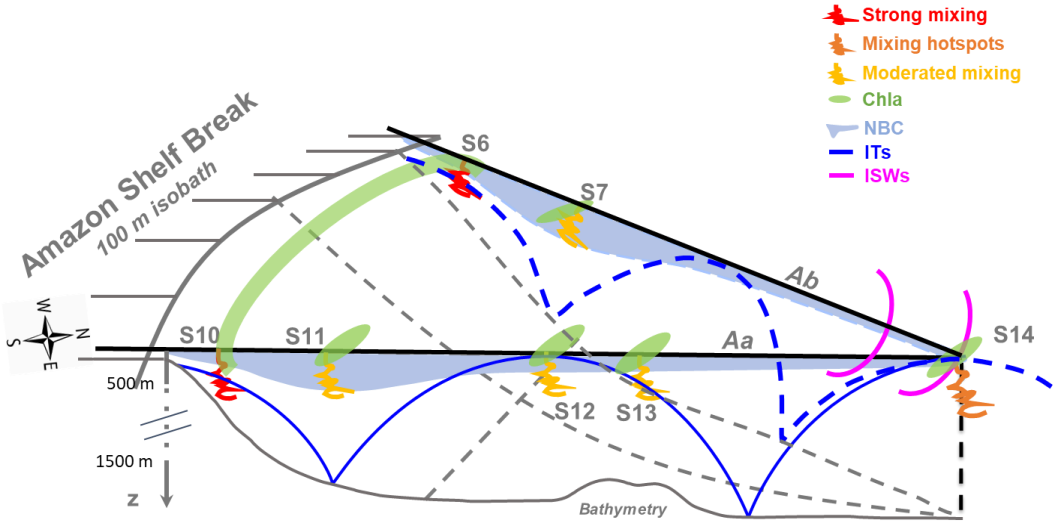

Figure 9: summary diagram illustrating the key processes driving mixing along the AMAZOMIX transects (e.g., Aa and Ab). At IT generation sites (e.g., S6 and S10; red zigzags), mixing rates are stronger, with ITs contributing around 65%, compared to mean circulation (NBC). Along IT pathways (e.g., S7 and S11; yellow zigzags), mixing decreases but remains notable, driven by nearly equal contributions from ITs and mean circulation. A key observation is the increased mixing ~ 230 km from two distinct IT generation sites at the shelf break. This hotspot at S14 (orange zigzags) coincides with the surfacing of IT rays (blue lines) from different sites, vanishing of the NBC (sky blue shaded areas) and the presence of ISWs (magenta lines), suggesting possible constructive interferences of IT rays may generate ISWs, amplifying mixing at S14. IT mixing observed close enough to the surface at these sites could influence the chlorophyll content (green shaded areas) off the Amazon shelf.

In other regions, dissipation rates exhibit values comparable to those observed in this study. For instance, at IT generation sites (S6 and S10), dissipation rates align with the range of [10^{-7}, 10^{-5}] W kg^{-1} reported for the Halmahera Sea, Indonesia (Koch-Larrouy et al., 2015; Bouruet-Aubertot et al., 2018), Kaena Ridge, Hawaii (Klymak et al., 2008), and the Changjiang Estuary (Yang et al., 2020). Conversely, along IT pathways off the Amazon shelf (e.g., S11 and S7), dissipation rates are higher ([10^{-8}] W kg^{-1}) than those documented in other regions, such as [10^{-10}, 10^{-8}] W kg^{-1} in the Southern Ocean (Gille et al., 2012) and the Halmahera Sea (Bouruet-Aubertot et al., 2018), that might be due to the cumulative effect of IT and NBC mixing and/or to their interaction that might intensified the local mixing. Lastly, in the open ocean, elevated dissipation rates were observed compared to previous studies. For instance, values of [10^{-9}, 10^{-8}] W kg^{-1} around 100 m depth at S25 were higher than values of [10^{-11}, 10^{-10}] W kg^{-1} reported by Takahashi and Hibiya (2019) for sites far from IT influence and under geostrophic current conditions. This discrepancy may be attributed to the strong mean background circulation investigated off the Amazon shelf (Dossa et al., in preparation).

Our study also found the highest dissipation rates at stations S3 and S5 of [10^{-6},10^{-4}] W kg^{-1} on the Amazon shelf , increasing near the bottom boundary layer. These findings compare well with values reaching up to 10^{-9} W kg^{-1} within a kilometer of the seabed in the Southern Ocean (Sheen et al., 2013) and up to 10^{-6} W kg^{-1} within a few meters from bottom topography off the Changjiang Estuary (Yang et al. 2020). This may indicate the presence of an active bottom boundary layer. Thus, kinetic energy of bottom flow was estimated using friction velocity, that was computed from total velocity averaged over the bottom-most 15 m for shallow stations. It showed bottom friction energy stronger between 16-35 J m^{-2} at S3 and S5 mainly and lower (< 3 J m^{-2}) in the other stations on shelf (e.g., at S8). These results are smaller but still important on the Amazon shelf and comparable to values (517 kJ m^{-2}) in the Drake Passage region (on the continental slope) of the Southern Ocean (Laurent et al., 2012). The bottom mixing at S3 and S5 can indirectly exert a control on pycnocline mixing on the Amazon shelf (Inall et al., 2021).

Enhanced surface mixing

The vertical eddy diffusivity coefficients were highest at the shelf break (e.g., at S3, S5, and S10), ranging from 10^{-3} to 10^{-0} m^2 s^{-1}. Away from the shelf break, diffusivity values were lower but remained substantial, within the range of 10^{-4} to 10^{-3} m^2 s^{-1} (e.g., at S2, S7, and S11). These mixing coefficients align with values reported in

other regions. For instance, vertical diffusivity falls within the range of 10^{-5} to 10^{-3} m^2 s^{-1}, as observed in the Luzon Strait (Tian et al., 2009), the Indonesian Sea (Koch-Larrouy et al., 2015; Bouruet-Aubertot et al., 2018), and the southern Yellow Sea (Xu et al., 2020).

Close to the surface, mixing coefficients remained significant, reaching up to 10^{-3} m^2 s^{-1} between 100-200 m depth and up to 10^{-2} m^2 s^{-1} above this layer at stations S6 and S10. These surface values are of the same order of magnitude as, but slightly higher than, those reported for the Halmahera Sea, Indonesia (Koch-Larrouy et al., 2015; Bouruet-Aubertot et al., 2018). In the open ocean, under the influence of ITs, mixing near the surface reached 10^{-4} m^2 s^{-1} at S14.

This elevated vertical eddy diffusivity close enough to the surface along IT paths may play a critical role in modulating heat transfer (e.g., Assene et al., 2024) and chlorophyll distribution (see green shaded areas in Fig. 9) (de Macedo et al., 2023; M'Hamdi et al., in preparation) observed off the Amazon shelf, as documented in the Indonesian region (Nugroho et al. 2018; Koch-Larrouy et al., 2010; Sprintall et al., 2014; Zaron et al., 2023).

Contribution of Background circulation and ITs to mixing

Mean baroclinic current shear

Another important aspect addressed in this study was quantifying the contributions of different processes to the observed heterogeneous mixing.

First, we analyse the mean baroclinic current (BC), a proxy for the background circulation. The BC was predominantly structured into a northwestward surface flow and a southeastward subsurface flow along the IT pathways. The strong surface flow toward the northwest is associated with the North Brazil Current (NBC), which originates from the northeastern coast of Brazil (e.g., Bourlès et al., 1999) and propagates along the Amazon shelf-break (e.g., at stations S7, S10, S11, S14, and S24). Conversely, the southeastward subsurface flow observed at stations such as S7 and S11 might result from NBC instability or the presence of a countercurrent at depth (Dossa et al., in preparation). At site E, the flow reversal observed at S21 - characterized by a southeastward surface flow and a northwestward subsurface flow - was located inside of the outer path of the Amazon plume. This reversal could be related with the influence of AWL formed by continental inputs (Prestes et al., 2018).

Both baroclinic flows demonstrated a significant potential for shear instability, with vertical shear ranging from 10^{-5} to 10^{-3} s^{-2} off the Amazon shelf. The shear associated with the NBC was particularly pronounced around the pycnocline (between 40 and 200 m depth) at sites Aa, Ab, and G (e.g., at S6, S7, S10, S11, S14, and S24). At site E, the shear instability was stronger (> 2.5 x 10^{-4} s^{-2}) at the base of the pycnocline (e.g., at S20), potentially associated with NBC retroflection near [5-6°N, 50°W] during the fall season (Didden and Schott, 1993). The higher BC shear observed at S21, where flow direction reversals occurred, could be associated with the presence of a subsurface cyclonic eddy (Dossa et al., in preparation).

ITs shear

Second, the baroclinic tidal current was extracted from the total baroclinic current, revealing significant semi-diurnal (M2) component signals around the pycnocline. These signals, characterized by higher tidal modes (3-5), were more pronounced at generation and propagation sites Aa and Ab (e.g., at S6, S10, and S14) compared to other sites. The tidal shear within the pycnocline layer (80-120 m) is consistent with the observed IT signal patterns and large vertical displacements. It was stronger, reaching up to 10^{-3} s^{-2}, near the generation sites Aa and Ab (at S6 and S10) and in the open ocean at S14. Further from the generation sites (e.g., at S7, S11, and S20), the IT shear was smaller but still notable (reaching up to 10^{-4} s^{-2}). This highlights the significant role of ITs in driving mixing processes, particularly within the pycnocline, where strong vertical shears were observed near the shelf-break compared to regions far away. Outside the IT fields, such as at S24, the persistent high vertical shear near the bottom topography could be attributed to the active bottom boundary layer (Inall et al., 2021).

IT/BC ratio

Both IT and BC shear contribute to mixing, with their relative dominance varying across sites. Near the generation sites on the shelf-break, IT shear dominated the IT/BC shear ratio, such as at S6 (61.4/38.6 %), S10 (65.8/34.2 %), and S21 (58.5/41.5 %). Along the IT paths, the contributions were nearly equal (~50/50 %) at locations farther from the generation sites (e.g., at S20, S7, S11, and S13), except at S14 in the open ocean, where IT shear remained dominant (58.5/41.5 %). These findings align with the presence of ITs at generation sites Aa, Ab, and E (Tchilibou et al., 2022; Assene et al., 2024) and the stronger energy associated with NBC cores, particularly at S7 and S11.

These results are consistent with previous studies that identified strong tidal shear near IT generation sites, such as the Halmahera Sea (Bouruet-Aubertot et al., 2018), the Changjiang Estuary (Yang et al., 2020), the northwest European continental shelf seas (Rippeth et al., 2005), and the southern Yellow Sea (Xu et al., 2020).

The most relevant finding of this study was the relative increase in mixing within the pycnocline layer, observed at S14 in the open ocean, far from the IT generation sites.

Discussion on the strong mixing at S14

Along the IT paths, elevated remote dissipation rates (within [10^{-7}, 10^{-6}] W kg^{-1}) were identified ~ 230 km from the shelf-break at S14.

This region is well known for intense IT dissipation, as shown by a realistic model (Tchilibou et al., 2022; Assene et al., 2024), and for the highest occurrences of ISWs generated by ITs (Fig. 1a; de Macedo et al., 2023), with large-amplitude ISWs exceeding 100 m clearly visible in satellite records (Brandt et al., 2002).

At station S14, where relative mixing increases, IT rays surfacing from two distinct IT generation sites coincide with the appearance of ISWs and mark the location where the NBC vanishes.

This region of wave-wave interactions can lead to the constructive interference of IT rays, potentially facilitating the emergence of higher tidal modes (New & Pingree, 1992; Silva et al., 2015; Barbot et al., 2022; Solano et al., 2023). These higher modes, in turn, could enhance the generation of nonlinear ISWs (e.g., Jackson et al., 2012) and contribute to the elevated dissipation rates (Xie et al., 2013), as observed at this station.

"

Line 426: "… It showed bottom FICTION"; I think you mean "bottom friction"?

R: Thanks for your remarks. We have rewritten it in line 490 of the revised manuscript, as shown in your previous comment.

In Figure 7 the legend for NBC is given, but it is not drawn in Figure 7.

R: Thanks for your comments. We have updated Figure 9 of revised manuscript as shown below in figure RC3.3.

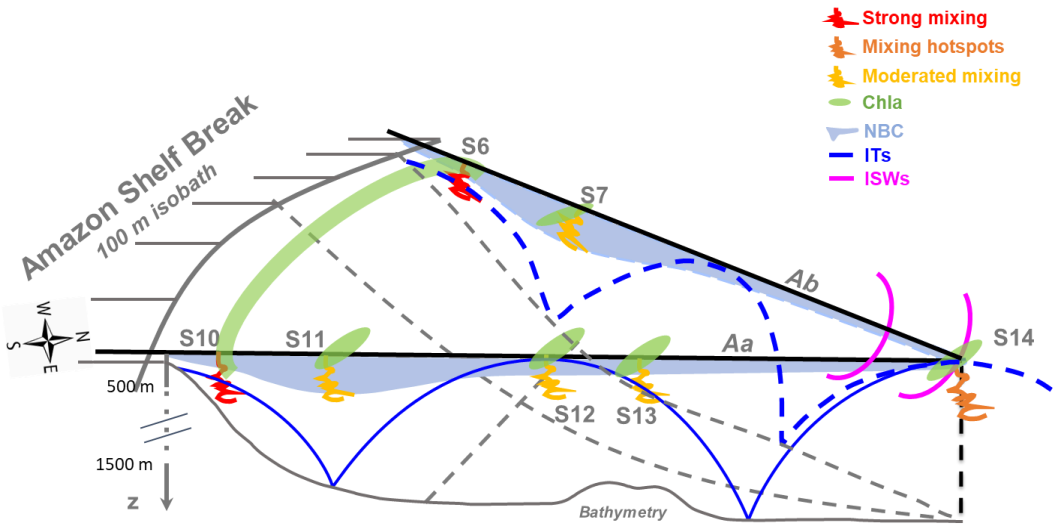

Figure RC3.3: summary diagram illustrating the key processes driving mixing along the AMAZOMIX transects (e.g., Aa and Ab). At IT generation sites (e.g., S6 and S10; red zigzags), mixing rates are stronger, with ITs contributing around 65%, compared to mean circulation (NBC). Along IT pathways (e.g., S7 and S11; yellow zigzags), mixing decreases but remains notable, driven by nearly equal contributions from ITs and mean circulation. A key observation is the increased mixing ~ 230 km from two distinct IT generation sites at the shelf break. This hotspot at S14 (orange zigzags) coincides with the surfacing of IT rays (blue lines) from different sites, vanishing of the NBC (sky blue shaded areas) and the presence of ISWs (magenta lines), suggesting possible constructive interferences of IT rays may generate ISWs, amplifying mixing at S14. IT mixing observed close enough to the surface at these sites could influence the chlorophyll content (green shaded areas) off the Amazon shelf.

Line 446: "This relative diminution….".; can you use another word for "diminution" that is more common in literature? Perhaps the word "decrease" suits what the authors want to say?

R: Thanks for your remarks. We have rewritten it in lines 538-549 of the revised manuscript, as shown in your previous comment.

Line 471: “The really new aspect raised in this study…”; Please avoid writing “The really new”. Something is either new or “not new”.

R: Thanks for your remarks. We have rewritten it in lines 553-554 of the revised manuscript, as shown in your previous comment.

Line 483: “ITs disintegrate into a package of ISWs events…”; Please use the word “packet” for ISWs because this is what became acknowledged in the literatute for groups of internal wave trains.

R: Thanks for your remarks. We have rewritten it in lines 557-567 of the revised manuscript, as shown in your previous comment.

Line 510: “…, ITs act as an important supplier of nutrient into….”; please use plural for “nutrients”.
R: Thanks for your remarks.
Ultimately, we decided to remove and reserve all sections on “Nutrients fluxes” for a separate paper in progress.

End

……

For Reviewer comments 3 RC3

Many thanks for the detailed correction of all typos and inconsistencies that were still present in the text. We have closely followed your recommendations to include the major and minor changes you have recommended and to restructure parts of the manuscript accordingly.

In this regard, we have revised and rewritten a few sections such as Abstract, method, results, discussion and conclusion in the revised manuscript. Quality control and revision of dissipation estimates, as well as current calculations were also done to ensure the validity of our results. We thought it useful to point out its detailed revisions (lines and sections) in the replies to your comments. Below (highlighted in blue and magenta) is an itemized response to the different issues raised in the review.
We believe that with all these additional changes and thanks to your valuable suggestions, we have achieved a marked improvement in the readability of the manuscript, as well as in the formal presentation and description of its main findings.

This paper reports on microstructure measurements off the Amazon shelf. This is an interesting area with a combination of various dynamical processes, internal tides, low frequency circulation and amazonian water lenses. Consistently with this dynamics contrasted dissipation rates are observed with the highest values at generation sites, and along internal tide pathways and the lowest values in no-tidal areas. The relative contribution to dissipation of the mean baroclinic current (North Brazil current) compared to that of internal tide was estimated : the contribution of IT shear was found larger than BC shear near generation sites, equal along IT pathways. In addition turbulent diffusive nutrient fluxes were computed : large values were obtained.

I think there is interesting material for publication but that part of the analysis must be revisited to provide convincing results before it could be accepted for publication. Some of the figures are overloaded and not easily readable, having many figures in the appendix does not facilitate a fluent reading. Part of the sections would need a careful polishing.

The main result to highlight is the spatial contrast of dissipation rates and give insights on the origin of these variations.

I list in the following my main general comments:

-More information on the background state should be given: bathymetry, sea surface salinity (Amazone plume), as well as the mean current and for instance information on generation sites for internal tides (reorganization of Figure 1 which is not easy to read, subplot (b) does not seem necessary)

R:Thank you for your comment.

We have updated the information on the background state, including bathymetry, the Amazon plume, internal tide generation sites, and mean circulation, and reorganized Figure 1 of the manuscript accordingly.

Revisions can be found in the "Introduction" section, lines 34-82, and the updated Figure 1 of the revised manuscript is provided below. We retained Figure 1b of the manuscript as it highlights the signature of the ISWs observed in the region during the AMAZOMIX cruise.

The revisions are shown below:

“

1 Introduction

Turbulent mixing in the ocean plays an important role in sustaining the thermohaline and meridional overturning circulation and in closing the global ocean energy budget (Kunze, 2017). These processes have strong implications for the climate, influencing heat and carbon transport, as well as nutrients supply for photosynthesis (Huthnance, 1995; Munk and Wunsch, 1998). Mixing processes can result from wind in the surface waters layer, internal waves and shear instability in the ocean interior, and bottom friction near the bottom layer (Miles, 1961; Thorpe, 2018; Ivey et al., 2020; Inall et al., 2021). Barotropic tides interacting with steep shelf-break topography trigger internal waves at tidal frequencies and harmonics, known as internal tides (ITs), which can propagate and produce mixing. These ITs can be expressed by large vertical displacements (up to tens of meters) of water masses (Garrett and Kunze, 2007). After their generation on the shelf-break, the (more unstable) higher modes of ITs may dissipate locally, while the lower modes can propagate far away (Zhao et al., 2016). IT beams (generated where the slope of the ITs and the topography match together on the shelf-break) can propagate vertically, resulting in reflection, scattering and dissipation of ITs at the bottom, surface waters, or thermocline levels (New and Da Silva, 2002; Gerkema and Zimmerman, 2008; Bordois, 2015; Zhao et al. 2016). They can also dissipate when energy fluxes interfere (Zhao et al., 2012) or interact with strong baroclinic eddies or currents (Rainville and Pinkel, 2006; Whalen et al., 2012). Furthermore, ITs may disintegrate into packets of higher-mode nonlinear internal solitary waves (ISWs), which can propagate and dissipate offshore (Jackson et al., 2012).

Previous and recent studies have shown that ITs-induced turbulent mixing can affect the surface, such as sea surface temperature (Ray and Susanto, 2016; Nugroho et al., 2018; Assene et al., 2024), chlorophyll content (Muacho et al., 2014; M’Hamdi et al., 2024; in preparation), marine ecosystems (Wang et al., 2007; Zaron et al., 2023), and atmospheric convection and the rainfall structure (Koch-Larrouy et al., 2010, Sprintall et al. 2014).

In the western tropical Atlantic, the Amazon River-Ocean Continuum (AROC) constitutes a key region of the global oceanic and climate system (Araujo et al., 2017; Varona et al., 2018). This region (Fig. 1a) is characterized by a system of western boundary currents, including North Brazil Current (NBC). NBC, which flows northwestward, has its core velocities (~ 1.2 m s^{-1}) that remain stable from the surface to a depth of 100 m (Johns et al., 1998; Bourlès et al., 1999; Barnier et al., 2001; Neto and Silva, 2014). This region also experiences

highly variable dynamics due to the Amazon River Plume. During the rainy season (May-July), peak discharge can extend the plume over 1500 km offshore, northwest along the NBC. In the dry season (September-November), reduced discharge and stronger saline intrusion may confine the plume to less than 500 km offshore, near the Amazon Shelf, with some eastward dispersion (Coles et al., 2013). The Amazon plume can generate vertical shear in underlying currents, enhancing mixing. Additionally, a system of Amazonian Lenses of water (AWL), influenced by continental inputs, may affect both the boundary layer and mixed layer patterns (Silva et al., 2005; Prestes et al., 2018).

In the AROC region, the Amazon shelf-break is a hotspot for the generation, propagation and dissipation of ITs and ISWs as a result of non-linear processes (Geyer, 1995; Brandt et al., 2002; Magalhães et al., 2016; Ruault et al., 2020; Tchilibou et al., 2022; Fig 1). Previous studies using Synthetic Aperture Radar (SAR) satellite images (Magalhaes et al., 2016) identified ISWs along the path of ITs propagating from two sites (i.e., sites Aa and Ab; Fig. 1a). Conversely, other sites showed no ISWs propagation (i.e., sites E and D; Fig. 1a, 1b and 1c) (see Magalhaes et al., 2016 for definition). Using numerical modeling, Tchilibou et al. (2022) showed that about 30 % of the M2 (dominant tidal component; Le Bars et al. 2010) ITs energy is dissipated locally (for higher-modes ITs) at sites E, Aa, Ab and D (Fig. 1a), while the remaining lower-modes ITs energy can be dissipated remotely. Dissipation away from the generation sites (E, Aa, Ab and D; Fig. 1a) can result from the shear instabilities caused by ITs-ITs and/or ITseddy/current interactions. Despite the presence of ITs, no direct measurements of dissipation rates have been conducted to our knowledge.

The mixing induced by these internal waves in the region was observed during the AMAZOMIX cruise (Bertrand et al., 2021). The cruise was designed with stations/transects inside and outside ITs fields (Fig. 1a and 1c) to measure ITs dissipation and study their impact on the AROC ecosystem. Direct microstructure measurements of temperature, salinity and velocity were conducted at the different repeated stations/transects over a M2 tidal cycle (~ 12.42 h). These cruise measurements offer an opportunity to explore whether ITs play a role in mixing within the AROC region. In this study, we will quantify mixing and identify the associated processes off the Amazon shelf. We will calculate turbulent kinetic energy (TKE) dissipation rates, vertical displacements of isopycnal surfaces and vertical eddy diffusivities using in situ microstructure and hydrography data. Finally, the baroclinic shear of currents and their contributions to mixing will be calculated from current data collected between stations and transects.

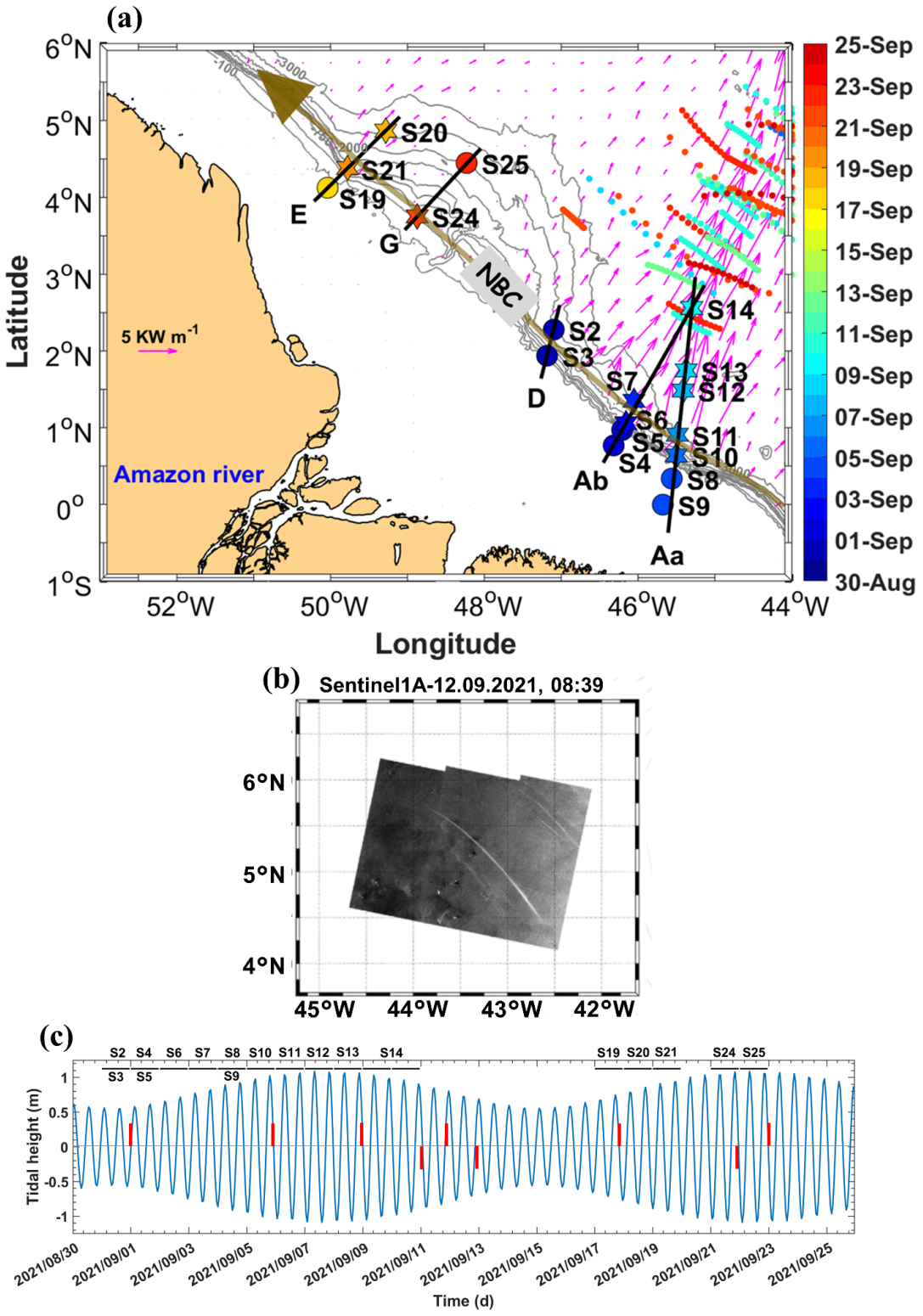

Figure 1: a) Map of a part of the AMAZOMIX 2021 cruise off the Amazon shelf, showing bathymetric contours (100 m, 750 m, 2000 m, and 3000 m isobaths) in gray. Colored circles and stars indicate short and long CTD-O2/L-S-ADCP stations, respectively, with the corresponding sampling dates represented by the color bar. Solid black lines depict SADCP transects (for Aa, Ab, D, G, and E). Magenta arrows show the 25-hour mean depth-integrated baroclinic IT energy flux (September 2015, from the NEMO model) originating from IT generation sites (Aa, Ab, D, and E) along the shelf break. The solid brown line represents the NBC pathways

illustrating background circulation. Shattered colored lines highlight ISW signatures. b) 1A Sentinel image acquired on 12th September 2021, showing ISW signatures. c) Tidal range at AMAZOMIX stations, with ISW signature dates marked by red bars.

“

-Baroclinic currents and energy : it is unclear why a parameterization of e is referred to as baroclinic total energy. The MG parameterization does not provide any relevant information (the correlation with epsilon is not clear and it is used as a proxy to evaluate the contribution of tidal shear and low frequency shear which I find questionable)

R: Thank you for your comment.

Indeed, the MacKinnon-Gregg parameterization was applied as a proxy to evaluate the contributions of tidal and low-frequency shear, primarily for comparison purposes. However, no scientific results were derived from it in this study.

Ultimately, we decided to remove the section using the parameterization and reserve the study and comparison of in-situ data to mixing parameterization for a separate paper in progress. In our paper, we used the vertical shear to assess the contributions of tidal and mean shear.

Revisions can be found in the "Methods" section, lines 120–230, as shown below:

“

2.2 Methods

TKE dissipation rates

The VMP data are processed using ODAS Matlab library (developed by Rockland Scientific International, Inc) to infer the TKE dissipation rate (ε). The processing methods for the VMP data are briefly described here and adhere to the recommendations of ATOMIX (Analyzing ocean turbulence observations to quantify mixing), as reported by Lueck et al. (2024), and have been validated against the benchmark estimates (presented in Fer et al., 2024).

First, the VMP data are converted into physical shear units, and the time series are prepared. Continuous sections of the time series are selected for dissipation estimation. Before spectral estimation, the aberrant shear signals caused by vessel wake contamination are removed. Collisions of the shear probe with plankton and other particles are removed using the de-spiking routine. The records from each section are then high-pass filtered (e.g., at station S6 and S10; Fig. 2a, and Fig. A1, Appendix).

Shear spectra are estimated using record lengths (L) and Fast Fourier Transform segments of 2 s, which are cosine windowed and overlapped by 50% (e.g., at station S6 and S10; Fig. 2b, and Fig. A1, Appendix). Additionally, vibration-coherent noise is removed. Different L and overlap (O) settings were selected and tested based on the environment (e.g., deep vs. shallow water), following Fer et al. (2024). For shallow stations, L (O) was shortened to 5 s (2.5 s), in contrast to the 8 s (4 s) used for deeper stations, due to evidence of overturns

observed in AMAZOMIX acoustic measurements at deeper stations (Koch-Larrouy et al., 2024; in preparation). This adjustment helped to optimize the spatial resolution of dissipation estimates in shallow water stations.

Finally, ε is determined using the spectral integration method and by comparison with the Nasmyth empirical spectrum (Nasmyth, 1970). Quality assurance tests are carried out in accordance with ATOMIX's recommendations (Lueck et al., 2024). A figure of merit < 1.4 is used to exclude bad data (e.g., at station S6 and S10; Fig. 2b, and Fig. A1, Appendix), and the fraction of data affected by de-spiking is < 0.05.

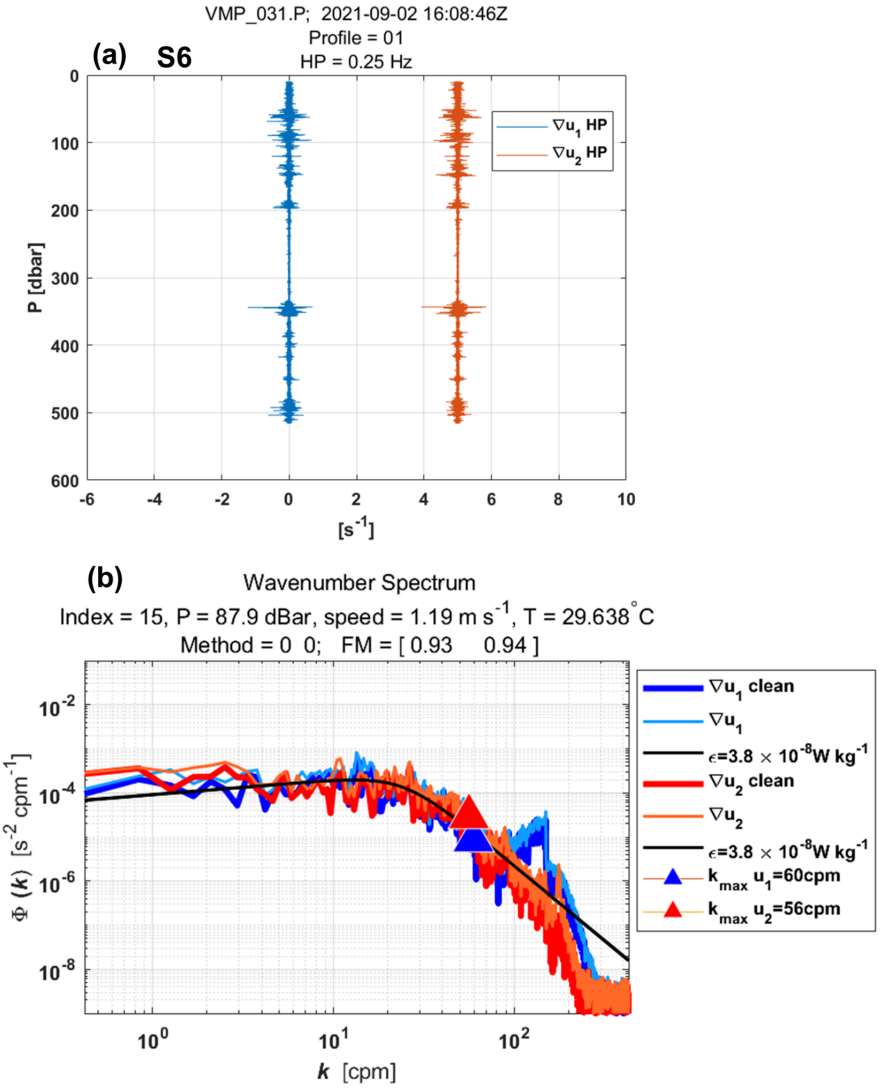

Figure 2: Example of wavenumber spectra from a dissipation structure segment used to determine the dissipation rate at station S6 at a pressure of 87.9 dBar. (a) Cleaned and high-pass filtered signals from shear probe 1 (blue) and shear probe 2 (red, offset by 5 s^{-1}). (b) Wavenumber spectra for shear probes 1 and 2. Thick lines (blue for probe 1, red for probe 2) show shear spectra with coherent noise correction, while thin lines (sky blue for probe 1, orange for probe 2) show spectra without correction. Triangles mark the maximum wavenumber used for dissipation rate estimation. Black lines represent Nasmyth reference spectra for estimated

dissipation rate of 3.8 x 10^{-8} W kg^{-1} for both shear probes. Dissipation rate estimates for shear probe 1 and shear probe 2 at a pressure of 87.9 dBar yielded a figure of merit of 0.93 and 0.94, respectively.

The vertical eddy diffusivity coefficient

The efficiency of turbulence in redistributing energy is assessed through the calculation of the vertical eddy diffusivity coefficient (K_z). This coefficient is particularly significant in regions such as pycnoclines, where stratification suppresses mixing, making turbulence-driven mixing a key mechanism for vertical energy transport (Thorpe, 2007).

K_z is calculated from ε following the formulation of Osborn (1980), given by $K_z = \varepsilon\ \Gamma\ N^{-2}$. Here, N^2 is the buoyancy frequency squared, which is calculated using the sorted potential density profiles (σ_θ) obtained from CTD-O_2 data. It is given by $N^2 = -\ (g/\rho_0)\ (d\sigma_\theta/dz)$, where ρ_0 is a reference density (1025 kg m^{-3}) and g is the gravitational acceleration. Γ is the mixing efficiency, defined as the ratio between the buoyancy flux and the energy dissipation, and is typically set to 0.2, which corresponds to the critical Richardson number Ri = 0.17 (Osborn, 1980). ε is linearly interpolated into the depths of N^2.

Turbulence within the pycnocline can reduce stratification and increase vertical eddy diffusivity below the mixing layer (Thorpe, 2007). Subsurface mixing, driven by the breaking of ITs and shear instabilities, plays a particularly important role below the mixed layer, especially in equatorial waters (Gregg et al., 2003).

There are several criteria for defining the Mixed Layer Depth (MLD). In this study, we use the commonly accepted density threshold criterion of 0.03 kg m^{-3}, as defined by de Boyer Montégut et al. (2004) and Sutherland et al. (2014), to estimate the MLD for each CTD-O_2 profile. Notably, comparisons with density thresholds of 0.01 and 0.02 kg m^{-3} revealed no major differences in MLD across the AMAZOMIX stations and transects (Fig. A2, Appendix).

The miXing Layer Depth (XLD) is defined as the depth at which ε decreases to a background level (Sutherland et al., 2014). Previous studies have applied various thresholds for background dissipation levels, such as such as 10^{-8} and 10^{-9} W kg^{-1} in higher latitudes based on in situ observations (Sutherland et al., 2014; Lozovatsky et al., 2006; Cisewski et al., 2008; Brainerd and Gregg, 1995) and 10^{-5} m^2 s^{-1} using an ocean general circulation model (Noh and Lee, 2008). In this study, XLD is specified as the depth where ε drops from its first minimum value. This aligns with previous dissipation thresholds and ensures that mixing is captured independently of surface influences. The Upper (UTD) and Lower (LTD/LPD) Thermocline/Pycnocline Depth are delimited as defined by Assunçao et al (2020). UTD corresponded to the depth where the vertical temperature gradient $\partial\theta/\partial z$ = 0.1 ℃ m^{-1}, while LTD/LPD were the last depth below the UTD at which $N^2 \geq 10^{-4}$ s^{-2}.

Baroclinic currents

To analyze the processes explaining dissipation and mixing, particularly along internal tidal (IT) paths, we estimate shear instabilities associated with the semi-diurnal (M2) ITs and mean circulation, as well as their contributions to mixing.

The M2 tidal component of the tidal current is derived by calculating the baroclinic (semi-diurnal) tidal velocity $[u'', v'']$ (Fig. A3, Appendix), following these equations:

$$[u', v'] = [u, v] - [u_{bt}, v_{bt}], \quad (1)$$

$$[u_{bt},\ v_{bt}] = \frac{1}{H}\int_{-H}^{0}[u,\ v]dz, \quad (2)$$

$$[u'',\ v''] = [u',\ v'] - [\overline{u'},\ \overline{v'}]. \quad (3)$$

Here, $[u,\ v]$ represent total horizontal velocities (Fig. A3, Appendix) obtained from SADCP data. The components $[u',\ v']$ and $[u_{bt},\ v_{bt}]$ represent baroclinic and barotropic components of horizontal velocities, respectively (Fig. A3, Appendix). H is water depth. The baroclinic mean velocities $[\overline{u'},\ \overline{v'}]$ (Fig. A3, Appendix), calculated to estimate mean circulation along IT paths, are decomposed into along-shore $\overline{u'}_l$ and cross-shore $\overline{u'}_c$ velocities. The overbar denotes the average over a M2 tidal period.

Note that continuously collected SADCP for some stations (e.g., S11) are not sufficiently resolved due to gaps filled by interpolating between time points. The similar processing are applied to the CTD-O_2 data collected alternately. SADCP time series data are less than 17 hours at all long stations, except for S14, which spans 42 hours. As a result, the diurnal and semidiurnal period fittings are not formally distinct (except at S14; Figs. A4 and A5, Appendix), and the inertial period (at least 5 days) cannot be resolved in our dataset. This limits our ability to separate currents by frequency and examine the associated dissipation.

The velocity profiles from LADCP are glued into our SADCP time series data below ~ 500 m depth at long stations.

To evaluate shear instabilities associated with ITs and the mean background circulation, we compute the baroclinic tidal vertical shear squared ($S^{2''}$) and mean shear squared ($\overline{S^{2'}}$) (Fig. A3, Appendix), as follows:

$$S^{2''} = (\partial u''/\partial z)^2 + (\partial v''/\partial z)^2, \quad (4)$$

$$\overline{S^{2'}} = (\partial \overline{u'}/\partial z)^2 + (\partial \overline{v'}/\partial z)^2. \quad (5)$$

To evaluate the impact of bottom friction on mixing, we calculate kinetic energy $\varepsilon_f = \frac{1}{2}\rho_s(u_f^2)$ near the bottom boundary layer at shallow stations using friction velocity $u_f = u_b\sqrt{C_d}$, where C_d=2.5 x 10^{-3} is a drag coefficient obtained from the NEMO model. Huang et al. (2019) showed that the bottom boundary layer thickness spatially varies between 15-123 m in the Atlantic Ocean, with a median of ~ 30-40 m in the North Atlantic. We define bottom layer thicknesses in our study area based on measured bathymetry from CTD-O_2 and near-bottom currents from ADCP. Here, u_b is the total velocity averaged over a thickness of 20 m above the seabed for shallow stations and 40 m for deep stations.

The individual contributions of semi-diurnal ITs and mean circulation are then expressed as follows: $E''/(\overline{E'} + E'')$ for tidal contribution and $\overline{E'}/(\overline{E'} + E'')$ for mean circulation contribution. Here, $E = N^2S^2$. N is the buoyancy frequency and S is vertical shear. S can be substituted by $S^{2''}$ and $\overline{S^{2'}}$.

Ray tracing calculation

Analyzing both the mean currents and the spatial dimension along the IT pathways offers another insight into the mechanisms responsible for observed mixing (Rainville and Pinkel, 2006). IT energy rays are generated in

regions with steep topography, such as the shelf break, where IT slope matches with the bottom slope (i.e., critical slopes) before propagating within the ocean interior. These rays, moving both downward and upward, encounter the seasonal pycnocline, resulting in beam scattering and the formation of large IT oscillations. As these oscillations steepen, they disintegrate into nonlinear ISWs, a process known as "local generation" of ISWs (New and Pingree, 1992). To explore IT paths, ray-tracing techniques are employed, as previously used by New and Da Silva (2002) and Muacho et al. (2014), to investigate the effectiveness and expected pathways of the IT beams off the Amazon shelf. One main assumption in our linear-theory-based hypothesis is that stratification remains horizontally uniform along the IT propagation path, although in reality, it may vary due to submesoscale and mesoscale variability. This limitation makes the ray tracing approach less realistic but still useful as a first-order estimate of energy distribution. The IT ray-tracing calculation assumes that in a continuously stratified fluid, ITs energy can be described by characteristic pathways of beams (or rays) with a slope c to the horizontal:

$$c = \pm\left(\frac{\sigma^2 - f^2}{N^2 - \sigma^2}\right)^{1/2}, \qquad (6)$$

where σ is the M2 tidal frequency (1.4052×10^{-4} rad s^{-1}), and f is the Coriolis parameter. N^2 are obtained from time-averaged AMAZOMIX CTD-O_2, glued with monthly N^2 profiles from Amazon36 (NEMO model outputs, 2012-2016) below 1000 m depth. Amazon36 is a NEMO configuration, specifically designed to cover the western tropical Atlantic from the mouth of the Amazon River to the open sea (see Tchilibou et al., 2022; Assene et al., 2024; for configuration details and model description). IT ray-tracing diagrams are performed along the transects. Seasonal sensitivity tests of rays (August, September, October, and April) are conducted by varying the critical slope positions and N^2 to explore its influence and generate a set of ray paths consistent with characteristics of IT pathways (Figs. A6 and A7, Appendix).

”

-Ray tracing calculation is applied but horizontal density gradients are neglected : this assumption is surprising owing to the major influence of the mean baroclinic flow.

Also in Figure 5 it would be more clear regarding the IT ray paths to consider the full water column

R: Thank you for your comment.

Indeed, our ray-tracing calculation neglected horizontal density gradients and the mean baroclinic flow, which we acknowledge as a limitation. In our study, the ray-tracing calculation superimposed with mean current data is used as another tool to gain insights into the mechanisms driving the observed mixing along the IT path. Indeed, change in density along the propagation path will affect the wavelength and beams of the rays.

To try to assess the potential influence of horizontal density gradients, we have tested different N2 profiles at specific stations (e.g., S10, S12, and S14) along transect Aa. The sensitivity tests (Figure RC2.1) demonstrated that ray paths align within the packets of rays observed when using mean N2 profiles at different times (e.g., in September and October; Figure RC2.2). Similarly, the influence of mean circulation could be very important for the ray. This question is beyond the scope of this study, and is tackled in

another paper we are working on using model results. Both influences-stratification and background circulation—are discussed in the sections "Methods" (lines 220–230) and "Results" (lines 232–414) of the revised manuscript.

In Figure 5 of the revised manuscript, we considered the full water column for internal tide (IT) ray paths, as depicted in the figure RC2.2. However, the y-axis in the manuscript is limited to 1000 m depth to enhance the visibility of dissipation profiles, density/stratification.

The influence of stratification and mean current on mixing and IT ray paths using ray-tracing calculations will be explored in a separate modelling paper.

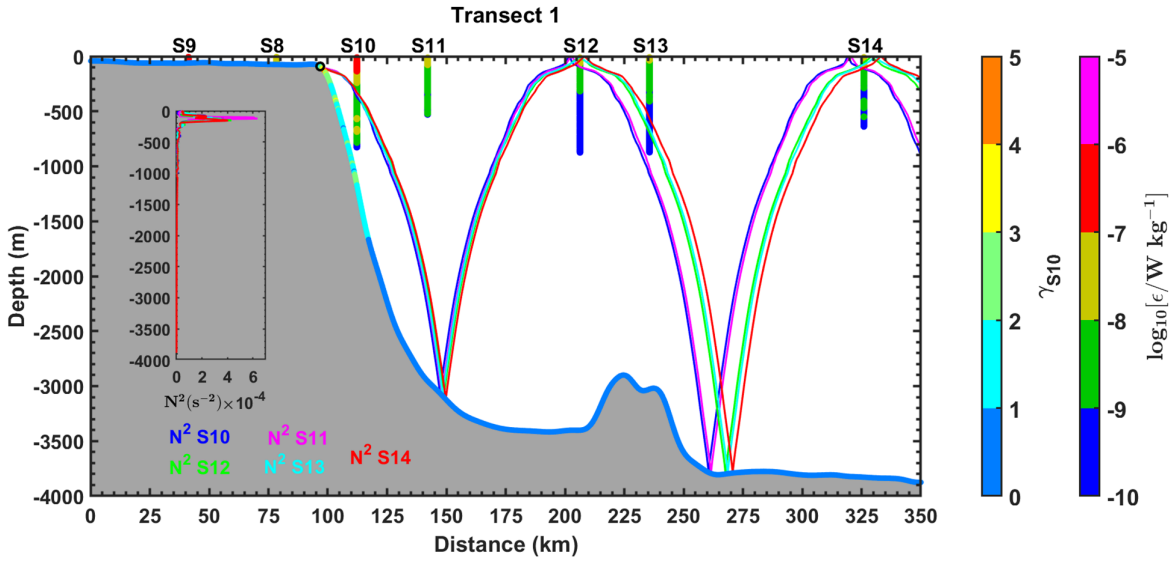

figure RC2.1: Example of sensitivity tests with different cross-sectional measurements of N^2 along the transect T1 N^2. colors are used to distinguish different cross-shore measurements of N^2 for corresponding stations on T1. Topography steepness (gamma = ray slope / topography slope) for T1 using measured N^2 of S10. Gamma is illustrated by the colored bar (named gamma S10).

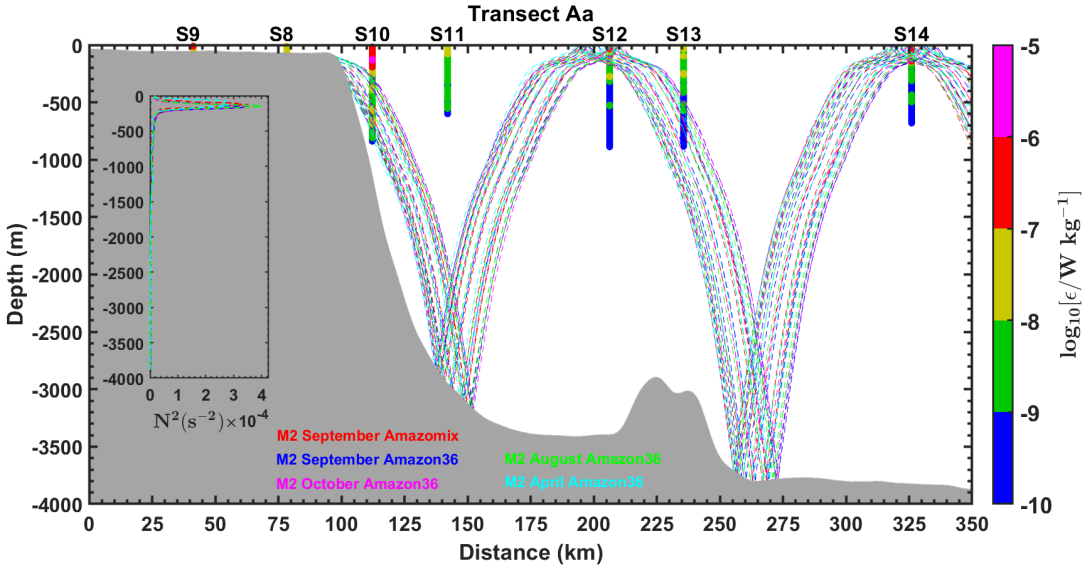

figure RC2.2: Sensitivity tests of M2 IT ray-tracing along the transects Aa, conducted by varying the location of the critical topography slope. The tests use mean buoyancy frequency squared (N^2, in s^{-2}) obtained from CTD-O_2 data (September 2021) and NEMO-Amazon36 model data (2012-2016). Dashed colored lines represent IT beams calculated for different seasons (April, August, October, and September) and for varying locations of the critical topography slope. Grey areas indicate local topography. Panel also includes dissipation rate profiles (ε, in W kg^{-1}, shown as vertical colored bars on a logarithmic scale) from the VMP measurements. Subpanels within each panel illustrate the N^2 profiles derived from AMAZOMIX and the NEMO-Amazon36 model, which were used in the ray-tracing calculations. For comparison, sensitivity tests using N^2 measurements from individual stations along the corresponding transect (e.g., at S10) revealed similar ray paths (not shown), consistent with the packet of rays obtained using the mean N^2.

Revisions can be found in the "Method/Ray tracing calculation" section, in lines 218–221 and 228-230 of revised manuscript, as shown below:

“

One main assumption in our linear-theory-based hypothesis is that stratification remains horizontally uniform along the IT propagation path, although in reality, it may vary due to submesoscale and mesoscale variability. This limitation makes the ray tracing approach less realistic but still useful as a first-order estimate of energy distribution..

“

“

Seasonal sensitivity tests of rays (August, September, October, and April) are conducted by varying the critical slope positions and N^2 to explore its influence and generate a set of ray paths consistent with characteristics of IT pathways (Figs. A6 and A7, Appendix)..

“

-Figure 3 : it is difficult to have a view on the evolution along the transects, why not show e profils along the transect with density superimposed, some large values at the end of the e profils would need to be checked (S12 and S14 in Fig. 3. and 3.e as well as S2 figA.1.c)

R: Thank you for your comment.

Indeed, the evolution of dissipation profiles, as well as, density along the transect were shown in Figure 8 of revised manuscript and figures in appendix. An example is shown in the figure RC2.4 below.

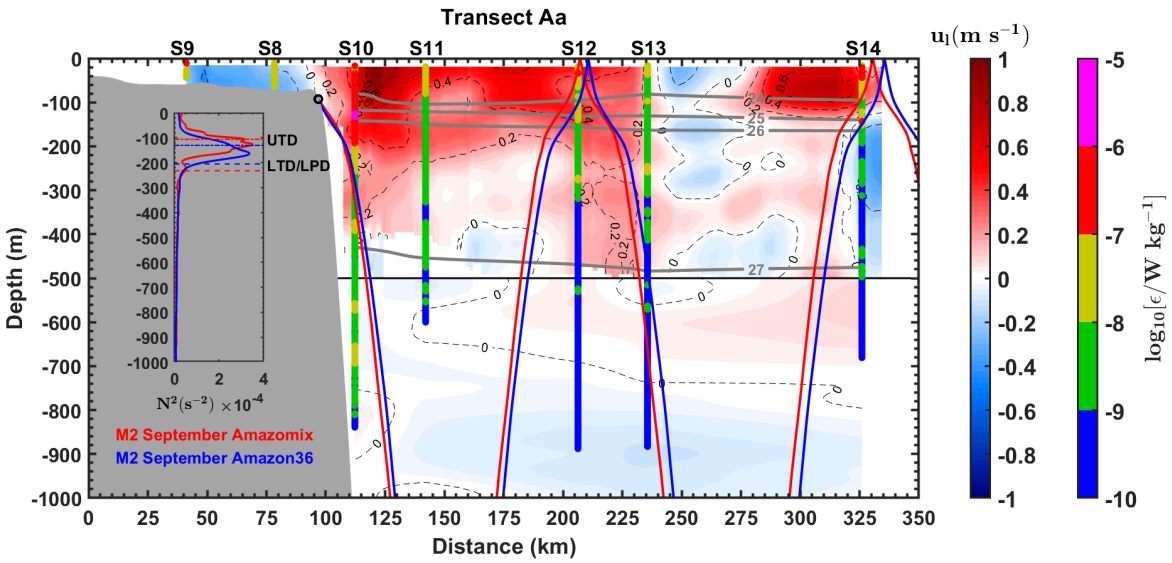

Figure RC2.4: IT ray-tracing diagrams for the M2 tidal constituent along transects Aa. The calculations were performed using the mean buoyancy frequency squared (N^2, in s^{-2}) obtained from CTD-O_2 data (ray in red) and NEMO-Amazon36 model data (ray in blue) for September. Grey areas represent local topography and black circles indicate the critical topography slope (ray generation sites). Panel also show along the transects Aa: along-shore mean total currents (u_l, in m s^{-1}) from ADCP (Dashed black lines), potential density from CTD-O_2 (grey contours), and dissipation rate profiles (ε, in W kg^{-1}, on a logarithmic scale) from the VMP (vertical colored bars). Subpanels within each panel illustrate the N^2 profiles from AMAZOMIX (red line) and the NEMO-Amazon36 model (blue line) used for ray-tracing calculations. Upper Thermocline Depth (UTD, dotted lines) and Lower Thermocline/Pycnocline Depth (LTD/LPD, dashed lines) are also indicated.

We have revised the important values at the end of the e profiles at these stations (S12, S14, and S2).

Revisions and checks of the VMP profile processing and dissipation estimates have been carried out, along with quality assurance tests, in alignment with all reviewers' comments and ATOMIX's recommendations (Lueck et al., 2024).

a) First, the revisions were focused on the VMP profile processing, particularly on:

- Parameters controlling shear spectra estimation, such as record lengths (L), which are cosine-windowed and overlapped (O) by 50%.
- Parameter for extracting the section or profile (continuous part of the time series), including the minimum depth of extraction (Pmin).

For shallow stations, we used L = 5 s and O = 2.5 s, instead of the previous L = 4 s and O = 2 s. Parameters for deep stations remain unchanged (L = 8 s and O = 4 s).

Additionally, we adjusted the minimum depth of extraction to Pmin = 10 m for deep stations and Pmin = 3 m for shallow stations, compared to the previously used value of Pmin = 1 m for both station types.

b) Second, the revisions and checks focused on the quality assurance measures for dissipation estimates, with quality control checks and adjustments applied across all stations (e.g., S2, S7, S12, S14).

For instance, at station S14, previous dissipation estimates showed some peaks at various depths, particularly between 100–200 m, 300–400 m, and 500–700 m. While the fraction of shear data affected by despiking during processing was <0.05, the figure of merit (FM)—used to filter out poor-quality data—for shear probe 1 was >>1.4 at certain depths (e.g., around 327 m compared to 122 m, as shown in figure RC2.5). In contrast, the FM for shear probe 2 remained <1.4.

After checks, quality control of dissipation estimates have been revised for all stations (e.g., S6, S10, S14). We have retained only dissipation estimates from either one or both probes that met the quality assurance criteria (FM < 1.4 and fraction of despiked shear data <0.05, as recommended by ATOMIX), as shown at S6 and S10 for example (figure RC2.6).

The final dissipation estimate was computed as the average of the estimates from both shear probes, followed by the mean of the dissipation profiles for the station, as illustrated in figure RC2.7.

The revision of section “methods/TKE dissipation rates” can be found in lines 169-194, in text, as shown below:

“

The VMP data are processed using ODAS Matlab library (developed by Rockland Scientific International, Inc) to infer the TKE dissipation rate (ε). The processing methods for the VMP data are briefly described here and adhere to the recommendations of ATOMIX (Analyzing ocean turbulence observations to quantify mixing), as reported by Lueck et al. (2024), and have been validated against the benchmark estimates (presented in Fer et al., 2024).

First, the VMP data are converted into physical shear units, and the time series are prepared. Continuous sections of the time series are selected for dissipation estimation. Before spectral estimation, the aberrant shear signals caused by vessel wake contamination are removed. Collisions of the shear probe with plankton and other particles are removed using the de-spiking routine. The records from each section are then high-pass filtered (e.g., at station S6 and S10; Fig. 2a, and Fig. A1, Appendix).

Shear spectra are estimated using record lengths (L) and Fast Fourier Transform segments of 2 s, which are cosine windowed and overlapped by 50% (e.g., at station S6; Fig. 2b, and Fig. A1, Appendix). Additionally, vibration- coherent noise is removed. Different L and overlap (O) settings were selected and tested based on the environment (e.g., deep vs. shallow water), following Fer et al. (2024). For shallow stations, L (O) was shortened to 54s (2.5s), in contrast to 8 s (4 s) used for deeper stations, due to evidence of overturns observed in AMAZOMIX acoustic measurements at deeper stations (Koch-Larrouy et al.,

2024; in preparation). This adjustment helped to optimize the spatial resolution of dissipation estimates in shallow water stations.

Finally, ε is determined using the spectral integration method and by comparison with the Nasmyth empirical spectrum (Nasmyth, 1970). Quality assurance tests are carried out in accordance with ATOMIX's recommendations (Lueck et al., 2024). A figure of merit < 1.4 is used to exclude bad data (e.g., at station S6; Fig. 2b, and Fig. A1, Appendix), and the fraction of data affected by de-spiking is < 0.05.

”

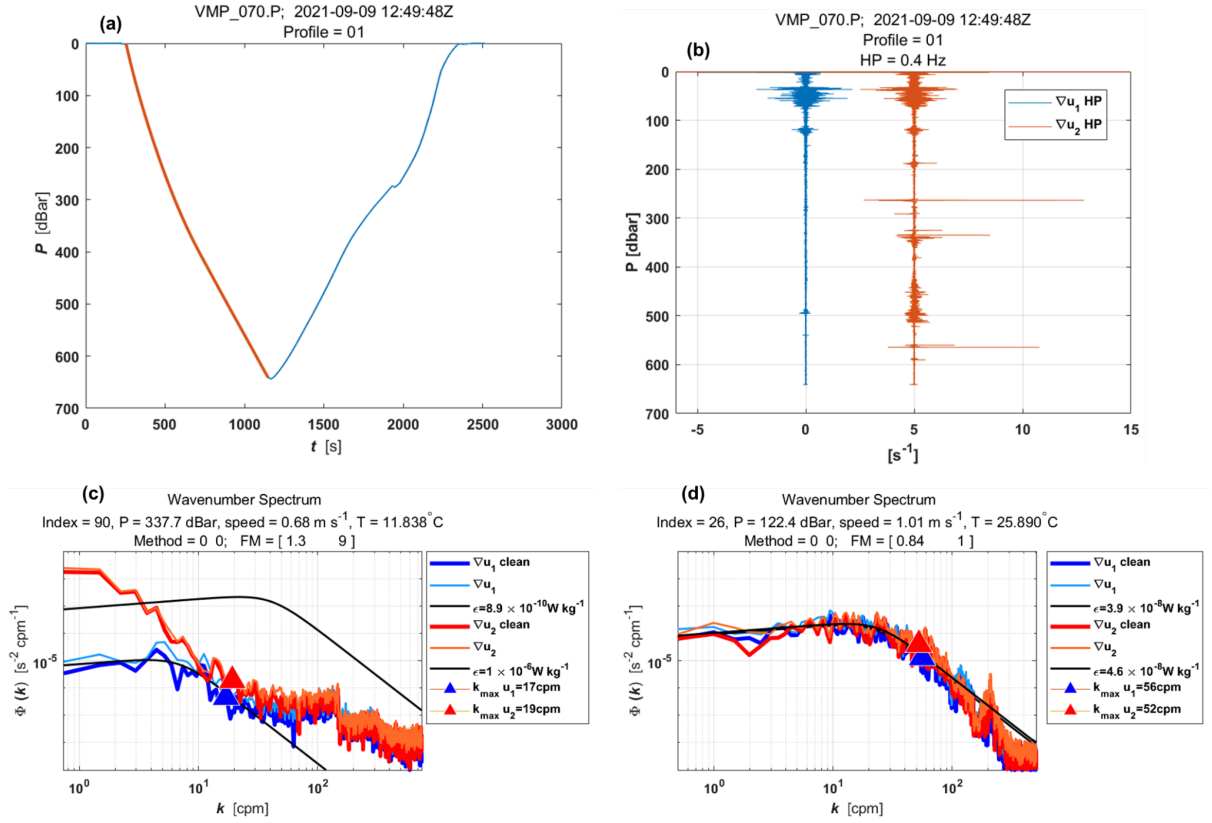

Figure RC2.5: Example of wavenumber spectra from a dissipation structure segment used to determine the dissipation rate at station S14 at a pressure of 337.7 dBar. (a) Pressure record for the entire data file (blue) and the specific segment being analyzed (red). (b) Cleaned and high-pass filtered signals from shear probe 1 (blue) and shear probe 2 (red, offset by 5 s^{-1}). (c) Wavenumber spectra for shear probes 1 and 2. Thick lines (blue for probe 1, red for probe 2) show shear spectra with coherent noise correction, while thin lines (sky blue for probe 1, orange for probe 2) show spectra without correction. Triangles mark the maximum wavenumber used for dissipation rate estimation. Black lines represent Nasmyth reference spectra for estimated dissipation rate of 8.9 x 10^{-10} W kg^{-1} and 1 x 10^{-6} W kg^{-1} for shear probes 1 and 2, respectively. Dissipation rate estimates for shear probes 1 and shear probe 2 at a pressure of 337.7 dBar yielded a figure of merit of 1.3 and 9, respectively. Panel (d) is similar to panel (c) but:- with Nasmyth reference spectra for estimated dissipation rate of 3.9 x 10^{-8} W kg^{-1} and 4.6 x 10^{-8} W kg^{-1} for shear probes 1 and 2. -wth dissipation rate estimates for shear probes 1 and 2 at a pressure of 122.4 dBar yielding a figure of merit of 0.84 and 1, respectively.

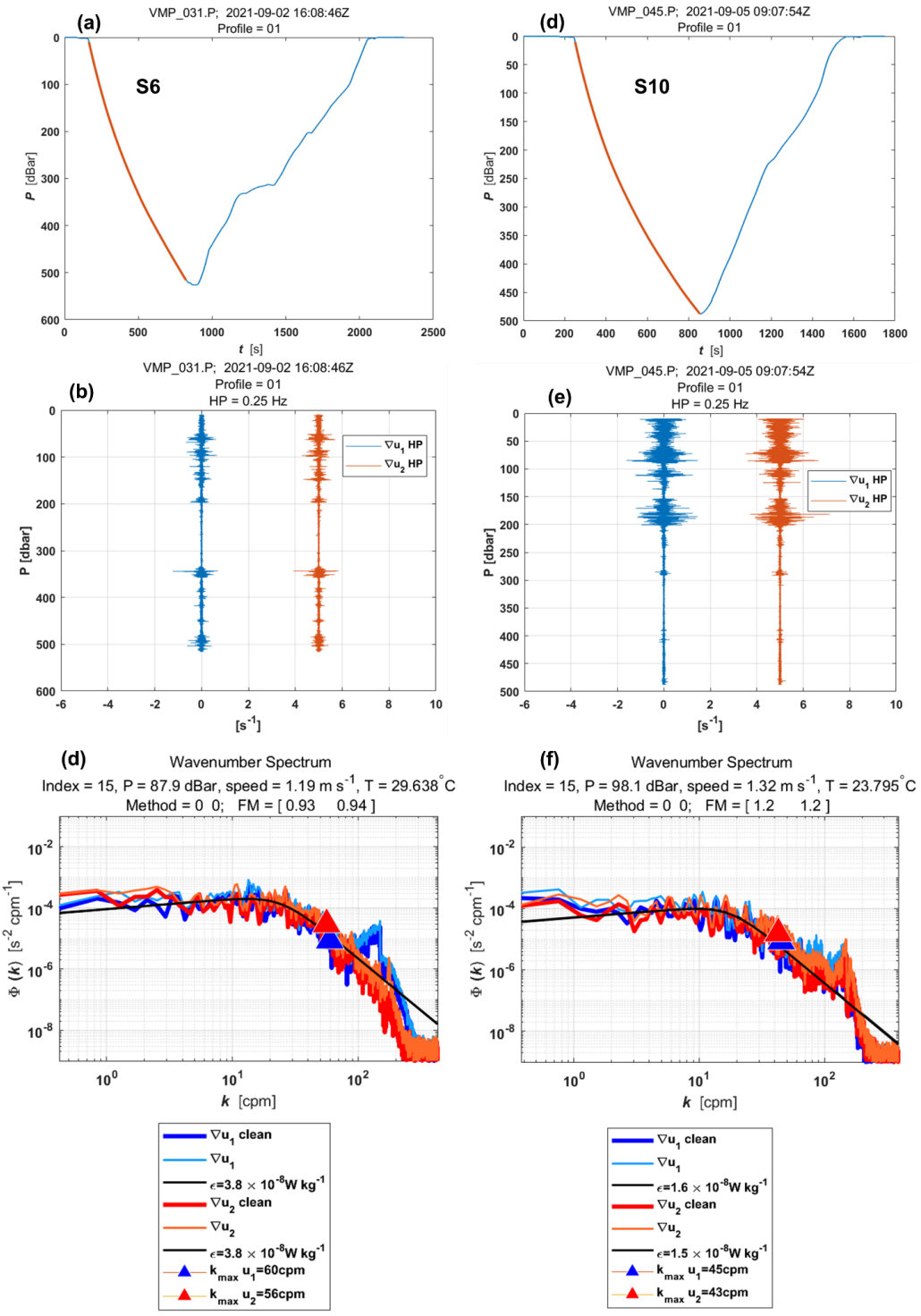

Figure RC2.6: Similar to Fig. RC1.1. but for stations (a)-(b)-(c) S6 and (d)-(e)-(f) S10. For S6 (panels c), Black lines represent Nasmyth reference spectra for estimated dissipation rate of 3.8 x 10-8 W kg-1 for both shear probes, and dissipation rate estimates for shear probes 1 and shear probe 2 at a pressure of 337.7 dBar yielded a figure of merit of 0.93 and 0.94, respectively. For S10 (panel f), Black lines represent Nasmyth reference spectra for estimated dissipation rate of 1.6 x 10^{-8} W kg^{-1} and 1.5 x 10^{-8} W kg^{-1} for shear probes 1 and 2, respectively, and dissipation rate estimates for both shear probes at a pressure of 337.7 dBar yielded a figure of merit of 1.2.

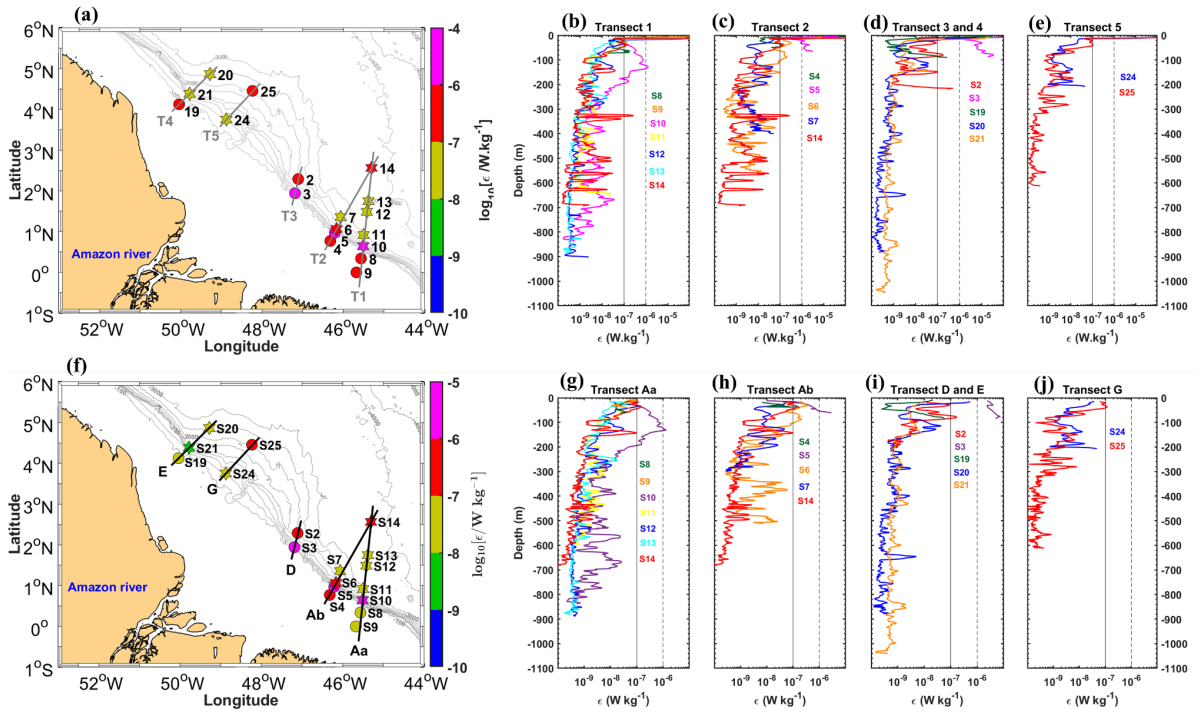

figure RC2.7: (a) Horizontal maximum and (b)-(c)-(d)-(e) vertical dissipation rates (ε, in W kg-1, on a logarithmic scale) before revisions and checks processes for all stations along transects T1 to T2. (f) Horizontal maximum and (g)-(h)-(i)-(j) vertical dissipation rates (ε, in W kg-1, on a logarithmic scale) after revisions and checks processes for all stations along transects Aa, Ab, D, E, and G. Distinct colors are used to represent each station within each transect. Dashed and solid black lines in panels (b) to (e) are included for comparison purposes.

-the relationship between step-like structures and strong internal tides is not convincing as it is presented

R: We agree that without prior knowledge of step-like features, this action can be difficult to understand. Thank you for highlighting this. In response, we have added arrows in Figure 3 of manuscript to indicate the "step-like structures" and "vertical displacement," making it easier for readers to understand the "step-like features" we are referring to (see figure RC2.8 below).

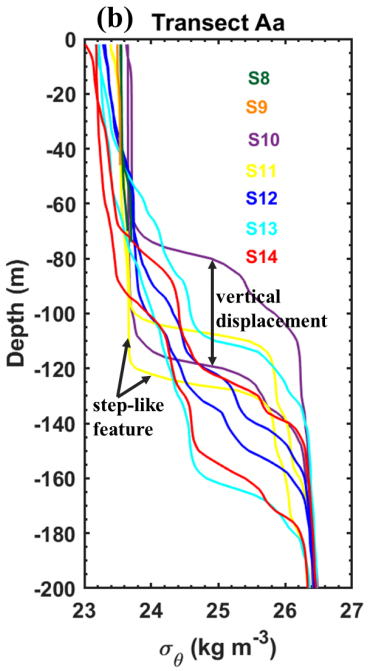

figure RC2.8: *Density profiles (σ_θ, kg m^{-3}) obtained from CTD-O_2 measurements during the AMAZOMIX 2021 cruise for stations S8 to S14 along transects Aa, located within IT fields. For long stations (S10-S14), two density profiles are shown to highlight step-like structures and isopycnal vertical displacements (illustrated by black arrows) along the transects. Distinct colors are used to represent each station within transect. The density values for stations S8, and S9 range between 23.4 and 23.8 kg m^{-3}*

-Figure 4 : Emphasis is made on shear instability, this is quite convincing at S10 but not at S14, this should be interesting to comment on.

R: Thank you for your comment.

Indeed, the focus is on the contribution of tidal and low-frequency shear instability in the mixing process. It was found that tidal shear and its influence are stronger at S10, located near the tidal generation site, compared to S14, which is farther from the generation site in the open ocean. This is discussed in the section "Discussion and Conclusion" (lines 426–567), with particular emphasis at S14 in lines 556–567 of the revised manuscript, as shown below at the end of this document.

-Competitive processes to generate mixing: the hypothesis of shear-driven dissipation is followed with the aim to discriminate between the low frequency shear contribution and the IT shear one. I find this subsection difficult to follow, and I don't understand why the MG parameterization is introduced to this aim.

R: Thank you for your comment.

Indeed, the MacKinnon-Gregg parameterization was applied as a proxy to evaluate the contributions of tidal and low-frequency shear, primarily for comparison purposes. However, no scientific results were derived from it in this study.

Ultimately, we decided to remove and reserve the mixing parameterization for a separate paper in progress. Instead, we revised the subsection and focused on vertical shear to assess the contributions of tidal and mean shear.

-Figure 5 : the ray tracing approach should be revisited with taking into account the low frequency current, mean along shore current displays some spatial variations that may modify the ray structure ;

R: Thanks for your comment.

Indeed, our ray-tracing calculation neglected horizontal density gradients and the mean baroclinic flow, which we acknowledge as a limitation. In our study, the ray-tracing calculation superimposed with mean current data is used as another tool to gain insights into the mechanisms driving the observed mixing along the IT path.

To try to assess the potential influence of horizontal density gradients, we tested N2 profiles at specific stations (e.g., S10, S12, and S14) along transect Aa. The sensitivity tests (Figure RC2.9) showed that ray paths align within the packets of rays observed when using mean N2 profiles at different times (e.g., in September and October; Figure RC2.10). Similarly, the influence of mean circulation was evaluated by superimposing on the figure RC2.10 the mean total current, as shown in the corresponding figure 8 of manuscript revised.

Both influences—stratification and background circulation—are discussed in the sections "Methods" (lines 218–221) and "Results" (lines 392–414) of the revised manuscript.

The influence of stratification and mean current on mixing and IT ray paths using ray-tracing calculations will be explored more in a separate paper.

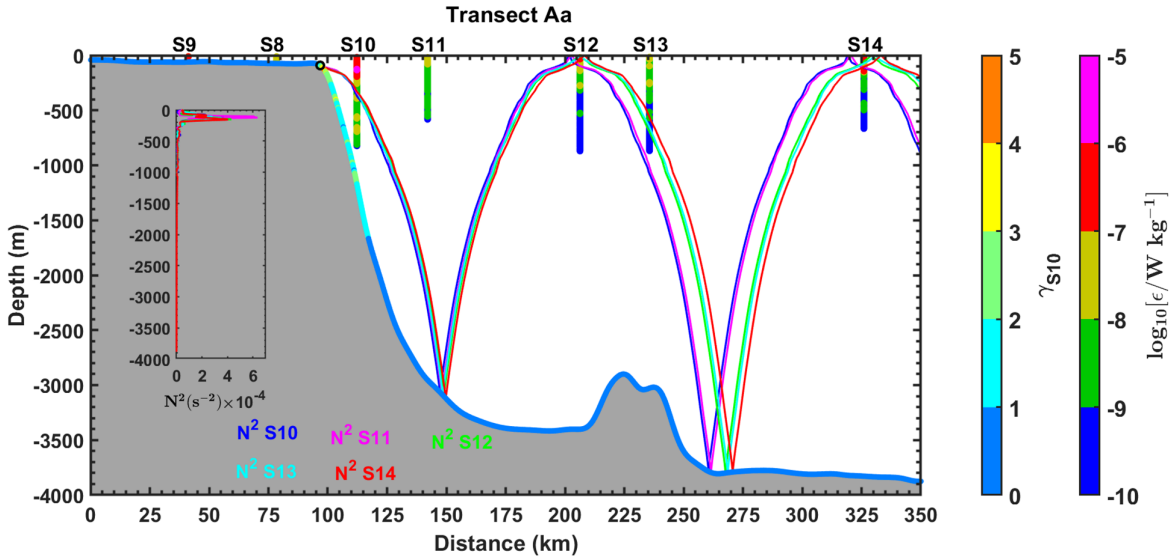

figure RC2.9: Example of sensitivity tests with different cross-sectional measurements of N^2 along the transect T1 N^2. colors are used to distinguish different cross-shore measurements of N^2

for corresponding stations on T1. Topography steepness (gamma = ray slope / topography slope) for T1 using measured N^2 of S10. Gamma is illustrated by the colored bar (named gamma S10).

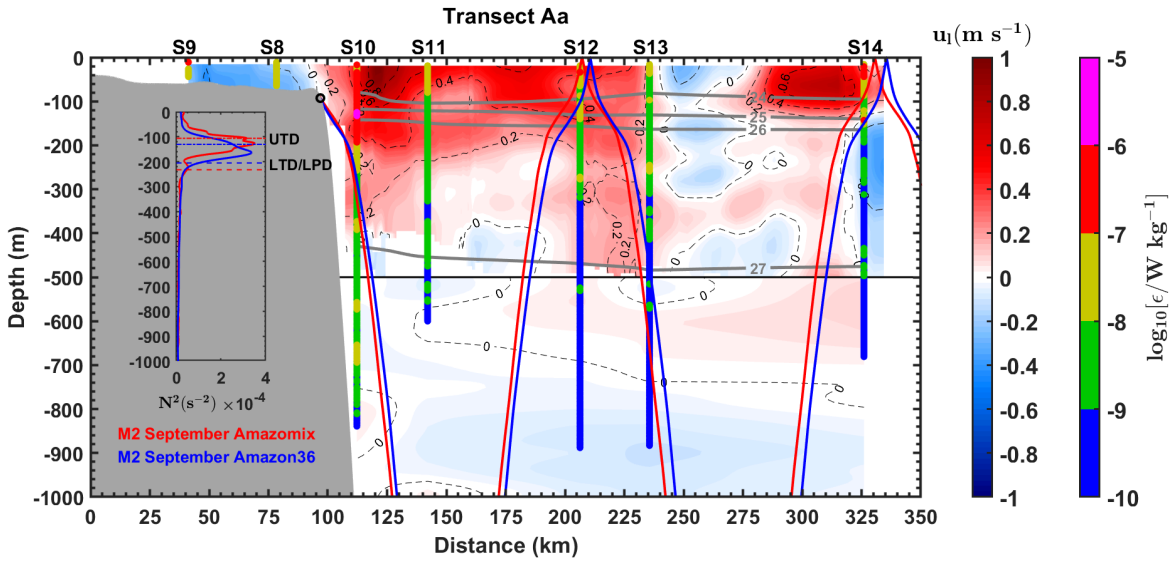

figure 10: IT ray-tracing diagrams for the M2 tidal constituent along transects Aa. The calculations were performed using the mean buoyancy frequency squared (N^2, in s^{-2}) obtained from CTD-O_2 data (ray in red) and NEMO-Amazon36 model data (ray in blue) for September. Grey areas represent local topography and black circles indicate the critical topography slope (ray generation sites). Panel also show along the transects Aa: along-shore mean total currents (u_l, in m s^{-1}) from ADCP (Dashed black lines), potential density from CTD-O_2 (grey contours), and dissipation rate profiles (ε, in W kg^{-1}, on a logarithmic scale) from the VMP (vertical colored bars). Subpanels within each panel illustrate the N^2 profiles from AMAZOMIX (red line) and the NEMO-Amazon36 model (blue line) used for ray-tracing calculations. Upper Thermocline Depth (UTD, dotted lines) and Lower Thermocline/Pycnocline Depth (LTD/LPD, dashed lines) are also indicated.

-Nutrients fluxes : profiles of Kz and nutrients fluxes are displayed. I don't see the point in giving values of nutrients fluxes without showing the concentration profiles and introduce the motivations and the issues.

R: Thanks for your comment.

Indeed, nutrient concentration profiles were analyzed prior to calculating nutrient fluxes.

Ultimately, we decided to remove and reserve all sections on “Nutrients fluxes” for a separate paper in progress.

-Discussion and conclusion : needs to be re-written and with convincing results for most part of it, one example : l442 « shear instabilities stronger >10-4s-2 », IT shear : high tidal modes are referred to but not shown etc

R: Thanks for your comment.

We have revised and rewritten the "Discussion and Conclusion" section, with updates found between lines 426–567 of the revised manuscript.
The tidal modes identified in the baroclinic tidal current time series (see figure RC2.11 below for an example) are presented in the section "Results" of the revised manuscript.

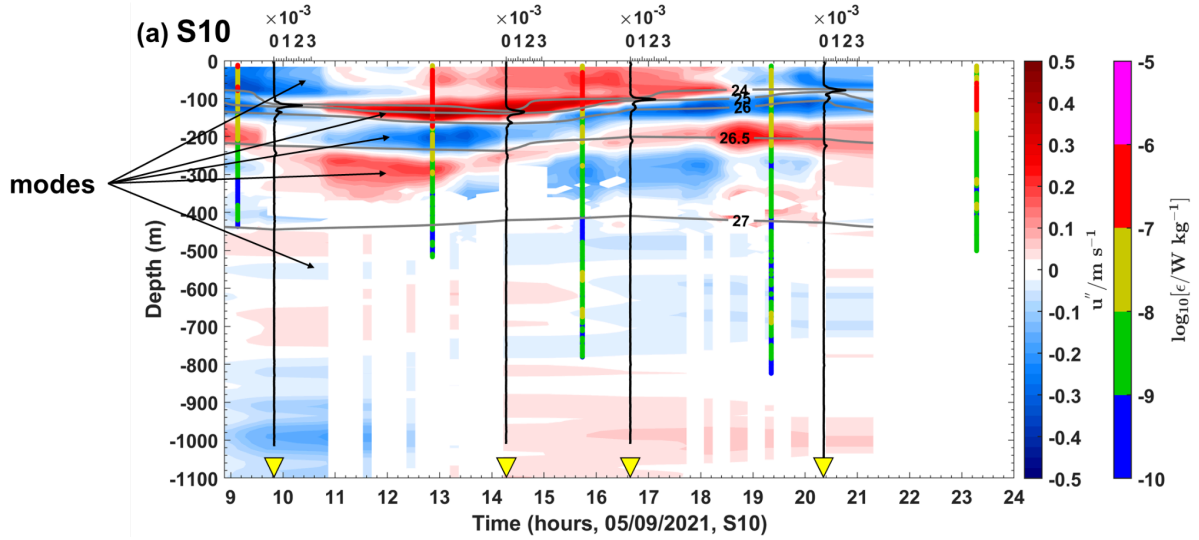

figure 11: Semi-diurnal baroclinic zonal currents (u", in m s-1) from the ADCP for stations (a) S10. Panel (a) also displays the buoyancy frequency squared (N2, in s-2) represented by vertical black lines, potential density represented by grey contours, and dissipation rate profiles (ε, in W kg-1, on a logarithmic scale) represented by vertical colored bars.

Revisions of section “Discussion and Conclusion” can be found below:

.

“

4 Discussion and Conclusion

The AMAZOMIX 2021 cruise provided, to the best of our knowledge, for the first time, direct measurements of turbulent dissipation using a velocity microstructure profiler (VMP) at multiple stations both inside and outside the influence of ITs. These measurements enabled the study of mixing processes at the Amazon Shelf break and the adjacent open ocean. To capture a full tidal cycle, data on turbulent dissipation rates, hydrography, and currents were collected alternately over 12 hours, with 4 to 5 profiles taken per station (see section 2). The locations of the 12-hour sampling stations were selected based on modeling results that provided realistic maps of IT generation, propagation and dissipation (Fig. 1a; Tchilibou et al., 2022). Stations were located in the most energetic regions of IT, specifically at sites Aa, Ab, and D, covering stations S2 to S14, as identified in previous studies (Magalhaes et al., 2016; Tchilibou et al., 2022; Assene et al., 2024). Stations S19 to S21 were positioned in less energetic IT generation areas at site E, while stations S24 and S25 were located outside the influence of the IT fields (site G). Stations were distributed across different areas, including the shelf (e.g., S4, S9, and S19), the shelf-break (e.g., S3, S6, and S10), and the open ocean (e.g., S14, S24, and S20).

Vertical Displacement, homogeneous layers

The results revealed that, over a semi-diurnal tidal cycle, relevant amplitudes of vertical displacements (up to 60 m in length) and pronounced step-like structures (up to 40 m thick) were observed along transects Aa and Ab. In contrast, smaller and thinner structures were identified along other transects, such as E. These differences are likely related to the propagation of ITs, which induce vertical displacements at tidal frequencies and promote mixing by creating homogeneous layers visible as step-like features in the density structure. The isopycnal displacements and step-like structures observed within the pycnocline are consistent with findings from other IT regions (e.g., Stansfield et al., 2001; Simpson and Sharples, 2012; Bordois, 2015; Koch-Larrouy et al., 2015; Zhao et al., 2016; Bouruet-Aubertot et al., 2018; Xu et al., 2020). Furthermore, IT propagation appears to have stronger energy along transects Aa and Ab compared to others, consistent with prior modeling studies (Tchilibou et al., 2022; Assene et al., 2024).

Direct measurements of dissipation rate

Dissipation rates measured with the VMP ranged from between [10^{-10}, 10^{-5}] W kg^{-1} below the XLD, spanning from the continental shelf to the open ocean.

The highest dissipation rates, within [10^{-6}, 10^{-5}] W kg^{-1}, were observed primarily at generation sites Aa, Ab, and D (e.g., at stations S6, S10, and S3), as represented for A region in Fig. 9 (red zigzags). Slightly lower but still substantial dissipation rates, ranging from 10^{-8} to 10^{-7} W kg^{-1}, occurred a few kilometers (~40 km) from these generation sites (e.g., at S11 and S7), along IT pathways (e.g., at S12, S13, and S20), and even in regions farther from IT influence (e.g., at S24). Interestingly, dissipation rates were higher within [10^{-7}, 10^{-6}] W kg^{-1} in the open ocean, such as at station S14, located ~230 km from generation site Aa, as summarized in Fig. 9 (orange zigzags).

Using dissipation measurements, we calculated the XLD, defined as the depth where the dissipation rate drops from its first minimum value. The XLD was found to be greater than the MLD at all stations except S8, S10, and S25. This exception may reflect larger mixing events at those stations that were not captured during the VMP deployment. For the other, it is consistent with regions exhibiting strong subsurface shear, such as the equatorial ocean and western boundary current areas (Noh and Lee, 2008).

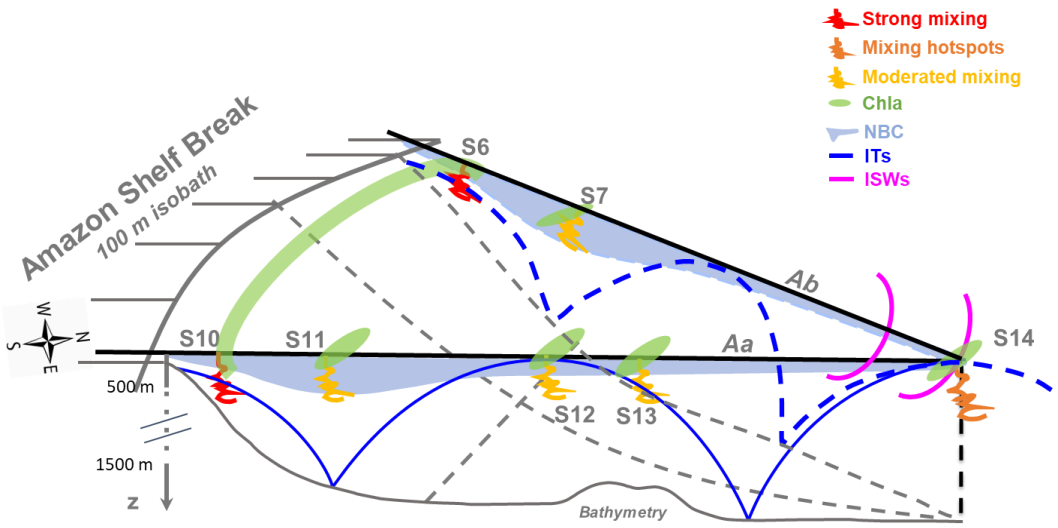

Figure 9: summary diagram illustrating the key processes driving mixing along the AMAZOMIX transects (e.g., Aa and Ab). At IT generation sites (e.g., S6 and S10; red zigzags), mixing rates are stronger, with ITs contributing around 65%, compared to mean circulation (NBC). Along IT pathways (e.g., S7 and S11; yellow zigzags), mixing decreases but remains notable, driven by nearly equal contributions from ITs and mean circulation. A key observation is the increased mixing ~ 230 km from two distinct IT generation sites at the shelf break. This hotspot at S14 (orange zigzags) coincides with the surfacing of IT rays (blue lines) from different sites, vanishing of the NBC (sky blue shaded areas) and the presence of ISWs (magenta lines), suggesting possible constructive interferences of IT rays may generate ISWs, amplifying mixing at S14. IT mixing observed close enough to the surface at these sites could influence the chlorophyll content (green shaded areas) off the Amazon shelf.

In other regions, dissipation rates exhibit values comparable to those observed in this study. For instance, at IT generation sites (S6 and S10), dissipation rates align with the range of [10^{-7}, 10^{-5}] W kg^{-1} reported for the Halmahera Sea, Indonesia (Koch-Larrouy et al., 2015; Bouruet-Aubertot et al., 2018), Kaena Ridge, Hawaii (Klymak et al., 2008), and the Changjiang Estuary (Yang et al., 2020). Conversely, along IT pathways off the Amazon shelf (e.g., S11 and S7), dissipation rates are higher ([10^{-8}] W kg^{-1}) than those documented in other regions, such as [10^{-10}, 10^{-8}] W kg^{-1} in the Southern Ocean (Gille et al., 2012) and the Halmahera Sea (Bouruet-Aubertot et al., 2018), that might be due to the cumulative effect of IT and NBC mixing and/or to their interaction that might intensified the local mixing. Lastly, in the open ocean, elevated dissipation rates were observed compared to previous studies. For instance, values of [10^{-9}, 10^{-8}] W kg^{-1} around 100 m depth at S25 were higher than values of [10^{-11}, 10^{-10}] W kg^{-1} reported by Takahashi and Hibiya (2019) for sites far from IT influence and under geostrophic current conditions. This discrepancy may be attributed to the strong mean background circulation investigated off the Amazon shelf (Dossa et al., in preparation).

Our study also found the highest dissipation rates at stations S3 and S5 of [10^{-6},10^{-4}] W kg^{-1} on the Amazon shelf , increasing near the bottom boundary layer. These findings compare well with values reaching up to 10^{-9} W kg^{-1} within a kilometer of the seabed in the Southern Ocean (Sheen et al., 2013) and up to 10^{-6} W kg^{-1} within

a few meters from bottom topography off the Changjiang Estuary (Yang et al. 2020). This may indicate the presence of an active bottom boundary layer. Thus, kinetic energy of bottom flow was estimated using friction velocity, that was computed from total velocity averaged over the bottom-most 15 m for shallow stations. It showed bottom friction energy stronger between 16-35 J m^{-2} at S3 and S5 mainly and lower (< 3 J m^{-2}) in the other stations on shelf (e.g., at S8). These results are smaller but still important on the Amazon shelf and comparable to values (517 kJ m^{-2}) in the Drake Passage region (on the continental slope) of the Southern Ocean (Laurent et al., 2012). The bottom mixing at S3 and S5 can indirectly exert a control on pycnocline mixing on the Amazon shelf (Inall et al., 2021).

Enhanced surface mixing

The vertical eddy diffusivity coefficients were highest at the shelf break (e.g., at S3, S5, and S10), ranging from 10^{-3} to 10^{-0} m^2 s^{-1}. Away from the shelf break, diffusivity values were lower but remained substantial, within the range of 10^{-4} to 10^{-3} m^2 s^{-1} (e.g., at S2, S7, and S11). These mixing coefficients align with values reported in other regions. For instance, vertical diffusivity falls within the range of 10^{-5} to 10^{-3} m^2 s^{-1}, as observed in the Luzon Strait (Tian et al., 2009), the Indonesian Sea (Koch-Larrouy et al., 2015; Bouruet-Aubertot et al., 2018), and the southern Yellow Sea (Xu et al., 2020).

Close to the surface, mixing coefficients remained significant, reaching up to 10^{-3} m^2 s^{-1} between 100-200 m depth and up to 10^{-2} m^2 s^{-1} above this layer at stations S6 and S10. These surface values are of the same order of magnitude as, but slightly higher than, those reported for the Halmahera Sea, Indonesia (Koch-Larrouy et al., 2015; Bouruet-Aubertot et al., 2018). In the open ocean, under the influence of ITs, mixing near the surface reached 10^{-4} m^2 s^{-1} at S14.

This elevated vertical eddy diffusivity close enough to the surface along IT paths may play a critical role in modulating heat transfer (e.g., Assene et al., 2024) and chlorophyll distribution (see green shaded areas in Fig. 9) (de Macedo et al., 2023; M'Hamdi et al., in preparation) observed off the Amazon shelf, as documented in the Indonesian region (Nugroho et al. 2018; Koch-Larrouy et al., 2010; Sprintall et al., 2014; Zaron et al., 2023).

Contribution of Background circulation and ITs to mixing

Mean baroclinic current shear

Another important aspect addressed in this study was quantifying the contributions of different processes to the observed heterogeneous mixing.

First, we analyse the mean baroclinic current (BC), a proxy for the background circulation. The BC was predominantly structured into a northwestward surface flow and a southeastward subsurface flow along the IT pathways. The strong surface flow toward the northwest is associated with the North Brazil Current (NBC), which originates from the northeastern coast of Brazil (e.g., Bourlès et al., 1999) and propagates along the Amazon shelf-break (e.g., at stations S7, S10, S11, S14, and S24). Conversely, the southeastward subsurface flow observed at stations such as S7 and S11 might result from NBC instability or the presence of a countercurrent at depth (Dossa et al., in preparation). At site E, the flow reversal observed at S21 - characterized by a southeastward surface flow and a northwestward subsurface flow - was located inside of the outer path of

the Amazon plume. This reversal could be related with the influence of AWL formed by continental inputs (Prestes et al., 2018).

Both baroclinic flows demonstrated a significant potential for shear instability, with vertical shear ranging from 10^{-5} to 10^{-3} s^{-2} off the Amazon shelf. The shear associated with the NBC was particularly pronounced around the pycnocline (between 40 and 200 m depth) at sites Aa, Ab, and G (e.g., at S6, S7, S10, S11, S14, and S24). At site E, the shear instability was stronger (> 2.5 x 10^{-4} s^{-2}) at the base of the pycnocline (e.g., at S20), potentially associated with NBC retroflection near [5-6°N, 50°W] during the fall season (Didden and Schott, 1993). The higher BC shear observed at S21, where flow direction reversals occurred, could be associated with the presence of a subsurface cyclonic eddy (Dossa et al., in preparation).

ITs shear

Second, the baroclinic tidal current was extracted from the total baroclinic current, revealing significant semi-diurnal (M2) component signals around the pycnocline. These signals, characterized by higher tidal modes (3-5), were more pronounced at generation and propagation sites Aa and Ab (e.g., at S6, S10, and S14) compared to other sites. The tidal shear within the pycnocline layer (80-120 m) is consistent with the observed IT signal patterns and large vertical displacements. It was stronger, reaching up to 10^{-3} s^{-2}, near the generation sites Aa and Ab (at S6 and S10) and in the open ocean at S14. Further from the generation sites (e.g., at S7, S11, and S20), the IT shear was smaller but still notable (reaching up to 10^{-4} s^{-2}). This highlights the significant role of ITs in driving mixing processes, particularly within the pycnocline, where strong vertical shears were observed near the shelf-break compared to regions far away. Outside the IT fields, such as at S24, the persistent high vertical shear near the bottom topography could be attributed to the active bottom boundary layer (Inall et al., 2021).

IT/BC ratio

Both IT and BC shear contribute to mixing, with their relative dominance varying across sites. Near the generation sites on the shelf-break, IT shear dominated the IT/BC shear ratio, such as at S6 (61.4/38.6 %), S10 (65.8/34.2 %), and S21 (58.5/41.5 %). Along the IT paths, the contributions were nearly equal (~50/50 %) at locations farther from the generation sites (e.g., at S20, S7, S11, and S13), except at S14 in the open ocean, where IT shear remained dominant (58.5/41.5 %). These findings align with the presence of ITs at generation sites Aa, Ab, and E (Tchilibou et al., 2022; Assene et al., 2024) and the stronger energy associated with NBC cores, particularly at S7 and S11.

These results are consistent with previous studies that identified strong tidal shear near IT generation sites, such as the Halmahera Sea (Bouruet-Aubertot et al., 2018), the Changjiang Estuary (Yang et al., 2020), the northwest European continental shelf seas (Rippeth et al., 2005), and the southern Yellow Sea (Xu et al., 2020).

The most relevant finding of this study was the relative increase in mixing within the pycnocline layer, observed at S14 in the open ocean, far from the IT generation sites.

Discussion on the strong mixing at S14

Along the IT paths, elevated remote dissipation rates (within [10^{-7}, 10^{-6}] W kg^{-1}) were identified ~ 230 km from the shelf-break at S14.

This region is well known for intense IT dissipation, as shown by a realistic model (Tchilibou et al., 2022; Assene et al., 2024), and for the highest occurrences of ISWs generated by ITs (Fig. 1a; de Macedo et al., 2023), with large-amplitude ISWs exceeding 100 m clearly visible in satellite records (Brandt et al., 2002).

At station S14, where relative mixing increases, IT rays surfacing from two distinct IT generation sites coincide with the appearance of ISWs and mark the location where the NBC vanishes.

This region of wave-wave interactions can lead to the constructive interference of IT rays, potentially facilitating the emergence of higher tidal modes (New & Pingree, 1992; Silva et al., 2015; Barbot et al., 2022; Solano et al., 2023). These higher modes, in turn, could enhance the generation of nonlinear ISWs (e.g., Jackson et al., 2012) and contribute to the elevated dissipation rates (Xie et al., 2013), as observed at this station.

"

As a conclusion, I think this manuscript is no ready for publication and needs significant work to produce convincing results. I think the most efficient way to proceed is a new submission.

End